博士論文

System Design of Cost-Effective Soil Monitoring Networks for Agriculture

(**コスト効率のよい農業用土壌モニタリングネットワークの設計**)

繁田　亮

指導教員:　**川原 圭博 准教授**

Abstract

In this thesis, system design of cost-effective soil monitoring networks is presented. The soil monitoring networks capture soil parameters such as soil moisture and soil temperature then collect measured data through wireless communication. Precision farming has large potential for enhancing farming productivity since it enables efficient natural resource management. The collection of environmental and crop data by using various sensors is a crucial part of precision farming; therefore, an agricultural wireless sensor network is considered as one of the most attractive Internet of Things (IoT) applications. As soil parameters significantly affect to plant growth, soil sensors play quite important role in agricultural sensing systems. While there are several commercialized agricultural sensing systems, their cost tends to be forbidding to large-scale implementation. As a result, IoT technologies have not much contributed to solve issues related with food and agriculture. To guarantee water resource sustainability and food supply through precision farming, huge scale deployments of agricultural sensors on developing country are required. Thus, reducing cost of agricultural sensors is the key challenge to enhance its potential. The cost of an agricultural sensing system can be broken down to initial and operational cost. Currently available sensors and data loggers are mainly designed and used for research purposes; therefore, they can provide very precise measurements, in various environments, but at increased cost. Thus, cost-effective soil moisture sensor leveraging printed electronics technologies is developed. The sensor can measure soil parameters in multiple depth and its sensor probe is detachable to select a target parameter. The sensed data is both stored locally and remotely so the real-time data is presented on Web app and the other clients. Its usability and durability were tested in iterations of experimental deployments all over the world. Several hundreds of the sensors were fabricated and tested in various fields from 2015 to 2017. Combining the irrigation control system and the soil monitoring network, more precisely automated irrigation system can be developed. Once it achieved, both farming productivity and labor efficiency should be significantly improved. As Japan is facing gradual population decreasing of farmers, automation will be a key to remain farming production. Such data driven irrigation should play important role on agriculture in India as well. As India is under monsoon climate, irrigation optimization is fundamental for farming in dry season and overuse of groundwater is considered as a social problem. If soil moisture is monitored in real time and farmers just supply appropriate amount of water based on the data, water consumption can be drastically reduced. Considering the background, the developed sensors were deployed and tested in India. The soil moisture sensors successfully captured soil moisture data which indicates relationship between irrigation control and soil moisture levels. As the next step, cooperation with efficient crop management strategy

and remote sensing is expected. Other than the sensors for professional farmers, a simple version of soil moisture sensor for hobby use was developed. In this package, sensor film for soil moisture sensing can be customized using ink-jet printer with silver ink. Since the artwork for sensor film can be drawn on PowerPoint, the rapid prototyping is suitable for soil sensor design workshops. Through the workshop, interesting ideas on sensor film design have been collected. The outcome would be reflected in the next version of the sensor. While initial cost is reduced by using printed electronics, operational cost is still significant and remaining problem because our sensor nodes are currently powered by batteries, which require additional labor expense for their replacement. Since the number of sensors is limited, battery replacement is not a serious matter; however, if a farmer introduced several hundred sensors in their farm field, and each sensor required battery replacement every year, the project would become unsustainable. With consideration to scalability issues, battery-less sensors are preferable to battery-driven sensor networks. Therefore, Unmanned Aerial Vehicle (UAV) assisted wireless power transmission (WPT) system and thermoelectrical energy harvesting are proposed as battery-less solution for agricultural sensing networks. Combining low-cost fabrication technics and battery-less solutions, cost-effectiveness is improved in both initial and operation cost. While sensing accuracy of the soil moisture sensor is not equivalent to the other precise soil sensors, according to the feedbacks from experimental deployments, the sensed data is useful enough to quantifying soil management knowledge and expand productivity eventually. Battery related troubles were matter on the experimental deployments, but they will be resolved by introducing the battery-less solutions and long-term usability will be significantly improved.

Table of Contents

List of Figures

List of Tables

Chapter 1

Introduction

1.1 Background

Agricultural sensing is considered as one of the most interesting application of Internet of Things (IoT) and various players such as start-ups, electric manufacturer, and IT vendors are exploring opportunities on the area. Introducing advanced technologies and innovative products to agricultural fields are called "agritech" and it attracted huge attention globally. Importance of agriculture is now revisited because of rapid growth of global population and potential risk of food shortage. Moreover, ongoing global climate changes make it difficult to keep food production in traditional ways. Expanding farming productivity to supply sufficient food without harming sustainability is considered as a major global challenge. Ensuring water resource sustainability is a key for this challenge because large scale grain farming, which is crucial for food supply, heavily depend on irrigation using underground water. Overuse of ground water starts causing serious water shortages and grain farming will be seriously damaged by the combination of climate changes and the lack of water. Thus, reducing water consumption is urgent matter for agriculture and appropriate irrigation considering soil moisture level is required. To achieve the smart irrigation, soil monitoring system need to be introduced in large scale as appropriate irrigation amount cannot be calculated without understanding the current soil moisture level. Irrigation strategy need to be optimized to maximize the harvest per supplied water based on the captured soil moisture data; however, reasonable sensing solution have not delivered yet.

Other than such large scale grain farming, soil monitoring plays important role for productive farming. Managing soil to be desired condition for crops is fundamental for agriculture. Even if hydroponic culture and plant factory is considered as modern agriculture, the most of farming production should keep relying on soil. Soil plays various role for plant growth as it works as storage of water and fertilizer so that plants can resist to lack of rain and fertilization for a while. Each crop has preferring soil condition e.g. rice likes wet conditions but cactus likes dry conditions and its growth and harvest is maximized under the appropriate condition. If a crop is left in not suitable soil condition, the risk of disease will be increased and it will be easier to beaten by insects and weeds. In the worst case, it will be killed. Soil moisture is the most important parameter as the other phenomena such as heat transfer, chemical transfer, and chemical reactions in soil are also affected by soil moisture level. Therefore, productive farmers should have deep knowledge about soil managements to maximize the harvest and quality of crops. However, it is highly depends on personal sense and experiences and it is not easily transfer to the others. Even if farmers understood importance of soil management, almost all farmers does not have detailed scientific guidelines or manuals. This is because there is no affordable soil monitoring solutions. While there are several commercialized soil sensors, they are developed mainly for research purpose so they are accurate but expensive. As a result, their cost is the most serious barrier for spreading the soil monitoring system.

Considering the background, developing cost-effective soil moisture monitoring networks is set as the eventual goal of the research. Through the network, various soil

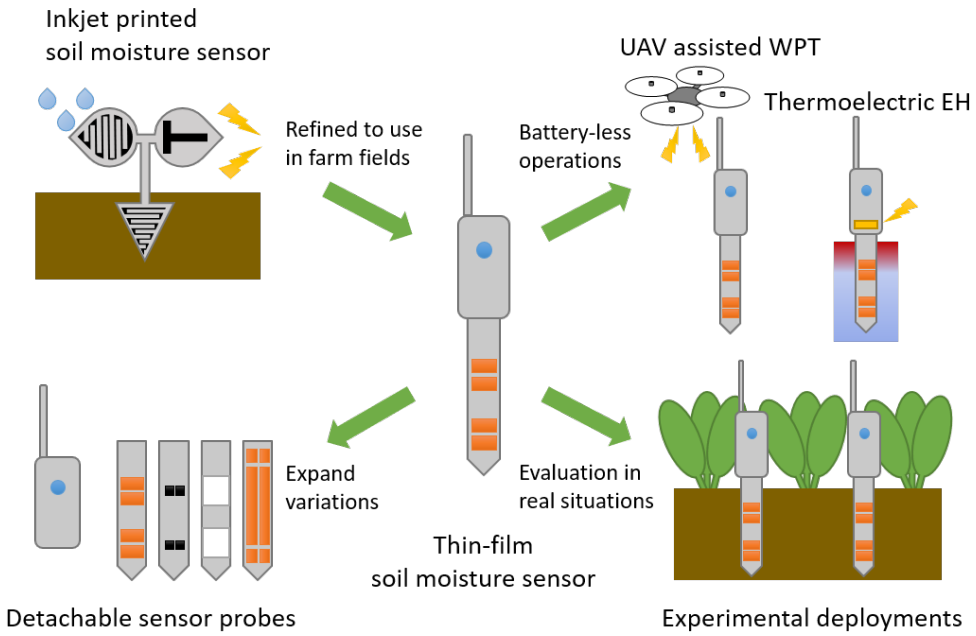

Figure 1.1: Developments of cost effective soil monitoring system

data is gathered and be ready for analysis to optimize irrigation then maximize farming productivity. Reducing cost is the design philosophy for this system and it is discussed from perspective of both initial and operational cost. Figure 1.1 shows the researches included in the thesis, the concept of the low-cost agricultural sensor is started from combined system of RF energy harvesting and ink-jet printing sensors. The concept itself was succeeded to give inspirations, it was actually not ready for deploying to the real fields. Therefore, the deployable model is developed. The sensor electrode is no longer ink-jet printed but still leveraging printed electronics to enable low-cost fabrication. The developed sensor can capture soil moisture in multiple depths and gather the measured data through wireless sensor networks. To proof of the practicality of the sensors, the developed sensor actively delivered and tested in the real farm fields in Japan and in India. On the other hand, RF energy harvesting part also had progress by leveraging unmanned aerial vehicles (UAVs) as a mobile power feeder. As another possible energy harvesting source, thermos energy harvesting is considered as temperature differences are occurred between surface and underground.

1.2 Application of Soil Monitoring Networks

Precision farming has large potential for enhancing farming productivity since it enables efficient natural resource management. The collection of environmental and crop data by using various sensors is a crucial part of precision farming; therefore, an agricultural wireless sensor network is considered as one of the most attractive IoT applications.

Figure 1.2: A center pivot irrigation system (Tifton, GA, USA)

In particular, appealing applications of precision farming are irrigated grain farming and greenhouse farming.

Grain Farming

In terms of ensuring food supply, grain farming is the most important area and impact of improvements on grain farming is much larger than the other area. Labor efficiency on grain farming have been improved by development of farm machines and irrigation system. The irrigation system called center pivots shown in Figure 1.2 enable automated irrigation in large scale and often applied to grain farming in dry climate. However, due to lack of sensing ability, conventional center pivots are not very efficiently use water resource and crop management is not sophisticated enough. There are several researches [1–3] to make decision on irrigation based on the sensed data about crops and the other environments including soil moisture. It imply that once reliable data about soil moisture can be collected, productivity on large scale farming should be improved significantly.

In India, irrigation optimization was considered as important challenge to enable efficient crop management and reserve water resource sustainability while they do not have modern irrigation system like center pivots. Since population of India is increasing, expanding farming production especially on grain farming is necessary to supply sufficient foods. However, current grain farming is not efficient and consumes too much water than required. Thoughtless expansion of farmland will cause severe water shortage by exhausting groundwater. The goal is maximizing farming productivity per consumed water. To achieve it, evapotranspiration and soil moisture need to be accurately estimated and just supplying minimum water not to damage expected harvest. It should be difficult challenge than just maximizing production. Soil moisture sensing will play crucial part for the advanced irrigation management.

Greenhouse farming

In Japan, the main application of the soil monitoring network is irrigation optimization for greenhouse farming. Effective greenhouse control enable maximize farming productivity and improving quality of crops. In recent developments on agricultural IoT, automation on greenhouse control have been enabled. For example, temperature control by air circulation, heating, and window controls with feedback from temperature sensors start to be common. Also current irrigation systems can electrically control irrigation valves and periodical irrigation with timer setting is enabled in the most of the system. Some automated irrigation system have rain detector to avoid unnecessary irrigation. In this meaning, automatic irrigation is already used but it is not reflect actual soil moisture level and it is far from optimal. Therefore, farmers usually take over irrigation strategy which supply more water than plants needed. If plants face to lack of water by insufficient irrigation, it will cause devastating results so supplying too much water is considered as better option than not supplying necessary water. However, too much irrigation also cause various issues like acceleration of salt accumulation. Of course retrieving underground water need electricity so consumption of underground water should be reduced even if there is no concern on sustainability of underground water. Moreover, crops under suboptimal soil moisture level more likely have diseases and easily damaged by insects and weeds because the condition may be preferred by weed, bacteria and insects rather than target crop. As a result, additional cost and labor for pesticide and removing weed are required. To leverage the robustness of crops toward these threats, keeping desired soil condition for the crops is quite important. Soil condition would not be uniform even in the same house so variance of crop size and weight is inevitable if it is uniformly irrigated. Markets require regulated size and weight on vegetables and imperfect vegetables are imposed significant discount. In some cases, shipping cost for the imperfect vegetables exceeds expected revenue so farmers decides to dispose the vegetables rather than shipping. That causes huge loss on food supply and damage income of farmers. If more precise and appropriate irrigation is applied with smaller granularity, such unevenness can be mitigated.

Experienced greenhouse farmers are highly productive because they have knowledge on the desired condition and they experimentally understand when and how much irrigation need to be applied. However, it is required quite difficult to transfer the knowledge to others because it mostly relies on tons of experiences and personal sense rather than quantified data. As far as the knowledge is experience base, new comer need to spend long time for learning. In Japan, population of farmers keep decreasing and elderly farmers mainly owns agricultural production but their valuable knowledge has not been transferred to younger ages. In order to record the knowledge and make it easy to educate younger farmers, collecting various data is quite important even for keeping current farming productivity. These days, some expert farmers works as a consultant to educate other farmers to expand their productivity but they also faced to difficulty on knowledge transfer. When the client remotely consult, it is almost impossible to literally tell the actual conditions of farm fields. Therefore, introducing sensors in client's fields

and giving advices through monitoring the data are considered for efficient consultation.

In more advanced vision, farming activities should be automated as much as possible to improve labor efficiency. Checking soil and crop condition and controlling irrigation are time consuming tasks for farmers and they would rather focus on sowing and harvesting if it is able to automated. To automate the irrigation, supports from professionals of cultivation are crucial as they should know when and how much irrigation is needed. Decision making logic should be designed to reproduce the decision made by such professionals. Combining their precious knowledge and affordable soil moisture monitoring system should enable automated and optimized irrigation. Once it is available, labor efficiency of farming should be dramatically improved as farmers currently spend many time to care irrigation. Meanwhile, consistency of farming production will be promised by precise controls on irrigation with fine granularity.

1.3 Soil Sensors and Probes

Soil moisture is one of the most fundamental parameter for agriculture because plants are highly rely on available water in soil. Soil moisture indicates how much water is included in the soil so it is crucial parameter for smart irrigation which leverages sensor data for decision-making in irrigation [1–3]. In order to determine irrigation amount and timing, continuous monitoring is preferred rather than periodical soil sampling. Although analyzing picked soil sample in lab should most reliable way to know soil parameters including soil moisture, it is too troublesome and time consuming for real time monitoring. The continuous monitoring of soil moisture started around 1940 with electrical resistance measurements using a gypsum block [4]. In this method, the sensor measures electrical resistance between electrodes in the block and the resistance reflects the soil moisture level of surrounding soil. The advantage of the method is simplicity and cost efficiency but the accuracy is not sufficient because resistance of the gypsum block is changed by temperature [5], the response of resistance change according to soil moisture change is slow [6] and it cannot handle various soil types since relationship between resistance and soil moisture is not universal [7]. A neutron attenuation probe was proposed as another alternative of soil moisture sensor in the 1950s [8]. The probe can count radioactive beams emitted from a source and calculate soil moisture from relationship between neutron attenuation and soil moisture. It was successfully applied for field measurements [9] but there is a health hazard concern. Time domain reflectometry (TDR) [10] is currently considered as one of the most accurate method for continuous monitoring. In electrical engineering, TDR is used to determine the characteristic of the transmission line like coaxial cables and optical fibers. Through TDR, both characteristic impedance of the target transmission line can be measured. Therefore, if transmission line affected by surrounding soil moisture is connected to TDR measurement equipment, soil moisture can be estimated from the TDR result.

In TDR method, parallel circular lines are often exploited as shown on fig 1.3. As the parallel line is not closed by conductive shields, its characteristic impedance is affected by

Figure 1.3: TDR probe (Campbell Scientific CS630-L)

Figure 1.4: Capacitive soil moisture sensor (METER 5TE)

conductivity, permeability and permittivity of surrounding materials and these parameter can be estimated from measured characteristic impedance. While permeability of soil will not significantly changed during monitoring periods, permittivity is easily changed by soil moisture because relative permittivity of water (around 80) is much larger than the other soil constituents (around 1 to 12) and permittivity of the soil is highly correlated to soil moisture level [11]. Hence, real part of the characteristic impedance reflects electrical conductivity of the soil and imaginary part of the characteristic impedance is mainly decided by permittivity which is correlated with soil moisture. Note that electrical conductivity is also informative soil parameter for agriculture as it represents salinity or fertilization level. TDR method has following advantages

- Simultaneous measurements of soil moisture and electrical conductivity [12]
- Measurement is not susceptible to temperature and salinity [10]
- Sampling volume can be selected by changing the design of electrodes [13, 14]

The disadvantage of TDR method is cost of the measurement equipment e.g., $3,000 US dollars or more. As it requires quite high sampling rate to capture detailed characteristics of reflected signal, it is difficult to reduce the cost. Frequency domain reflectometry (FDR) [15] and amplitude domain reflectometry (ADR) [16] are also used for soil moisture measurement. Since they all use theories of RF transmission line, basics of the measurement are same. Both FDR and ADR could be enabled with a little lower cost than TDR; however, as far as they rely on high frequency measurements, there is limitation on cost reduction so TDR is still de-facto standard for precise measurement.

The capacitive soil moisture sensors are attractive alternatives to TDR [17–20]. As relative permittivity of soil and capacitance of sensor electrodes covered by soil is correlated, capacitive measurement is usable for soil moisture sensing [21]. Although some disadvantages like sensitivity to soil temperature [22], limitation on applicable soil [23] and small sampling volume [24] were reported, capacitive soil moisture measurement is reliable enough for practical usage. It has potential to make it low-cost so various capacitive soil moisture sensors are developed and commercialized [1, 25, 26]. For example, METER Group (Previously known as Decagon Devices) commercialized capacitive soil moisture sensors and they are known to be reasonably accurate and inexpensive solutions so the sensors are widely used in research areas [27, 28].

Cost effective solution on soil monitoring is required to enable precision farming in large scale for enhancing farming productivity and reserving sustainability of natural resource

Figure 1.5: Damaged alkaline batteries due to extreme heat

usages. It is unrealistic that installing a lot of TDR sensors in the field considering its cost and relatively low-cost capacitive soil moisture sensors are still expensive and not easy to use for farmers in terms of usability. Generally speaking, there is a trade-off between cost and accuracy. Currently available sensors intend to be used for research area so they spend much attention on accuracy rather than cost of the sensors. However, considering practical usage of soil moisture sensors in agricultural fields, cost should have higher priority because even if the sensor just capture relative differences or changes on soil moisture, it is enough useful for decision making on irrigation and optimization on crop managements. Also usability and ease of setting up are important aspect for developing practical sensors. Different from researchers, farmers need to accomplish various farming activities in their limited working time. If the labor cost for setting up and using sensor system overcomes benefit by introducing sensor system, they should not have motivation to introducing the sensor system. Therefore, setting up and maintenance process should be as simple as possible. For example, many connections of cables, frequent battery replacements, complicated processes for data analysis and difficulty on fixing troubles need to be avoided. Simple and quick usability is necessary for productive farming.

1.3.1 Challenges of Battery Driven Sensors

According to the experimental deployments of the proposed monitoring networks, several challenges were brought up on its operation. The most serious matter is battery replacements. The most of agricultural sensors including our proposed sensor are battery driven and its battery life is usually around a year. It is reasonable to be designed to work for a year because the most of the crop is harvested in a half year or less except fruits trees. Since the number of sensors is limited, battery replacement is not a serious matter; however, if a farmer introduced several hundred sensors in their farm field, and each sensor required battery replacement every year, the project would become unsustainable. Large scale farming, in particular, will not accept the cost as replacing batteries of many

sensors distributed in huge field requires unacceptable additional labor expense. In this case, automated recharging system should be desired. In large scale farming, various equipments and farming activity will be automated to expand farming productivity. UAVs are expected to play important roles in agricultural area for remote sensing and pesticide and auto driving tractors will be actively introduced. If we can leverage these automated vehicles to feeding power to sensors, the issue of battery replacement will be mitigated.

Battery driven sensor has another weakness that the working temperature range of alkaline battery is not sufficient in some cases as shown in Figure 1.5. Lithium battery could be alternative as it has more wider working temperature range but it is too expensive compared to alkaline battery. In our deployments, sensor nodes experiences from -15 °C to 47 °C while working range of alkaline battery is 5 °C to 45 °C. Also higher relative humidity accelerate self-discharging and condensation water may cause short. In short, the battery driven sensor is weak to extremely low temperature and high humidity which could happen in subarctic area and tropical area, respectively. If an energy source that can rather work better in such extreme conditions is available, it should be used as alternative of battery. Temperature differences tend to be larger in such situation. For example, temperature of half frozen soil is stuck around 0 °C while surface temperature is vibrating and daily temperature vibration tends to be larger in dry season in tropical climate.

1.3.2 Energy Harvesting and Microwave Wireless Power Transfer

With consideration to scalability issues on operations, battery-less sensors are preferable to battery-driven sensor networks. Energy harvesting is a fascinating alternative for battery-less solutions. Energy harvesting devices such as solar panels, piezoelectric devices, thermocouples, and RF energy scavengers are attracting a great deal of attention, especially in applications related to low-power Wireless Sensor Networks (WSNs) [29–31]. Ample research focusing on energy harvesting devices and their operations is being conducted [29]. Energy harvesting can dramatically extend the operating lifetime of nodes in wireless sensor networks. Furthermore, this technology enables a battery-less operation and reduces the operation cost of WSNs, which is mainly due to battery replacement, thus making it very important for a sustainable “near-perpetual” WSN operability. Thus, energy harvesting is important for the sustainable operations of a WSNs. In this study, we focus on RF energy harvesting, which can produce only a small amount of energy; however, it is more stable than solar and wind power. Almost all energy harvesting wireless networkare leveraging solar panels, wind power, and piezoelectric devices. These harvester are significantly dependent on environmental conditions, which may result to unstable sensor systems.

Thus, various energy management methods have been discussed [29,32,33] since major natural energy sources such as solar and wind power are often unpredictable. Even if such methods can mitigate the stability issues of energy harvesting, concerns still exist with regard to long-term operations; therefore, energy harvesting sensor nodes usually

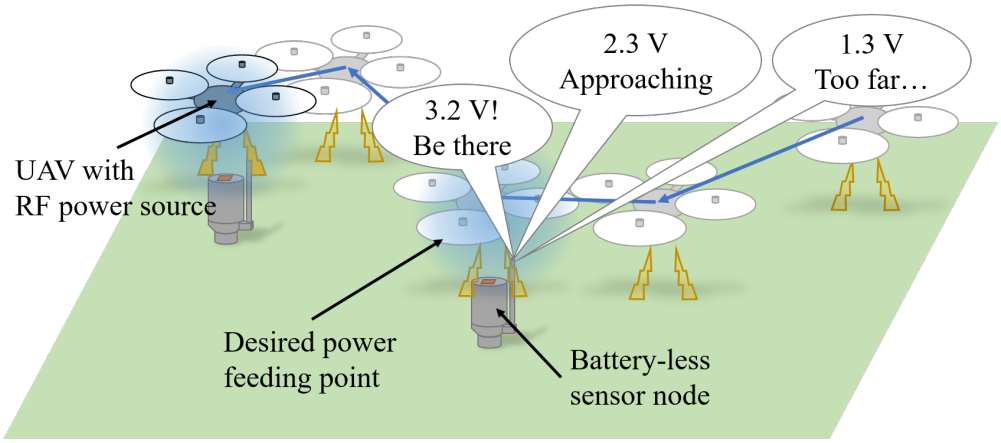

Figure 1.6: Overview of UAV-assisted microwave wireless power transfer system. The UAV tries to reach the desired power feeding point by leveraging a position estimation method using the measured transmission efficiency by the target sensor node.

have much larger harvesting and energy storage capacities than the required minimum. Preparing such spare capacity may not be allowed considering system requirements in terms of package size, weight, and cost. Ambient RF energy such as digital TV broadcast radio waves, is relatively stable so it can be used as a suitable power source in urban areas [34, 35, P1]. In farm fields, however, a strong RF signal is not observed; therefore harvesting would be limited.

The RF energy harvesting technique can also be used for microwave wireless power transfer (WPT). In microwave WPT systems, RF sources are intentionally prepared for supplying power to sensors. Using this technology, we developed the prototype of an agricultural sensor system with microwave WPT [36]. If the RF sources are movable, its coverage can virtually be expanded to a much larger area than the fixed RF source, therefore, an unmanned aerial vehicle (UAV)-assisted WPT system was proposed [37,38]. Note that the same concept is applicable for WPT using magnetic resonance [39]. In such a system, UAV has an RF source and feeds power to the sensor node through radio waves. The application of the UAV-assisted WPT system to our agricultural sensor networks was considered [P14]; Fig.1.6 shows the overview of a sensor system using UAV-assisted WPT. In that system, microwaves are distributed from the UAV, which periodically goes around the farm field. The conversion of RF energy to DC power is achieved using a rectenna, which is the combination of an antenna and rectifier. Then, the sensor node stores the DC power to an energy storage medium such as a capacitor, until it is needed for sensing. In the near future, UAVs will be commonly used in large scale farming applications for remote sensing [40], pesticide spraying, direct seeding and the collecting of sensor data. Therefore, equipping a UAV with an RF source will enable it to power the sensor concomitantly to performing the other tasks. Thus, farmers will not need to prepare UAVs solely for delivering energy.

1.4 Organization of Thesis

This thesis composed as following. The first prototype of low-cost agricultural sensor is introduced in Chapter 2. The first prototype including RF energy harvesting sensor node, ink-jet printed capacitive sensor, and adaptive duty cycle control. To expand the applicable area in large scale farming, UAV assisted microwave power transfer and navigation strategy for quick charging is introduced in Chapter 3. In Chapter 4, the detailed design of soil monitoring networks are presented. As the network composed by gateway and sensor node and each of them have 4 variations, the design and evaluation are described one by one. These developed sensor is deployed in various farm fields in Japan and India. The several of them are presented in Chapter 5. The longest experiment is continued for 2 years and relationship between soil moisture and harvest was evaluated through the deployments. Finally, the thesis is warped up in Chapter 6 by revisiting the research and discussing the future works.

Chapter 2

Inkjet Printed Soil Moisture Sensor with Microwave Wireless Power Transfer

2.1 Introduction

In this chapter, a prototype implementation of agricultural sensors using printed electronics and RF energy harvesting is presented. That is the start point of the project but it contains mostly all concepts. While we modified materials and shapes of the sensor electrodes and tentatively switched to battery driven sensor node rather than energy harvesting sensor node, our eventual goal should be identical to the first concept model. In this system, RF energy harvesting technology is exploited which is also called ambient RF scavenging when it capture energy from ambient radio wave like TV radio wave. When there are some intentional radio source for supplying power to sensor node, it will be called as microwave wireless power transfer; however, it basically use same components. Initially the sensor consider to be driven by TV broadcasting radio wave but a modified version adapted to microwave wireless power transfer is developed as well. Thus, in this chapter, firstly, the design of the ambient RF harvesting device is introduced and adaptation to microwave wireless power transfer and agricultural sensor application follow it.

As described in Chapter 1, almost all energy harvesting wireless sensor networks are relying on solar panels, wind power, and piezoelectric devices and energy management strategies are mostly optimized for them.

On another front, RF energy harvesting has specific characteristics not found in other energy sources. For instance, because we rely on "ambient" RF signals, which are originally intended for other communication and broadcast systems, the amount of harvested energy comprises both a long-term fluctuation due to radio tower service schedules and human activity patterns, and short-term variability due to fading and noise. Therefore, in this chapter we introduce a novel energy management method that is robust against both these issues. In low-power WSN systems, the sensor nodes attempt to save energy by being in "sleep" mode almost throughout the entire time and periodically switching to the active mode only when a sensing task is assigned. The ratio of the active time to total cycle time is called a duty cycle. A typical ultra low-power microcontroller operates in the following three modes: active, sleep, and off. Unlike the off-mode, the sleep mode consumes a few dozen nA; however, the microcontroller can maintain the status of the register and resume the task with a minimum time and power overhead. The adaptive duty cycle management plays an important role in balancing the energy intake and expenditure. When a sensor node is set in a duty cycle that is too high compared to harvested energy, the sensor node consumes the stored energy and finally turns off because of energy shortage. After the sensor node is off, it consumes 5 times more energy for turning into active mode compared to wake up from sleep to active. Therefore, a duty cycle control method should be designed to avoid the energy shortage risk, which we call a "dead" risk. On the other hand, a lower duty cycle is not desirable because of the leaky characteristics of energy storages. In this study, we used capacitors for energy storage because of their charge and discharge efficiency. Capacitors are better than batteries in this respect and have no limitation on the number of recharge/discharge cycles. However, capacitors yield more energy leakage than batteries, for example, the leakage

of a NiMH battery, which is the most leaky battery, is 30% per month, while the leakage of a super capacitor is 5.9% per day [41]. Therefore, we had to deal with the capacitor leakage problem as it results in a relatively large amount of energy loss in comparison to scavenged amount of energy obtained from a harvester.

The contributions of this study are summarized as follows; (1) implementation of low-cost RF energy harvesting sensor nodes using inkjet printing; (2) Introduction of the optimal stored energy level calculation by the aggregate evaluation of capacitor leakage and the energy shortage risk; (3) adaptive optimal operation point tracking, taking into account harvested energy variability; and (4) evaluation of the duty cycle control algorithm via simulation with measured TV radio wave data. By using the proposed method, we achieve a 5.34% leakage reduction compared with a method that does not involve operation point tracking. Our proposed method can reduce the capacitor leakage by the determination of the optimal capacitor stored energy. In addition, the optimal stored energy adjustment is adaptively performed with regard to both short-term and long-term transitions of the harvested energy. We can achieve an optimally efficient energy usage and a maximized sampling/sending rate applying the energy management strategies introduced in this chapter.

2.1.1 Related Work

Ambient RF energy harvesting has been discussed in several feasibility studies and prototype implementations. The target frequencies of the ambient RF energy harvesting are mainly on 500 MHz, 900 MHz, and 2.45 GHz. For example, Parks et al. successfully performed a sensor node operation using RF energy harvesting from a 500-MHz digital TV broadcasting radio wave. Their sensor node could operate at a distance of 10.4 km from broadcasting tower with a transmission power of 1 MW [35]. In addition, they implemented a sensor node powered by a cellular Base Transceiver Station (BTS) at a distance of 200m from the BTS. Dolgov et al. designed a Maximum Power Point Tracking (MPPT) mechanism for RF energy harvesting, considering the variability in the transmitted power from the BTS's [42]. They considered wireless sensors for cellular tower monitoring that can harvest energy from the side-lobe or reflected RF power and monitor the tower activities [43]. The frequency of 2.45 GHz is widely used for communications such as Wi-Fi and Bluetooth. Some of the researchers conducted a feasibility study on the RF energy harvester using a signal at the abovementioned frequency [44], and Olgun et al. developed a technique to continuously drive a temperature and humidity sensor with a LCD using Wi-Fi RF energy harvesting [45]. A compact and efficient rectenna operating at 2.45 GHz was designed by the optimization of patch antennas and a charge pump [46]. On the other hand, 2.45 GHz is commonly used for microwave wireless power transmission [47], using the technologies that are almost the same as those applicable for ambient RF energy harvesting. 5.8GHz is more suitable as a power source for compact RF energy harvester [48] it will occur less collisions with communication signal compared to 2.45 GHz. In this study, we considered a low-cost ambient RF energy harvesting sensor node using a digital TV broadcasting signal. The

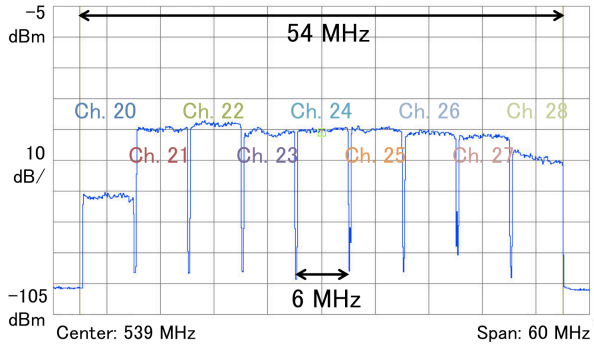

Figure 2.1: Spectrum of ISDB-T digital TV signal.

sensor node should be applicable in structural health monitoring or "rugged" environmental monitoring because these applications do not require sensing at fixed intervals; however, a battery-less and low-cost operation is desirable. As mentioned above, there have been some of studies on the design of a RF energy scavenger using a TV signal. Nishimoto and Vyas designed a RF energy scavenger that could capture the RF power of a TV signal using an inkjet-printed dipole antenna and a charge pump [49, 50]. Vyas, Kawahara and Tentzeris were the first to identify and exploit the multi-channel OFDM nature of TV signals for powering an embedded microcontroller [34]. However, several challenges faced by energy management software remain unsolved. A TV broadcasting signal wave is much more stable than wireless communication signals such as those utilized in cell phones; however, it commonly varies dynamically around midnight because of the scheduled facility maintenance as shown in Figure 2.2. To address this issue, we develop a capacitor-leakage-aware duty cycle control method for ambient RF energy harvesting. A general software management method for energy harvesting sensor node has already been developed. However, a method particularly focusing on the ambient RF energy harvesting is yet to be developed. We proposed capacitor-leakage-aware duty cycle control method that considers generic energy harvesting sensor nodes [P4]. Our method can work more effectively when energy supply from harvester has both long-term and short-term fluctuations, thus being very appropriate for RF energy harvesting.

2.2 Variability of Harvested TV Energy

There have been some previous studies of RF energy harvesting [34, 49, 50]. An RF energy harvesting system with the objective to scavenge energy from the TV broadcast radio waves, which are continuously supplied from the TV radio towers almost 24 hours per day in urban areas, has been previously designed. The digital TV broadcast in Japan is performed using the Integrated Service Digital Broadcasting-Terrestrial (ISDB-T) standard. In addition, the ISDB-T standard is used in the Philippines and South America, while the Digital Video Broadcasting-Terrestrial (DVB-T) standard is mainly used in Europe. Both ISDB-T and DVB-T have many common features, that is, both

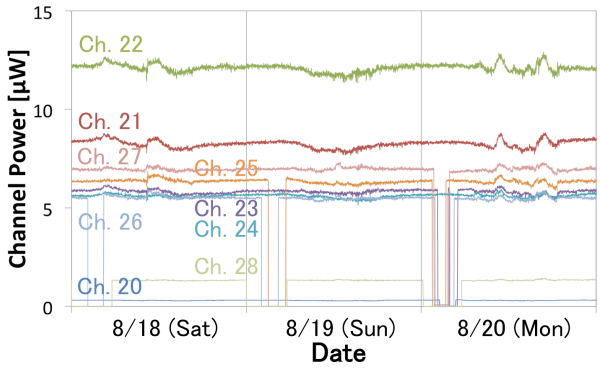

Figure 2.2: Channel power of digital TV broadcasting signal for 3 days. Some channels stop transmitting in midnight, thus accentuating channel power time- variability

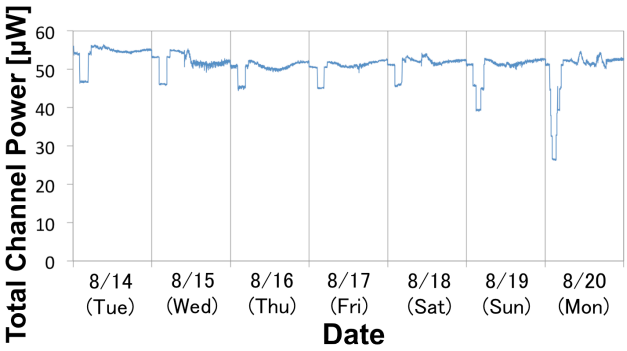

Figure 2.3: Total channel power of digital TV broadcasting signal for a week.

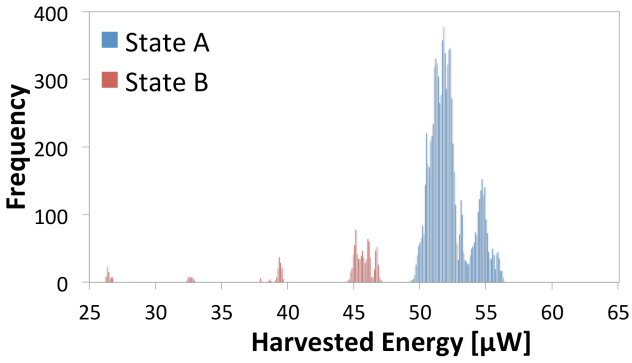

Figure 2.4: Histogram of total channel power of TV signal. Some channels are interrupted at midnight, thus total channel power state shifts to State B.

of them use OFDM modulation, and therefore, they can be considered as almost the same signal for ambient RF energy harvesting. Figure 2.1 show the spectrum of the ISDB-T broadcasting signal used in Tokyo. There are nine channels (Ch. 20 to 28) each with a bandwidth of 6 MHz at frequencies ranging 512 MHz to 566 MHz. Ch. 21 to 27

are transmitted from the Tokyo tower with 48 kW (Equivalent Radiated Power: ERP). In this spectrum, Ch. 20 and 28 are comparatively weaker than the other channels because Ch. 20 is transmitted with 5 kW (ERP) and Ch. 28 with 19 kW (ERP). In this case, we plan to continuously operate the sensor node that can measure temperature data at our building that is approximately 6.3 km away from the Tokyo tower. Using following Friis's equation, the received power at the dipole antenna at this position can be estimated as from 30 to 100 μW [34, 50].

$$P_R = P_T G_T G_R (\frac{\lambda}{4\pi R})^2 \tag{2.1}$$

An accurate estimation of the received power is quite difficult because the received power is affected by the reflection at the ground and fading; however, several dozen microwatts is required to periodically drive the sensor node. Considering these circumstances, we use digital TV signals as an energy source. Figure 2.2 shows typical average channel power data of these channels measured in 3 days. These data are measured at 1-min interval. Each channel occupies in total 6 MHz. The channel power is measured using a 5-dBi YAGI UwPA UHF antenna [51] connected to a Tektronix RSA-3308B real-time spectrum analyzer. Although the measurement setup is not the same as our sensor node setup, the objective of this measurement is to measure the relative change in the channel power, thus the absolute value of individual channel power levels does not need to be accurately measured. As can be observed from the measurement result, the total channel power level is divided into two states. This is mainly because some of the channels stop the broadcasting service at midnight for energy saving and/or maintenance purposes. It is quite difficult to predict when and which channel stops sending signal. When all the channels are broadcasting, the total amount of channel power varies because of fading and noise; however, the variation is not abrupt. We defined this "total-channel-power" state as State A. From 12 a.m. to 2:30 a.m., only Ch. 28 is stopped, but the power does not drastically change. After that, Ch. 20 and Ch. 22 are also shut down from 2:30 a.m. to 4:15 a.m., At midnight, some of channels are turned off owing to the broadcasting schedule and maintenance. Ch. 26 and Ch. 28 are stopped almost every midnight; however Ch. 22 and 21 are not stopped all the time and the remaining channels are only stopped from midnight to early morning during weekends. We define this "total-channel-power" state as State B. Figure 2.3 shows the total power from the TV radio signal consisting of 9 channels for a week including the daily fluctuation, which is given by the broadcasting schedules. However, these signals exhibit a short-term variability. Figure 2.4 shows a histogram of the channel power that represents the probability distribution function of the supplied energy required for the death risk estimation. When some of the channels are turned off and the transmitted energy decreases, the variability in the harvested energy decreases, and therefore, we should recalculate the optimal stored energy level at this transition. The current variability can be estimated from the average harvested energy, and our proposed method appropriately sets the optimal level in each state. This type of daily transition of the channel power can be observed in the communication signal transmitted from the cellular BTSs [52]. Thus, energy management methods for ambient RF energy harvesting should consider

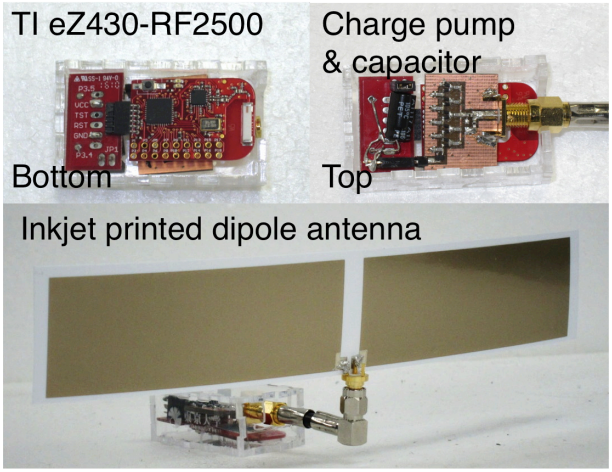

Figure 2.5: Prototype of TV radiowave energy harvesting sensor node.

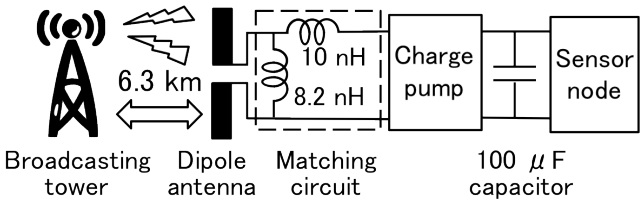

Figure 2.6: System overview of RF energy harvesting sensor node.

the signal characteristics.

2.3 Design of Sensor Node

To evaluate the performance of our novel energy management approach, we design a prototype of an ambient RF energy harvesting sensor node, as shown in Figure 2.5, using the scavenged energy from the digital TV broadcasting signals. As shown in Figure 2.6, this sensor comprises of the following four modules: (1) inkjet-printed dipole antenna, (2) 5-step modified Dickson charge pump with matching circuit, (3) 100-μF capacitor and (4) a Texas Instruments eZ430 RF-2500 sensor node with temperature sensor [53]. In this section, we discuss the design of these components. Note that the combination of an antenna and a rectifier including charge pump is called "rectenna" and it works as a converter of the RF ambient signal to DC power.

2.3.1 Ink-jet-Printed Dipole Antenna

We use the inkjet printing technology with a conductive silver nano ink manufactured by Mitsubishi Paper Mills Limited [54], to fabricate an antenna at a low cost. In this process, specific ink-jet printer and paper are not required and commercial printer [55] and polyethylene coated photo paper [56] are enough. The ink-jet printer is 165 US

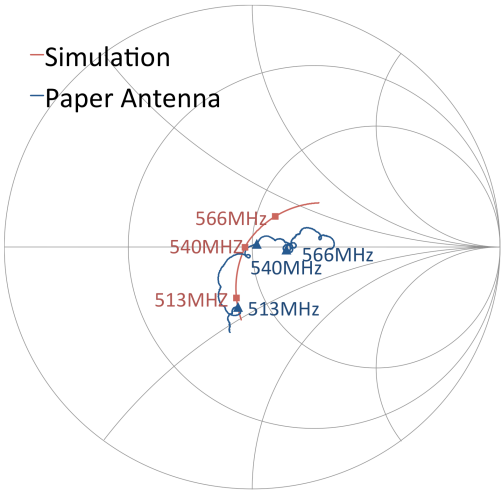

Figure 2.7: S11 parameter of inkjet-printed dipole antenna on Smith chart.

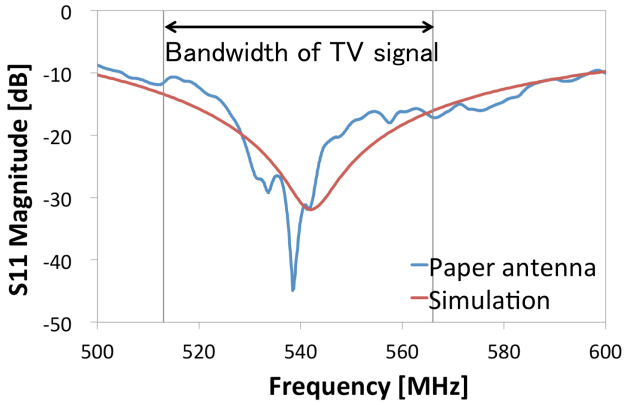

Figure 2.8: S11 parameter of inkjet-printed dipole antenna, with magnitudes in dB.

dollars so initial cost is quite low. The photo paper is 55 cents and silver ink required for printing patterns on an A4 paper is around 60 cents and four dipole antennas can be printed on each A4 paper. It means that cost for a printed dipole antenna is only around one third dollar. If we use FR-4 substrate, about dozen dollars are needed for each antenna at least. Moreover, the silver ink does not require heating to get conductivity and quickly get high conductivity. After the printed-paper is laminated, its durability is improved and it can be applicable for not only indoor usage but also outdoor usage. The antennas for ambient RF energy harvesting from TV radio wave should have a wide bandwidth to cover spectrum of 54 MHz around the central frequency in order to capture energy from 9 ISDB-T channels that can be observed in Tokyo area. By increasing the width of the element, it is possible to expand the bandwidth of the dipole antenna. We conducted a simulation of the antenna design using Sonnet to determine the optimal width of the antenna elements. In this simulation, we used a 0.35-mm thick PET-film photo paper model, with a relative permittivity of 3.0 and a loss tangent of 2.1%, and

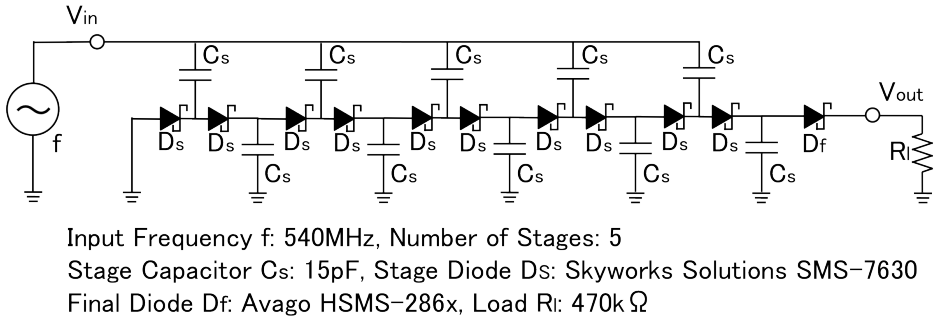

Figure 2.9: Schematics of a 5-stage modified Dickson charge pump.

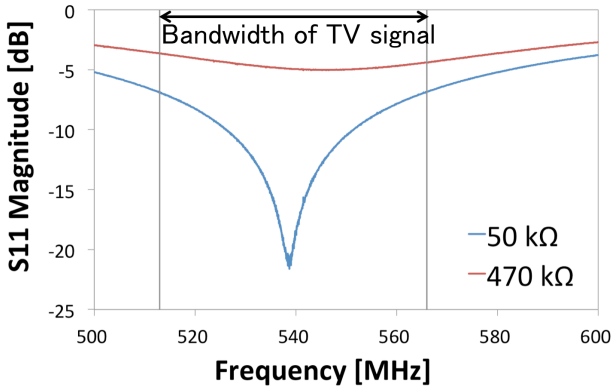

Figure 2.10: S11 values for the charge pump in dB.

1-μm thick conductive pattern model. Finally, we achieve the optimal elements size of 104 mm x 36 mm. The thickness of the ink is only 1 micrometers and the conductivity of the silver ink is 7.7 MS/m which is less than metal so the resistance of the elements are higher. However, if the element width is wider its current is distributed and resistance is lower. The wider pattern contributed to reduction in the antenna resistance. Figure 2.7 and 2.8 show the value of the return loss S11 of the printed antenna with good agreement between the simulations and the measurements. The simulated antenna gain value was 1.33 dBi. Unlike the simulation result, the printed antenna has multiple resonant frequencies because printed conductive pattern is composed by nano scale particles of silver but evaluated as homogeneous metal on the simulation. It is still difficult to simulate such ink-jet printed pattern on electromagnetic simulator. Although there are some errors, the simulated S11 parameter is roughly fit to the actual S11 at the working bandwidth.

2.3.2 5-Stages Modified Dickson Charge Pump

A modified Dickson charge pump is often used as a RF/DC converter for the RF energy harvester because it converts RF power to DC and works as a voltage multiplier [57]. On the other hand, some RF energy scavenging systems use a half-wave rectifier or

a voltage doubler rectifier, connected to an ultra low-power charge pump IC such as S882-Z manufactured by Seiko Instruments [58]. When the distance from the TV tower is far and the received power is not enough high (lower than -10 dBm approximately), the combination of a rectifier and a charge pump IC works better than the Dickson charge pump. However, if the signal is strong enough, the Dickson charge pump can efficiently supply higher amounts of energy [35]. In our scenario, although the sensor node is placed several kilometers far from the TV tower, the received power is sufficient to enable the Dickson charge pump to operate efficiently and supply the sufficient voltage. Although some of the suppliers have begun to develop ultra low-power charge pump ICs, only a few types of the product are available on the market and they have not been commonly used yet. Considering the mass production of low-cost sensors, the Dickson charge pump is more suitable because it is composed of easily available capacitors and Schottky diodes, that are commonly used for signal detection applications. Obviously, whenever ultralow-power charge pump ICs become common and inexpensive, we should reconsider the design of a RF/DC converter. SMS-7630 [59] manufactured by Skyworks Solutions is often chosen for low-power charge pump circuits owing to its lower threshold voltage [60]. Figure 2.6 shows our charge pump schematics. We use SMS-7630 for the charge pump except for the final diode that blocks the reverse current from the energy storage due to the very low value of its reverse resistance [59]. Avago HSMS-286C [61] exhibits a higher resistance and is more suitable to use as the final diode instead. If we increase the number of stages in the charge pump, a higher voltage is generated; however the total efficiency decreases, thus making it necessary to choose the minimum number of stages that supplies sufficient voltage to activate the sensor node. In our case, the received power is estimated as several dozens to a hundred microwatts as reported by Nishimoto and Vyas in [49] and [34]. With a 100-μW input power, a 3-stage charge pump generates 1.8 V, a 4-stage charge pump generates 2.2 V, and a 5-stage charge pump generates 2.7 V on a circuit simulation. Typical sensor nodes turn-on voltages range between 1.8 V - 3.6 V, thus requiring at least four-stage charge pumps. For the sake of safety, considering an input power fluctuation, a 5-stage charge pump is suitable for our study. The input resistance of the charge pump was measured using a Rohde & Schwarz ZVL-3 vector network analyzer with -10 dBm input signal. The resistance in the TV signal bandwidth (from 513 MHz to 566 MHz), without connecting a matching circuit, show losses of between 5.88 and 7.58 Ω and capacitive reactance between 34.9 and 41.1 Ω for a 470 kΩ load. In addition, it shows losses of between 8.09 and 10.13 Ω and capacitive reactance between 33.6 and 40.0 Ω for a 50 kΩ load respectively. Note that we utilized 470 kΩ load to simulate the sensor node in sleep-mode, while a load of 50 kΩ maximizes the charge pump performance because output resistance of the charge pump is several dozen kΩ and it matches to a 50 kΩ load. In actual sensor nodes, the charge pump is connected to the storage capacitor and the load impedance is lower than 470 kΩ due to the shunt impedance of the storage capacitor. As we can see, the original impedance of the charge pump is not matched to 50 Ω. Therefore, it is necessary to insert a matching circuit as shown in Figure 2.6. which consists of 8.2 nH and 10 nH high-frequency inductors welded on the surface of the charge pump circuit board,

enabling a sufficient matching in the TV signal bandwidth as shown in Figure 2.10. In this bandwidth, the S11 values are lower than -6.85 dB when a 50 kΩ load is connected and is lower than -3.64 dB when a 470 kΩ load is connected.

2.3.3 Energy Storage and Sensor Node

The rectified energy is stored in the energy storage, that is, the capacitor in our system. The sensor node wakes up from the sleep mode and senses and transmits the data to the access point. The energy consumption during the process W_C is approcimately 200 μJ for a sensing task including wake-up and sensing operation, and it only consumes several microwatts in the sleep mode. After the sensor node completes the sensing operation, the capacitor voltage must be maintained over V_{min} of 1.8 V. Otherwise, the sensor node turns off because of energy shortage and the sensor node requires 1.03 mJ for initialization, which is five times greater than the power required for a sensing action. Sufficient voltage is necessary to prevent the sensor node in reverting to the "off" mode. The required condition for the capacitor voltage V_C before a sensing task begins is represented as $\frac{C}{2}(V_C^2 - V_{min}^2) \geq W_C$, with capacitance C. As a result, the requirement for capacitor voltage V_C is

$$V_C \geq \sqrt{\frac{2W_C}{C} + V_{min}^2} \tag{2.2}$$

It means that V_C can maintain a value over V_min after the sensing operation is finished, if the V_C is larger than the threshold voltage before the sensing. For example, when a 47-μF capacitor is selected, V_C should be greater than 3.5 V. When we use a 100-μF, V_C should be greater than 2.7V, and when a 200-μF is used, V_C should be greater than 2.3V. Considering a charge pump output voltage close to 3V upon simulation, it is difficult to increase this voltage above 3.5 V. Thus, a capacitance with a value larger than 100 μF is required as also verified by Nishimoto and Vyas [34,49]. In addition, a larger capacitance contributes to the suppression of the voltage ripple. The DC leakage of the capacitor is denoted as kCV_C (k is a constant of leakage). A very large capacitance value yields a greater leakage loss. As described on Section 2.2, although the total channel power level dynamically changes when the total channel power state shifts from State A to State B or from State B to State A, the fluctuation range of the harvested energy stay within a dozen μW except such state changes. It allows the sensor to operate with a low energy buffer. Considering these aspects, we select the capacity of energy storage as 100 μF.

2.4 Evaluation of Sensor Node

Without loss of generality and for proof of concept verification purposes, we implement a sensor node including an antenna and a charge pump, the design which is discussed in Section 2.3, and evaluate its performance. First, we measured the RF/DC conversion efficiency of our charge pump and connected the charge pump to a vector signal generator that generates a multi-carrier signal in order to simulate the ISDB-T and confirm

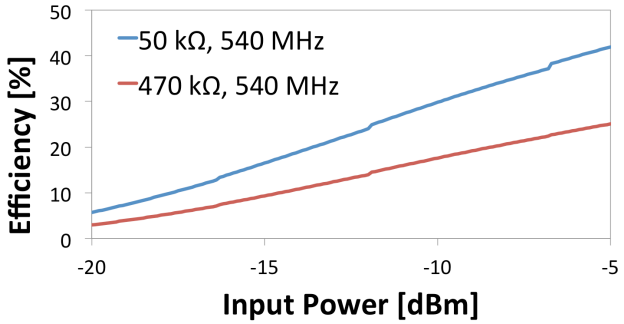

Figure 2.11: Performance of charge pump: RF/DC conversion efficiency.

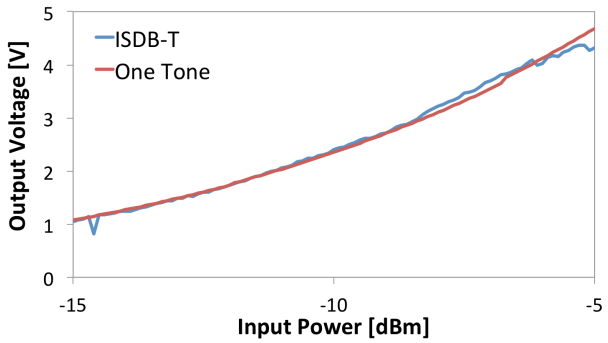

Figure 2.12: Performance of charge pump: single-tone vs. ISDB-T TV signal.

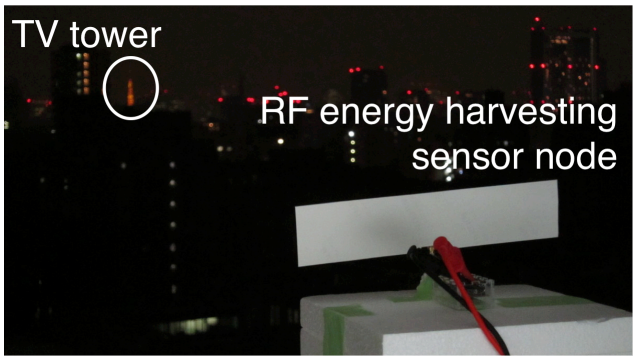

Figure 2.13: Experiment with RF energy harvesting sensor node.

the performance of the charge pump when the input signal is not a single-tone signal. Further, we evaluated the activation/performance of the sensor in realistic deployment conditions, that is, on 11th floor of our building that is 6.3 km far away the Tokyo tower.

2.4.1 Performance of Charge Pump

We connected the charge pump to a signal generator, supplying a 540 MHz single-tone signal whose power values swept from -20 dBm to -5 dBm in order to measure

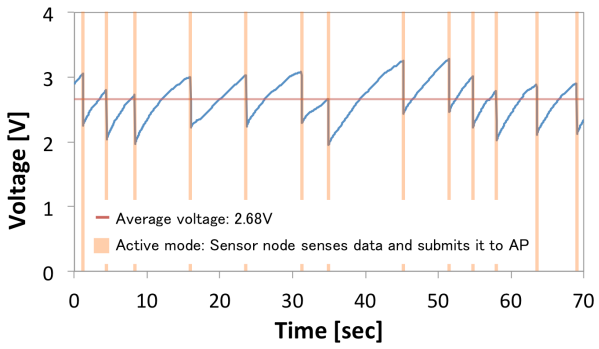

Figure 2.14: Capacitor voltage when sensor node periodically wakes up.

the RF/DC conversion efficiency. RF/DC conversion efficiency η which is given by the following formula.

$$\eta = \frac{P_{DC}}{P_{RF}} \tag{2.3}$$

Note that P_{DC} is the output DC power that is supplied to the load and P_{RF} is the input RF power. Figure 2.11 shows the efficiency values for our benchmarking sensor configuration. When the input level is -10 dBm, the efficiency is 10.0% with 470 kΩ load and 30.0% with 50 kΩ. In this measurement, we utilize a single-tone signal instead of a ISDB-T signal to simplify the testing environment while the input level is estimated to be around -10 dBm using aforementioned Equation 2.1 [34]. Thus, the measurement result would be slightly different from the actual performance of charge pump because of the effects of multi-career signal. As described in Section 2.2, the Japanese digital TV broadcasting uses the ISDB-T standard and OFDM modulation. Thirteen segments are used to construct a channel of ISDB-T signal. One segment is allocated for mobile TV broadcast and the remaining twelve segments are for high-definition TV broadcast. The bandwidth of each segment is 429kHz, and a 430-kHz guard band is additionally used, thereby the total bandwidth of a channel is 6MHz. A segment can be divided to 432 carriers that are QAM -modulated. Thus, the total number of carriers for a ISDB-T channel is 5617. The ISDB-T signal was simulated by using a Rohde & Schwarz SMBV100A vector signal generator with an arbitrary-waveform baseband signal generator. A unique characteristic of the signal is that its peak envelope power is higher than the average power. This peak can be observed only for a short period, and therefore, the typical sampling rate of the spectrum analyzer is not sufficient to observe the peak; however, it affects the charge pump performance. Figure 2.12 shows the comparison between the case where the input signal of the charge pump is a single-tone signal (540 MHz) and the case where it is a simulated ISDB-T signal. With the simulated signal, the charge pump performance is better than that obtained with a single-tone signal. When a chaotic spectrum signal is inputted into the rectifier, its output DC voltage and RF-to-DC conversion efficiency are improved [62], an effect that explains the performance improvement when an ISDB-T signal is inserted as verified by Vyas, Kawahara and Tentzeris [34].

2.4.2 Performance in Actual Situation

We placed the sensor node on the balcony of our building from where we could observe the Tokyo tower line of sight (Figure 2.13). We measure the output voltage of the rectenna and confirm the operation of the sensor node. As described in Section 2.2, the channel power tends to be unstable at daytime and stable at nighttime. This is mainly caused by the different types of fading including k-type fading and duct-type fading due to refractive-index change owing to air temperature change at daytime [63]. We performed the measurement from 11 p.m. to 12 p.m. in order to eliminate the effect of fading. First, we monitored the output voltage when the capacitor is not connected to the sensor node. The capacitor voltage is saturated at approximately 3.8 V; however the output voltage estimated from charging process of the storage capacitor is slightly different. The transition shows that the charge pump operates as 4.1 V equivalent DC voltage source with an output impedance of 100 kΩ. The characteristic of the equivalent DC source (e.g. output voltage) strongly depends on the supplied power. However, the equivalent power source is valuable for the design of a DC circuit including a microcontroller.

2.4.3 Performance of Sensor Node

Figure 2.14 shows the capacitor voltage when the rectenna, which is placed in the same setup of the previous experiment, is connected to the sensor node, which periodically wakes up and senses the temperature and transmits the sensed data to the access point. The wake-up timing of the sensor node is determined by using the simple duty cycle control method to get robustness of the energy harvester to short-term variability. The duty cycle control method sets the duty cycle to minimize the objective function $f(B_t) = (B^* - B_t)^2$. In this formula, B_t denotes the current stored energy level and B^* denotes the desired stored energy level. The stored energy level is calculated as $\frac{V_C^2}{V_{max}^2}$ using the current capacitor voltage V_C and maximum voltage V_{max}. The duty cycle u_{t+1} is set as $u_{t+1} = u_t - a(B^* - B_t)$ (a is a constant used for adjustment sensitivity). In this case, we set the desired voltage to 2.8 V, which implies that $B^* = 0.6$ when V_{max} is 3.6 V, which is a limitation of the DC supply level for the sensor node. We calculated the average voltage during the 70 seconds that are enough long to observe the periodical sensing operation and enough short to avoid effects of TV channel fluctuations. As a result, the average voltage is 2.68V, which is slightly lower than the desired level because the sensor node can sense the capacitor voltage only in the "active" (ON) mode. The duty cycle control method obtains only two parameters: current voltage and current duty cycle. It does not consider the level of the harvested energy, thus it is too sensitive to the harvested energy variability. To make matters worse, the voltage is not convergent under the naive duty cycle control and swinging over the desired voltage, similar to the one shown in Figure 2.14. Sometimes such unstable control sets the duty cycle too high and the sensor node consumes the stored energy too quickly, consequently switching to the off-mode and requiring significant energy to restart from

off-mode to active-mode, thereby reducing drastically its energy efficiency. This duty cycle determination approach is far from optimal control necessitating the development of the much more effective approach introduced in this paper. Although Nishimoto and Vyas have proposed numerous duty cycle determination methods [34, 49], they have not focused on the variability of harvested energy in midnight and leakage characteristics of an energy storage. Our proposed method is focusing on these two factors that commonly prevent the efficient operation of ambient RF energy harvesting sensor node.

2.5 Adaptive Duty Cycling for Robust Operation

Most microprocessors used for WSNs can reduce the current consumption by entering the sleep state. The transition time between the active mode and the sleep mode is rather short. The energy management software for WSNs is typically realized by using the abovementioned feature, and the objective of the energy management is to determine the duty cycle, that is, the ratio of the duration of the active state to the total period of a repetitive cycle. Kansal et al. introduced the energy neutral operation (ENO) concept [32]. In ENO, the duty cycle is always determined to maintain the condition that the consumed energy is always less than the harvested energy. The ENO concept achieves $B_t > B_0$ for $\forall t > 0$, with an initial stored energy level of B_0 and a current stored energy level of B_t. ENO is required for system sustainability. By extending the ENO concept, Vigorito et al. proposed ENO-MAX [33]. The objective of this operation is to sustain the condition of $B_t = B_0$ for $\forall t > 0$ because if the harvested energy overshoots the energy consumption, the system does not efficiently use the available energy. Therefore, these researchers defined an objective function as the average of $(B_t - B_0)^2$ for $\forall t > 0$ and applied a control method for minimizing it by using the linear quadratic (LQ) tracking control [64]. In short, this control method enables the system to sustain stored energy level B_t as B_0 even if the energy supply is unstable. Thus, B_0 is a significantly important parameter of this control method and is considered as the optimal stored energy level.

In the LQ tracking control system, the system operation point is represented by the stored energy level. For an efficient operation, the operation point should track the optimal point, that is, the operation should be performed at the optimal stored energy level. In this study, we propose a calculation method for the optimal stored energy level and a tracking method to enable the operation point to keep the optimal point. By applying the LQ tracking control to the energy harvesting systems, along with the adaptive duty cycle control, an efficient energy management under unstable harvested energy supplies is achieved. However, this method does not obtain the optimal stored energy level. If the energy storage device is a battery, energy loss from energy storage does not depend on its stored energy level, thus the optimal stored energy level is not crucial for energy efficiency. Therefore, Vigorito et al. have heuristically determined the optimal stored energy level [33]. However, when the energy storage device is a capacitor, the energy loss caused by the leakage is related with its stored level. In this case, the optimal stored energy level determination method is required for energy

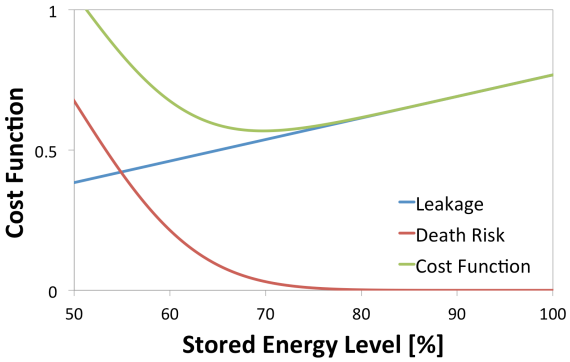

Figure 2.15: Aggregate cost function to calculate optimal stored energy level.

efficient operations. The objective of our previous study was to calculate and track the operation point; however, it still contained a heuristic parameter [P4].

2.5.1 Leakage Aware Optimal Operation Point Calculation

In this section, we demonstrate the optimal stored energy level calculation, considering both capacitor leakage and energy shortage risk. The parameters of this method depend on the specific sensor node designs, such as the characteristics of the energy storage configurations and harvested energy fluctuation patterns that can be estimated by measurements. First, we discuss the capacitor leakage. The capacitor leakage current can be calculated as to be $kCV_C(k \sim 0.01)$ with capacitor voltage V_C and capacitance C. The constant value of k is dependent on the type of capacitor and 0.01 is typical value for chemical capacitor. The capacitor leakage energy is denoted as $P_l = kCV_C^2$. Further, the leakage power is proportional to stored energy level B_t, which is $\frac{V_C^2}{V_{max}^2}$(V_{max} is the maximum capacitor voltage) and is expressed as $P_l = kCV_{max}^2 B_t$. Finally, in T seconds, the normalized leakage energy is given by

$$f_{leak}(B_t) = W_l = k_l B_t T (k_l = kCV_{max}^2) \tag{2.4}$$

Note that all the energy values, in this section, are normalized by the maximum stored energy in the capacitor $\frac{1}{2}CV_{max}^2$. Second, we attempt to evaluate the energy shortage risk and the loss when the sensor node is dead and forced to restart. Although a microprocessor consumes only several microamperes while in the sleep state, its input voltage is almost always greater than a specific value of 1.8 V. When the input voltage decreases below the specific value, the microprocessor is forced to enter the off state. Thus, we define the minimum stored energy level for the sensor node operation as B_{min}. The energy for restarting the sensor node is denoted as W_r, the harvested energy is denoted as W_h and the energy used for sensing is denoted as W_c in T seconds. Under this condition, stored energy B_t after T seconds is $B_{t+T} = B_t + W_h - W_c - W_l$. The condition of $B_{t+T} > B_{min}$ is required to continue the sensor node operation. Thus, when $W_h \leq W_c + W_l - (B_t - B_{min})$, the sensor node becomes dead node, the probability of

which is expressed with the following probability distribution function:

$$P_{dead}(B_t) = \int_0^{W_c+W_l-(B_t-B_{min})} p(W_h)dW_h \tag{2.5}$$

By applying the LQ tracking, the relationship between the stored level in next wake-up time and the system parameters including the duty cycle, previous stored energy level, and the optimal stored energy level, is estimated and adjusted to the current system condition including the amount of harvested energy. With the appropriately estimated relationship of these parameters, $W_c + W_l$ is controlled to be close to the average of the harvested energy $E[W_h]$. Therefore, this probability can be approximated by

$$P_{dead}(B_t) = P(E[W_h] - (B_t - B_{min})) \tag{2.6}$$

using the cumulative distribution function (CDF) $P(W_h)$ of the harvested energy. This implies that the variability in the harvested energy is a significant parameter for eliminating the risk of the sensor to become a dead node. The CDF can be estimated from the harvested energy data like the TV channel power histogram (Figure 2.4). According to the histogram, the TV channel power fluctuation can be simulated by the normal distribution. Note that the standard deviation represents the level fluctuation of the harvested energy when the CDF is based on the normal distribution. Finally, the energy loss during the sensor node restart due to energy shortage is expressed as

$$f_{dead}(B_t) = P_{dead}(B_t)W_r \tag{2.7}$$

We determine the aggregate of the losses by summing the above two terms and define the sum as a cost function $f(B_t)$.

$$f(B_t) = f_{leak}(B_t) + f_{dead}(B_t) \tag{2.8}$$

The aggregated cost function is shown in Figure 2.15. A stored energy level that minimizes the cost function is the optimal level.

2.5.2 Linear Quadratic Tracking

An optimal control method is applied to the LQ tracking problem. In this case, we consider a linear dynamical system with colored noise. This system is expressed by the formula

$$B_{t+1} = aB_t + bu_t + cw_t + w_{t+1} \tag{2.9}$$

where B_t is the current stored energy level; u_t is the duty cycle; w_t is the noise; and a, b, and c are the real-valued coefficients. When B^* represents the desired stored energy level, the duty cycles should be set to a value obtained as

$$u_t = \frac{B^* - (a+c)B_t + cB^*}{b} \tag{2.10}$$

for the optimal power control and it does not depend on w_t, but does depend on coefficient c of previous noise terms [33]. In typical situations, a, b, and c are initially

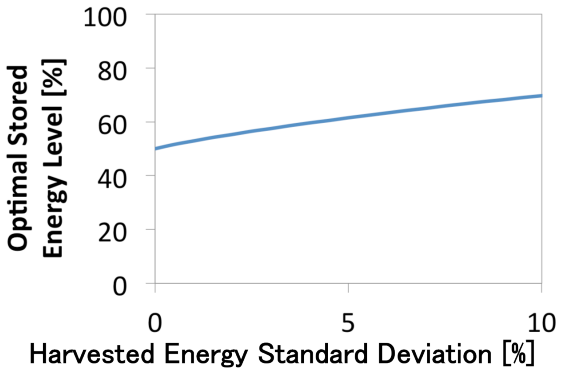

Figure 2.16: Relationship between the harvested energy variation and the optimal stored energy level.

unknown and can be estimated using a stochastic gradient descent method, with which we determine the duty cycle u_t. Further, we define a parameter vector $\theta = (a + c, b, c)^T$ and a feature vector $\phi_t = (B_t, u_t, -B^*)^T$. The estimated vector $\hat{\theta}_{t+1}$ is expressed as

$$\hat{\theta}_{t+1} = \hat{\theta}_t + \frac{\mu}{r_t}\phi_t(B_{t+1} - \phi_t^T\hat{\phi}_t) \tag{2.11}$$

Where μ is the a step size and $r_t = \sum_{k=1}^{t} \phi_k^T\phi_k$. Using $\hat{\theta}_{t+1}$, u_{t+1} can be calculated by the aforementioned formula. The step size does not significantly affect to the performance so it should be set to reasonable value as Vigorito et al. reported in [33]. The duty cycle update interval should be short enough to adapt to the harvested energy fluctuations. In our case, the duty cycle should be updated every few minutes to get robustness to TV signal fluctuations.

2.5.3 Optimal Level Adaptation with State Awareness

As mentioned above, the aggregated cost function depends on the level fluctuation of the harvest energy. Thus, when the state of energy supply changes and the level of harvested energy fluctuates, the optimal stored energy level should be recalculated. However, a simple LQ tracking uses the static optimal stored level and therefore, sometimes, leads to inefficient condition of system in some states. Taking the lack of state awareness under consideration, we propose an optimal level adaptation method considering the possible level fluctuation of harvested energy, using standard deviations. We calculate the aggregated cost function and find the minimum point of the cost function for each standard deviation, acquiring a relationship between the standard deviations of harvested energy and the optimal level as shown in Figure 2.16. In this example, when the fluctuation of harvested energy is sufficiently small, the optimal stored energy level is around 50% that means the sensor node should keep storing 50 % energy of the maximum energy capacity in an energy storage device that is restricted by the maximum operating voltage of a sensor node. On the other hand, when the harvested energy fluctuation is large (above 10%), the optimal stored energy level is around 70 % that means sensor node should keep storing more energy in order to avoid the energy

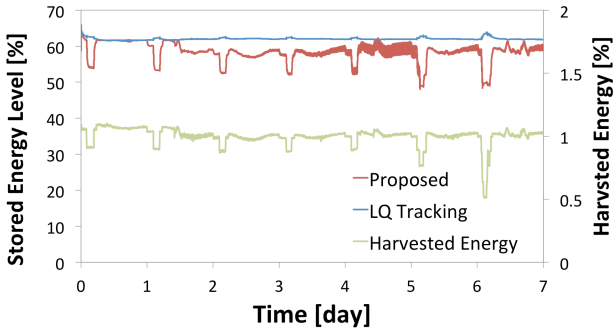

Figure 2.17: Simulation result: stored energy level for a week.

shortage that occurs accidentally caused by the large variabilities of harvester energy. We need to appropriately select an optimal level, considering the harvested energy level fluctuation and aforementioned relations. Furthermore, we attempt to maintain the sensor node operation at the optimal point by the LQ tracking. This proposed method can adjust the optimal level of each state estimated by the level of the harvested energy. When the harvested energy decreases over 10 %, the system considers this event as a state transition and modifies its optimal stored energy level profile. This scheme enables the stored energy level to be set to the optimal level always. As well, the optimal level adaption achieves a significant capacitor leakage reduction.

2.6 Evaluation of Duty Cycle Control

We evaluated the RF energy harvesting system by both actual measurement and simulations. First we confirmed the system 's operations in a realistic deployment situation. Our laboratory is on the eleventh floor of a building that is 6.3 km away from the TV tower. We can see this tower line of sight, and the rectenna can charge up to 2.82V at the location, which is enough to drive the sensor node. In this case, our sensor node could sense data and could transmit it around once per minute. We determine the adaptive duty cycle control with the energy supply state awareness. When the harvested energy decreases, the system considers this event as a state transition and modifies its optimal stored energy level profile. This control enables the stored energy level to always be guided to the current optimal level. We evaluate the operation performance by simulation using the measured TV channel power data in comparison to the LQ tracking without state awareness. The duty cycle is adaptively selected by using the LQ tracking method such that it sustains the optimal stored energy level. By observing the stored energy level as shown in Figure 2.17, we can observe that the level was adjusted to be optimal level. The capacitor leakage is proportional to the stored energy level. Thus, the sensor node operation at lower energy level is desirable for leakage reduction. However, the sensor node operation at a very low energy level can cause an energy shortage and consume a large amount of energy to restart the operation. This implies that balancing is quite important for efficient and stable operations. As demonstrated by the simula-

Table 2.1: Simulation result: total amount of energy used in simulation.

Method	LQ Tracking	Proposed
Sensing	73.2%	74.6%
Leakage	26.8%	25.4%

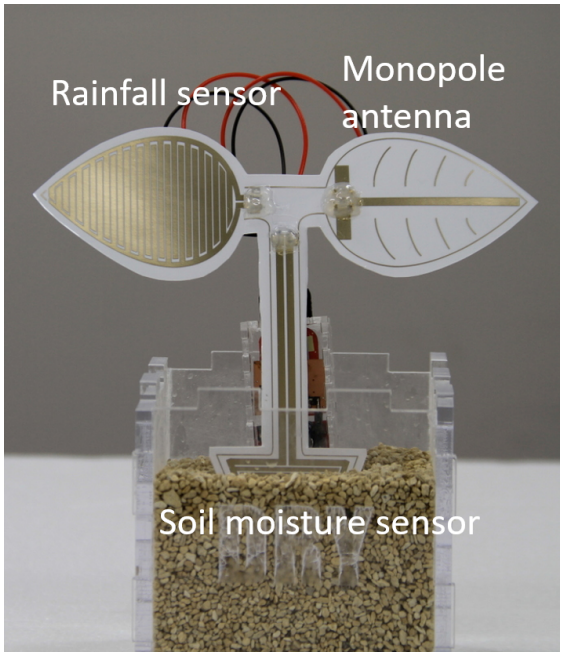

Figure 2.18: Overview of the low-cost agricultural sensor

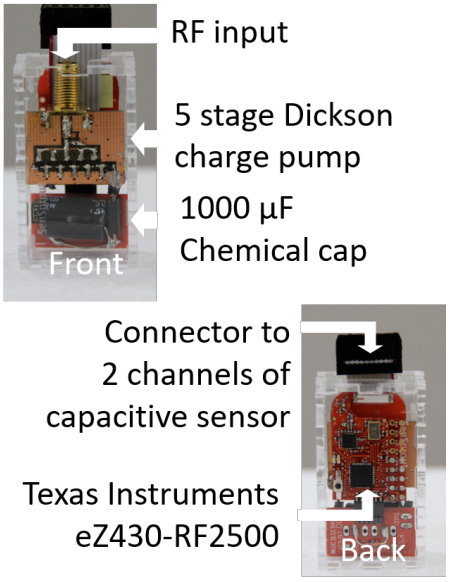

Figure 2.19: Components of the low-cost agricultural sensor

tion results, the proposed method achieves an appropriate balance that can reduce the capacitor leakage without affecting the sustainable operation. We performed the control simulation for a week to evaluate the long-term operation efficiency. As summarized in Table 2.1, the simple LQ tracking uses 73.2% of the supplied energy for sensing operations and loses 26.8% of the energy through leakage. By contrast, the proposed method uses 74.6% of its energy for sensing and loses 25.4% through leakage. This implies that the proposed method achieves a 5.34% leakage reduction. The state awareness enables the system to efficiently use the energy for sensing, thereby reducing the leakage loss. As a result, this method achieves an improvement in the sensing reliability and accuracy by maximizing the sampling rate of the sensing operation.

2.7 Prototype of Battery-Less Soil Moisture Sensor

The ambient RF energy harvesting sensor device and its adaptive duty cycle control strategy are generally usable for any sensing application but its advantages that low-cost and battery-less should be suitable for agricultural sensing area. Thus, we connected the sensor node to capacitive soil moisture sensor and leaf wetness sensor whose sensor

patterns are printed with a receiving antenna by ink-jet printing. As antennas and sensors can be printed at once, fabrication cost for the sensor will be reduced. In addition to that, the frequency for RF energy harvesting is switched from 500 MHz to 920 MHz to enable microwave wireless power transfer in ISM band which is allowed for RFID. TV broadcasting radio wave is suitable energy source for RF energy harvesting in urban area; however, in farm field, strong broadcasting and communication signals may not be expected. Even if ambient RF signal is not available, it is possible to set up RF power source near target farm field because farmers usually have electrical energy supply to pump ground water. In addition to that, some green houses have electrical power supply for automatic environmental controls. However, it doesn't mean power supply is available anywhere in the farm field. It is available only near electrical pumps or automatic control dashboards so setting up RF energy source near power source and transferring energy to sensor nodes using RF energy harvesting techniques can be reasonable solution.

Figure 2.18 shows the overview of the agricultural sensor prototype. This sensor node has 2 inter-digital capacitors (IDCs) which work as leaf wetness sensor and a soil moisture sensor. These sensors are printed on a photo paper by a commercially available ink-jet printer and laminated to be water proof. The IDC placed on the "root" works as soil moisture sensor and the IDC placed on the "leaf" works as leaf wetness and rainfall sensor. Also it has a printed monopole antenna which can receive 920 MHz. Received RF signal is converted to DC, the sensor can work without having batteries. As shown on Figure 2.19, components for the prototype is mostly identical to the aforementioned ambient RF energy harvesting sensor node. Note that 5 stage modified Dickson charge pump is used for rectifier and voltage multiplier, 1000 μF chemical capacitor exploited is for energy storage and Sensor node is a Texus Instruments Texas Instruments eZ430-RF2500 [53] is leveraged as sensor node. Except these components, antenna and sensors are disposable since they are just printed pattern on photo paper. In agricultural sensing area, sensors are exposed to large temperature changes, solar radiation and attacks by animals so it is quite difficult and costly to acquire durability for long term operation. As a result, super low-cost, easily exchangeable and disposable solution should be preferred.

2.7.1 Microwave Wireless Power Transfer Component Designs

To change the target frequency, the antenna and charge pump need to be redesigned. Considering the suitable packaging, receiving antenna is changed to monopole antenna from dipole antenna. While the basic design of the charge pump is same as the ambient RF harvester, stage capacitors and diodes are revisited.

Even if dipole antenna should work well on this application , in this sensor design, one of the leaf part is occupied for the rainfall sensor and there is no sufficient space to place 2 antenna elements; therefore, monopole antenna is chosen instead. It is a bit difficult to simulate antennas fabricated by ink-jet printing on electro magnetic simulators so after confirming the basic design on the simulator, final design need to be determined by

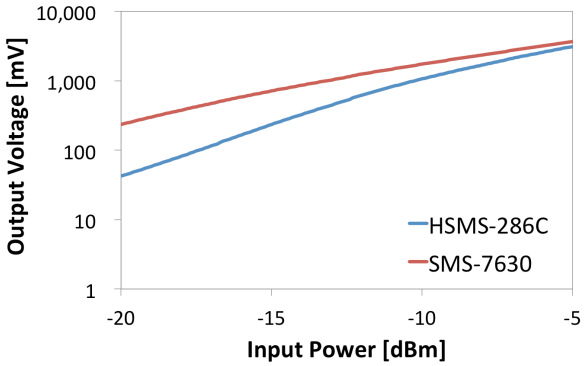

Figure 2.20: IN/OUT characteristic of the charge pump

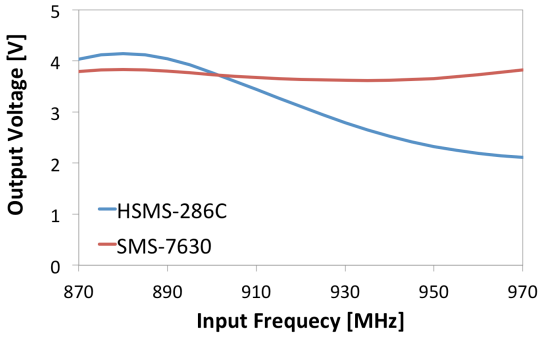

Figure 2.21: Frequency characteristic (Input: - 5dBm)

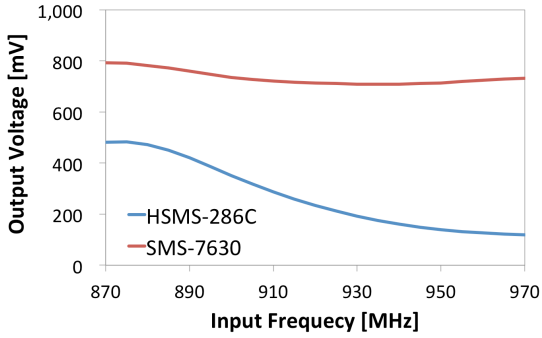

Figure 2.22: Frequency characteristic (Input: - 15dBm)

trials and errors. However, ink-jet printing accelerate the iterations of the prototyping and suitable element length, 56 mm, is quickly figured out.

The charge pump exploited for the sensor node is mostly identical to the charge pump mentioned in section 2.3.2. Through a circuit simulation, stage capacitors are set as 12 pF. Since input power would be stronger than ambient RF harvester, Avago HSMS-286C diode can be usable as well as SMS 7630 so comparison between HSMS-286C and SMS 7630 was conducted.

Firstly, Figure 2.20 shows the output performance of these 2 charge pumps where input power was swept from - 20 dBm to -5 dBm in 920 MHz. Note that a 470kΩ load was connected to charge pump output. Generally, SMS-7630 outperform HSMS-286C but its advantage was not very significant when the input power was sufficiently large. The appealing point of the SMS-7630 is its quite low threshold voltage which is from 135 to 240 mV for 1.0 mA. Meanwhile, the threshold voltage of HSMS-286C is from 250 to 350 mV which is 100 mV higher than SMS-7630. According to the result, SMS-7630 should be chosen especially when input power is not sufficient to overcome threshold voltage of HSMS-286C.

Secondly, these frequency characteristic were investigated for 2 input powers. The result with -5dBm was presented on Figure 2.21 and with -15 dBm is on Figure 2.22.

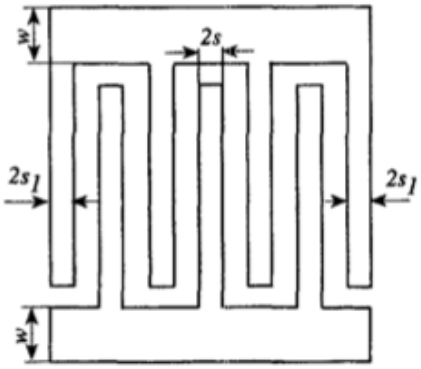

Figure 2.23: Pattern of inter-digital capacitor [65]

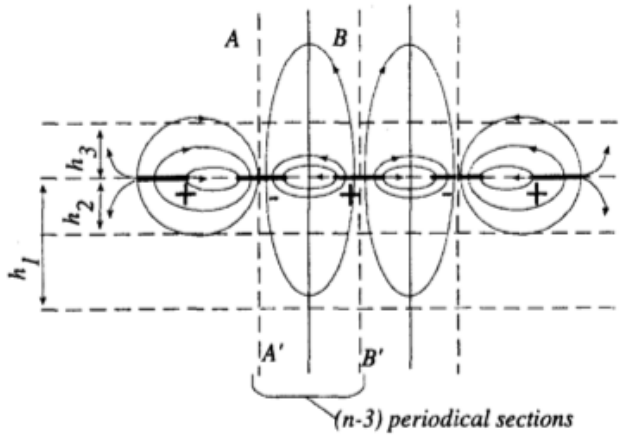

Figure 2.24: Electrical field caused by IDC [65]

As mentioned before, when input power is high enough, differences caused by the stage diodes is not significant and differences caused by the impedance matching is rather emphasized. As charge pump with HSMS-286C had better matching around 880MHz, it outperform SMS-7630 in some part but SMS-7630 usually give better performance. Especially, with lower input power, SMS-7630 gave totally better performance in any frequency. Moreover, the charge pump with SMS-7630 has wide band matching since its series resistance (20Ω) is larger than HSMS-286C (6Ω). As far as impedance of the charge pump need to be matched to 50Ω, higher resistance is preferred for matching; however, it also means loss by the resistance is higher and SMS-7630 cannot accept too strong input power. If over -5dBm input power is expected, using HSMS-286C may safer option.

2.7.2 Capacitive Sensing

The IDCs on the leaf and root part works as rainfall sensor and soil moisture sensor respectively. The fundamentals of these sensors are simple capacitive sensor which is achievable with charge-discharge cycles.

Figure 2.23 shows the typical design of an IDC. IDC is often used for capacitive base sensor because it can effectively occur capacitance in single side conductive pattern. When it is connected to power source, electrical fields shown in Figure 2.24 will be occurred. The main factors of determining capacitance of the IDC is element width, element pitch and relative permittivity of surrounding mediums. Thus, relative permittivity change can be detected by measuring the capacitance of the IDC. Since water has much higher permittivity than air and soil particles, most part of the changes of permittivity is caused by existence of the water around IDC. When rainfall happened and the IDC for rainfall sensor capture some water, capacitance of the IDC will drastically increase so rainfall detection is easily enabled. Soil moisture sensor is much more complex compared to rainfall sensor because soil has various parameters which would cause

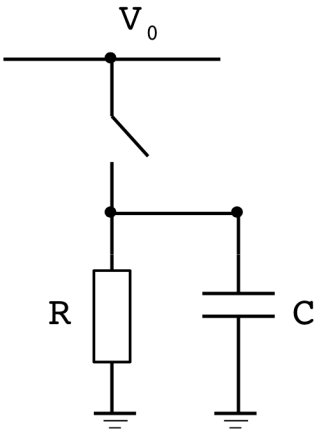

Figure 2.25: Measurement circuit of capacitive sense

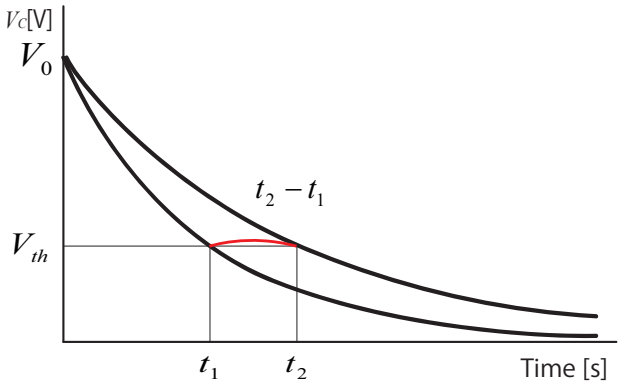

Figure 2.26: Fundamentals of capacitive sense

capacitance changes on the IDC other than the moisture level. For example, salinity level changes on soil will cause electrical conductivity changes and it also appeared as capacitance changes as far as the measurement frequency is not high enough. In order to mitigate the effect by the salinity level, a few hundred MHz is required which is not usually available for general purpose microcontrollers (MCUs). However, if accuracy requirements are not strict, the IDC still can be used for capturing relative soil moisture changes because soil moisture is primary factor for causing capacitance changes in short term. The relative soil moisture change detection is useful enough for hobby farmer and gardeners.

To measure the capacitance, the RC circuit shown on Figure 2.25 is used. Firstly, MCU turned on the charging switch and supply power to IDC and resistance and then wait a while to finish charging. Secondly, MCU measured initial voltage V_0 and set interruption setting to capture a timestamp when the capacitance voltage V_C underrun the threshold voltage V_{th}. Thirdly, cut the charging switch then discharging through resistance is started. Ideally, the capacitance voltage V_C will follow the equation

$$V_C = V_0 e^{-\frac{t}{\tau}} \tag{2.12}$$

$$\tau = RC \tag{2.13}$$

so if the timestamp t_1 is captured when V_C is V_{th} as shown on Figure 2.26

$$\log \frac{V_{th}}{V_0} = -\frac{t_1}{\tau} \tag{2.14}$$

$$\tau = -\frac{t_1}{\log \frac{V_{th}}{V_0}} \tag{2.15}$$

$$C = -\frac{t_1}{\log \frac{V_{th}}{V_0} R} \tag{2.16}$$

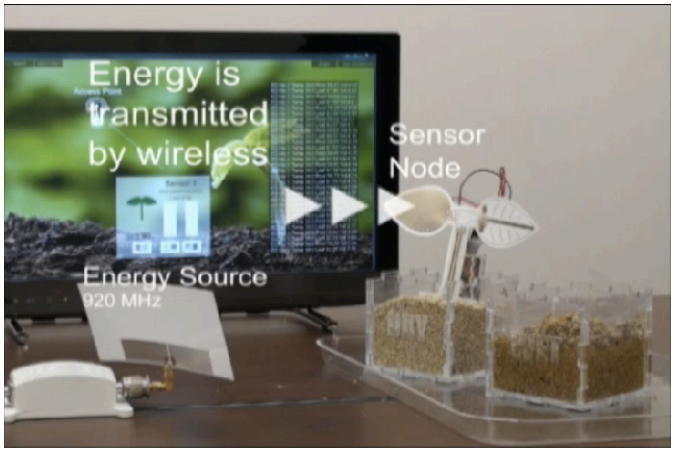

Figure 2.27: Overview of the agricultural sensing prototype

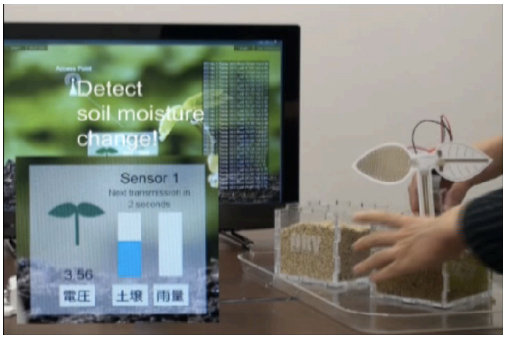

Figure 2.28: Detection of soil moisture changes

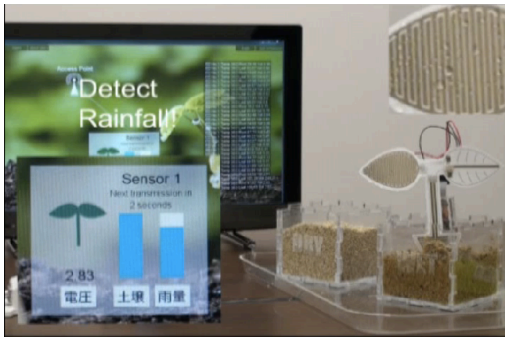

Figure 2.29: Detection of rain falls

Since $\log \frac{V_{th}}{V_0}$ and R are set as fixed value, relative capacitance change ΔC is

$$\Delta C = a(t_2 - t_1) \tag{2.17}$$

$$a = \frac{1}{\log \frac{V_0}{V_{th}} R} \tag{2.18}$$

Thus, it is simplified to a subtraction of timestamps.

2.7.3 Demonstration as Agricultural Sensor Node

Figure 2.27 shows a demonstration setup for the agricultural sensing prototype. RF energy source supply power through 920 MHz, single tone radio wave and its output power is 250 mW. Sensor node captures the RF energy and convert it to DC then drives a MCU. The sensor node operated with adaptive duty cycle control introduced in 2.5 with some simplifications because it works with constant radio wave rather than ambient RF energy source.

Sensor node measures 2 channels of capacitance, its board temperature and its supplied voltage with 16 bits ADC. In addition to the sensor data, sensor node ID and its current

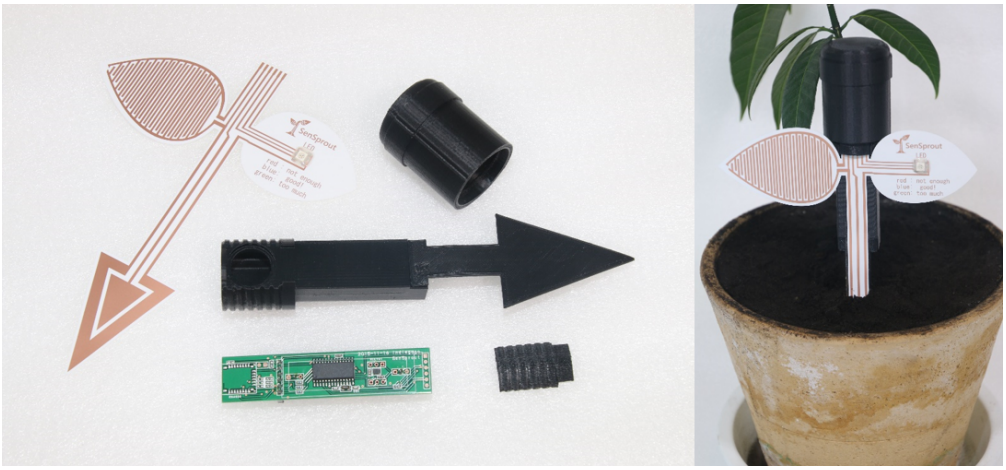

Figure 2.30: Craft kit of simple soil moisture sensor

duty cycle setting is expressed in 8 bits respectively and added so total 10 bytes data are transmitted through SimpliciTI wireless connection. Note that SimpliciTI is a low-power RF protocol developed by Texus Instruments and implemented with TI CC2500 communication module in the eZ430-RF2500 sensor node.

Received sensor data and the other information is displayed on the GUI program as shown in Figure 2.28 and figure 2.29. Its sensing interval is adaptively adjusted by the duty cycle control from 3 seconds to 30 seconds so it is robust to distance and condition changes which cause receiving energy changes.

2.8 Adjustable Sensor Design Using Inkjet Printing

The printable sensor electrodes provide flexibility on design and drastically accelerate fabrication speed; therefore, we can easily collect various design ideas through sensor design workshops. The workshop was held as a Global Design Workshop (GDWS), Workshop C, which is part of graduate program for Social ICT Global Creative Leaders. The purpose of GDWS is clarifying the social issues and the new opportunities. Through the workshop, participants would consider what are issues and requirements on soil moisture sensor design and organizers could find another opportunity on the design by gathering ideas provided by participants.

In this workshop, participants could design their own soil moisture and water level sensors using rapid prototyping enabled by ink-jet printer with silver nano particle ink. As simple capacitive sensing is exploited for our moisture sensing, 2 conductive patterns separated by small gap can work as sensor electrodes, which is not necessarily IDC. Therefore, there are various options on the electrodes design and potential that participants can come up with innovative ideas on the sensor design. During the workshop, participants sketched sensor patterns using PowerPoint and they printed them out on PET film using ink-jet printer. Then, they laminated the film for water proofing, cut

its outline and put chip LED for moisture indication. Once the sensor film is ready, it will work as a moisture sensor by connecting to a measurement circuit that is used for a craft kit of soil moisture sensor "SenSprout" which is shown on Figure 2.30. Unique and impressive designs are also important when we consider consumer version intended to be used by hobby farmers or gardeners, while currently available agricultural sensors mostly focus on toughness and ease of use. Thus, including consumer side people on the designing process through such workshop will be helpful to figure out attractive designs for possible users. In addition to that, some electrical engineers were joined to the workshop and they could give practical ideas on sensor design. Through the first workshop held in November 15th, 2016 at Sony Creative Lounge, all 17 participants could implement some sensor films and 13 participants could design their own patterns while the time was quite limited. There are several designs related with plant like plant pot, leaves and root which is also considered as the motif of original "SenSprout" sensor but designs that imply some company or product logos or animals were also proposed. These outcomes of the workshop should have interesting variety and inspiration on the soil moisture sensor design. Since time is limited, it might be difficult to finish up all the implementation in time and there was no enough time to share and evaluate ideas each other. For further improvement, we would need to brush up the implementation processes to be accomplished more quickly and may need to ask participants some preliminary works. In the second workshop held in May 27th, 2017 at DMM.make AKIBA, we prepared several samples before the workshop and also reserved more time for workshop so more participants reached their own design and satisfying the output. In addition to that, the firmware for the craft kit is updated to reset threshold to turn on LED when a battery is inserted so that the issue on capacitive touch switch was resolved. As a result, the second workshop is more successful compared to the first one. The workshop was generally enjoyable for participants, gave impressive outputs and imply valuable aspects on sensor design. It would be interesting to iterate similar workshops with other participants.

2.8.1 SenSprout Craft Kit and Custom Film Fabrication

The craft kit is simplified version of the concept of the sensor mentioned in 2.7. In this kit, components for wireless power transfer and communication module were eliminated and work offline with a AAA battery. For the sensor electrodes in the kit shown on Figure 2.31, we shifted to ordinary flexible printed circuit board rather than ink-jet printed one considering durability but it keeps compatibility to printed one. The capacitive sensor on the left leaf part is turned to the touch switch to turn on the sensor rather than a rainfall sensor, right leaf have a 3 color LED to indicate soil moisture level and its root part is still soil moisture sensor while its shape was modified from IDC. The LED indicate soil moisture in 3 level: "too much" with green color, "good!" with blue color and "not enough" with red color. The MCU scanned capacitance on the leaf touch switch in every 1 second and when it detect a capacitance change caused by touching finger of users, it turns on LED with a color determined by the soil moisture sensing result. Threshold to changing color can be adjustable by tap and holding the

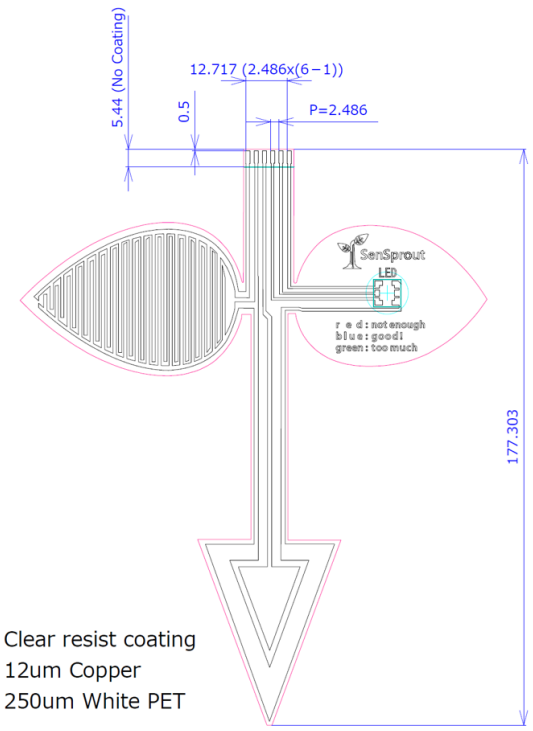

Figure 2.31: Sensor film design and specifications

touch switch. After blinking the LED 3 times with white color, the adjustment will be finished. Then, current soil moisture level is set as a "good" level and it indicates relative moisture from this level. Since the sensor electrodes composed by only capacitor like conductive patterns, 3 color LED and connection lines, it is not difficult for non-specialists of electrical engineering to modify the design of the sensor electrodes. For example, a custom design inspired by sailboat shown on Figure 2.32 or inspired by Pokemon shown on Figure 2.33 are applicable. These pattern can be made on PET film either drawing software like Microsoft PowerPoint with ink-jet printer or hand writing with silver ink pens [66]. After print or draw the conductive pattern with silver nano-particle ink [54], it is laminated with 100 μm thickness laminate film to be water proof except connection areas for LED and MCU board. Note that laminate film need to be cut not to cover these area before lamination. After lamination, a LED chip on the right leaf is putted on using conductive pastes, then insert connector to MCU board and it is ready for use.Summarizing the processes, it contains following steps.

1. Designing pattern on drawing software
2. Printing the pattern on PET film by an off the shelf ink-jet printer with silver ink
3. Cutting laminate film to avoid connection part
4. Laminating the printed film using an off the shelf laminator

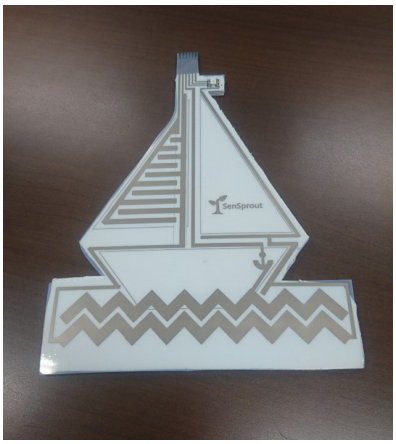

Figure 2.32: Sailboat shape sensor for moisture detection

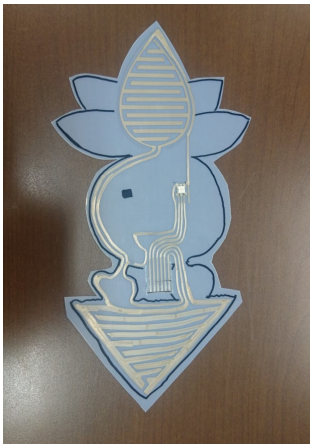

Figure 2.33: Soil moisture inspired by a Pokemon

5. Put 3 color LED for moisture level indication
6. Cutting outline
7. Insert connection part to a MCU board
8. Insert AAA battery then the touch switch setting is calibrated to custom design
9. Adjust soil moisture in suitable level
10. Insert sensor to soil and make sure surrounding soil stick to the sensor pattern
11. Tap and hold the touch sensor to memorize suitable soil moisture level
12. Tap the touch sensor and confirm current soil moisture level

The mechanism can be applicable to water level sensor as well because it can detect water level changes. Therefore, participants have option to make water level sensor instead of soil moisture sensor like Figure 2.34.

Initially, it did not consider making custom sensor electrodes so the threshold to turn on the sensor was fixed and adjusted for the leaf touch sensor. This limitation cause always ON or always OFF cases during the first workshop because capacitance of the touch sensor varies with its design and sensor size. To solve the issue, we modified the firmware to make the MCU reset the touch switch threshold to bit above the capacitance of touch switch when a battery is inserted. By this modification, the sensor can be turned on by relative capacitance changes and absorb variability of the touch switch capacitance.

2.8.2 Workshop Reports

1st Workshop at SONY Creative Lounge, Nov 15th, 2016, From 18:30 to 21:00
As the first workshop is held in the Sony (Shinagawa, Tokyo, Japan), the large part of participants already have some experiences and knowledge about electrical circuit

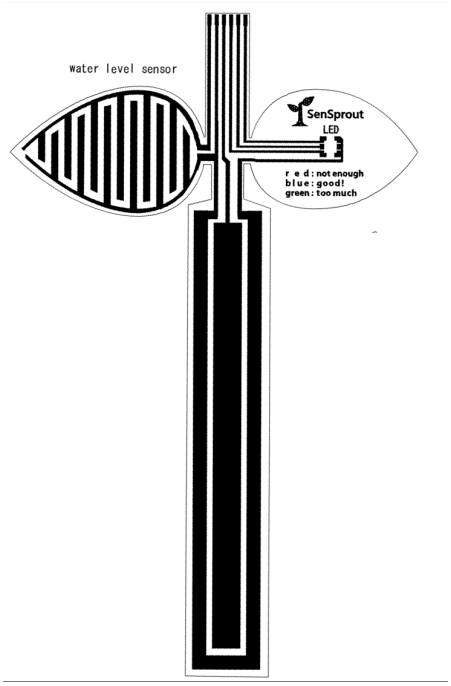

Figure 2.34: Sensor design for water level sensor

design while it is open to anyone who is interested in the agricultural sensing and digital fabrication. Through an online ticketing site, we had 18 entries and 17 were actually joined. The schedule was following

- 18:30-18:40 Introduction
- 18:40-19:00 Guidance for how to use tools
- 19:00-20:00 Implementation of custom sensors
- 20:00-20:10 Presentation about currently available agricultural sensors
- 20:10-20:40 Implementation of custom sensors
- 20:40-21:00 Presentation for created sensors and discussion
- 21:00-21:10 Closing

After the introduction about the processes to make the custom sensor patterns, requirements on custom sensor and some working examples, participants start designing their own sensors. Skill and experiences about electrical engineering seemed to be varied from beginner to expert so we separated participants to 3 groups.

1. Replicate working examples
2. Draw patterns other than connectors using silver ink pen (Like Figure 2.35)

Figure 2.35: Fabricating sensor by hand drawing with a silver ink pen

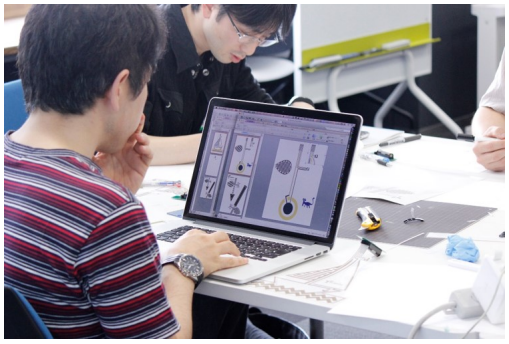

Figure 2.36: Designing sensor on PowerPoint for ink-jet printing

Figure 2.37: Participants and outcomes of 1st workshop

3. Design artwork on PowerPoint and print own design using ink-jet printer (Like Figure 2.36)

In fabrication processes, attaching LED would be a little difficult for participants because it requires experiences with conductive paste and number of printers are limited so organizers supported on these steps. To provide inspirations, brief presentation about currently available sensor designs and case studies on agricultural sensing was given and it would stimulate participants to come up with new design on sensors.

Overall, they did not face difficulties on fabrication processes but created sensor sometimes did not work well mainly due to lack of touch switch setting adaptation. However, we were able to find more various designs than expected (Figure 2.37). At the end, we asked participants to present their own ideas to others and gave feedback each other.

Through the workshop, some novel ideas we had not considered are proposed. For example, one of the participant make connection line under the LED chip to expand design options and another participants set connection part to the MCU board at the center of the sensor film. While our original design is basically inspired by a shape of plants and large part of participants also follows plant like shapes, some of them did not

stick to the motif and freely included company logo or mascot on their design and reached unique designs. The challenges on the 1st workshop is time limitation. Finishing sensor design and fabrication in 2 hours was quite difficult and we need to cut down the idea sharing time instead so we may not leverage collaboration between participants. Also success rate for sensor film fabrication should be improved by optimizing processes or some modification on the tools. In workshop process, asking all participants to replicate example at first and try to make their own design afterword will be more efficient to learn the fabrication process and outcomes will be more promising by the iterative processes.

2nd Workshop at DMM.make AKIBA, May 27th, 2017, From 13:00 to 17:00 As the second workshop was held after a half year from the 1st workshop with some improvements. Through the internet ticketing site, 17 are registered and 16 are joined actually. In this time, participants interests tended to be creative stuff and workshop itself rather than electrical engineering. Although its overview was not changed much as shown on the following schedule, we reserved more time for it and introducing iterative process rather than separating groups. Additionally, the threshold adjustments of touch switch was enabled.

- 13:00-13:10 Introduction
- 13:10-13:20 Guidance for how to use tools
- 13:20-13:40 Demonstration of sensor fabrication
- 13:40-14:30 Implementation of custom sensors
- 14:30-14:50 Presentation about currently available agricultural sensors
- 14:50-16:00 Implementation of custom sensors
- 16:00-16:40 Presentation for created sensors and discussion
- 16:40-17:00 Closing

In the first attempt, all participants focus on follow the fabrication process using sample design shown on Figure 2.32. The sample had been printed before the workshop so they can skip the first 2 steps on fabrication. It worked better for learning processes and they can smoothly started designing their own sensor by understanding the processes and fundamentals of the sensor. In this workshop, designing water level sensor was promoted in addition to soil moisture sensor because it is more easy to test and come up with its applications. As almost all users reached successful results by following the sample, they would be motivated to make their own in addition. Later part of the implementation participants try to develop their own designs. Interestingly, in this workshop more participants use silver ink pen rather than ink-jet printer and efficiently made unique design with it. That is probably because the background differences from 1st workshop.

Figure 2.38: Participants and outcomes of 2nd workshop

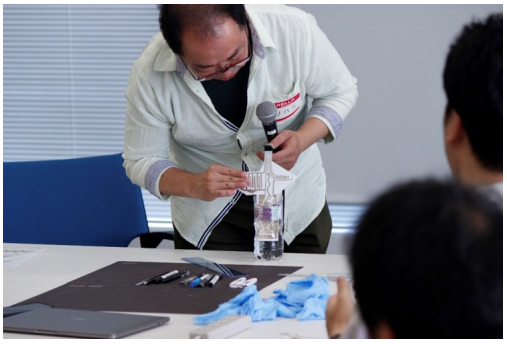

Figure 2.39: Demonstration of water level sensor inspired by fishing

Figure 2.40: The LED is putted on the fire ball to fit the design motif

Outcome was more various than the 1st workshop as shown on Figure 2.38. For example, one made a water level sensor inspired by fishing and tried demonstration on his presentation (Figure 2.39) and another carefully designed LED position to match the motif (Figure 2.40). The workshop implied the potential of the craft kit for educational purposes because around half of them succeeded to fabricate sensors using hand writing and came up with interesting ideas and which mean we may not necessarily prepare ink-jet printer and PC for the prototyping. If that is possible, the workshop may applicable for children to learn basics of electrical engineering and sensor technologies. In the next time, probably asking participants to use their sensors in actual situations and redesign their sensor considering the usability on another day would be interesting to gather practical ideas. The outputs through the workshops are informative for designing simple soil moisture sensors and water level sensors for hobby and gardening usages. Also enabling to create own sensor designs could be an attractive feature of the craft kit.

2.9 Summary

In this chapter, a prototype implementation of agricultural sensors are presented. By introducing RF energy harvesting technologies, battery-less operations are enabled and it can be driven either 500 MHz TV broadcasting radio wave and 920MHz RFID radio wave. As the sensor has capacitor leakage aware adaptive duty cycle control, it can calculate an optimal stored energy level calculation and sustain the optimal stored energy level under the condition of unstable and fluctuating harvested energy. The proposed method defines and minimizes the cost function by aggregation of the capacitor leakage characteristics and of the energy shortage risk to calculate the optimal level. In addition, the proposed method focuses on both long-term and short-term harvested energy transitions, which are specific characteristics of RF energy harvesting, especially for TV signals. This method monitors the harvested energy and adjusts its optimal stored energy level when long-term changes are detected. This environmental awareness enables an efficient energy usage by capacitor leakage reduction. For a benchmarking sensing topology, the proposed method achieved a 5.34% leakage reduction as compared to simple LQ tracking.

The RF energy harvesting node was generally applicable for environmental monitoring but we narrowed down the focus to agricultural sensing area and add capacitive sensors for rainfall detections and soil moisture monitoring which are also printable with an off the shelf ink-jet printer. Combining the printed electronics and energy harvesting, a prototype of low-cost, printed, disposable and battery-less agricultural sensor was developed. While its accuracy is not very high but it can roughly detects relative moisture level changes, it implies potential of applying printed electronics on soil moisture sensing. In the workshops for soil moisture sensor, rapid prototyping using ink-jet printing on sensor design stimulated creativity on the sensor design and it should contribute to accelerate developments. Although harvested energy from ambient radio wave is tiny, modifying it to microwave wireless power transfer, its potential will be expanded. In

order to drill down on each feature, we separated the project for enabling battery-less solution utilizing energy harvesting including microwave wireless power transfer and developing low-cost soil moisture sensor leveraging printed electronics. Therefore, in the following chapters, we focus on either part separately. However, the eventual goal remains to be with the concept so the printable sensors and the energy harvesting sensor node should be integrated again in the future.

Chapter 3

UAV-Assisted Microwave Wireless Power Transfer for Agricultural Sensors

3.1 Introduction

As introduced in Chapter 1, UAV has large potential on agricultural applications including UAV assisted WPT. Also various sensors including soil moisture sensors will be deployed in the field for precision farming. Therefore, combining UAV and agricultural sensor to enhance both potential is desired. Soil parameters are difficult to measure through remote sensing technologies so deploying soil sensors are needed even if UAVs are introduced for remote sensing. On the other hand, current agricultural sensors requires frequent battery replacement which will be too troublesome when expanding the deployment scale. UAV assisted WPT enable powering the sensors remotely and UAVs can deliver power to sensors in spare time for the other activities so that manual battery exchanges are no longer required.

For power to be supplied from a UAV using WPT, the UAV needs to keep hovering over points suitable for power feeding, which are usually located right above a sensor node. UAV navigation above sensor nodes using GPS might seem easy but the power transmission efficiency will decrease drastically, when GPS localization errors result in the UAV navigating a half a meter away from the sensor. Since GPS tends to err by a few meters [67], its accuracy is not good enough for the intended purpose. While more accurate GPS technologies are available, such as the RTK GPS, which can achieve centimeter order accuracy, they are too expensive to be used in this system. Therefore, in addition to GPS, an additional navigation system is required to ensure that the UAV reaches the correct point.

For navigating a UAV to an appropriate power feeding point, the position of the sensor node needs to be estimated. Localization methods using RF propagation characteristics have been actively discussed both for indoor [68] and outdoor situations [69]. There are various RF signal localization methods based on signal parameters such as received signal strength indication (RSSI) [70], time-of-arrival (TOA) [71] . Additionally, UAV navigation strategies have been proposed in order to minimize localization errors [72,73]. However, these were designed for searching moving signal emitting targets. On the contrary, the targets considered here are stationary and will not have sufficient energy to emit signals continuously, unless a UAV approaches to power feed them. UAV navigation strategies for power feeding had not been discussed at the time of our study, including the situations described above. Thus, we proposed a position estimation technique for power feeding [P11] , which is being improved on an ongoing basis.

This paper presents an efficient sensor position estimation method for implementation in the navigation system for UAV-assisted WPT. The method is inspired by trilateration, which is a widely used process in position estimation systems such as GPS. The sensor node conveys the transmission efficiency to a UAV and the UAV then attempts to estimate the optimal power feeding point based on the information it was given. Then, the UAV moves to the estimated point. We initially used a simple hill climbing method to conduct the estimation [P14]; however, a more time efficient method is needed in order to complete the power delivery quickly, within the limited flight time of the UAV. In simulation, the trilateration-inspired method can navigate the UAV to a near optimal

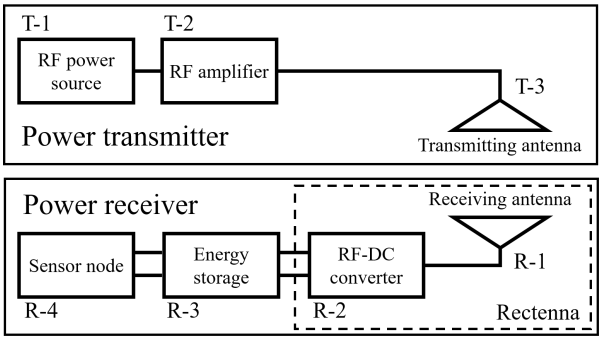

Figure 3.1: Components of microwave power transfer system.

power feeding location 52% faster than the hill climbing method.

This paper is organized as follows: in section 3.2, we describe the WPT system implementation and the measurements that relate location dependency to transmission efficiency. In section 3.3, navigation algorithms for position estimation are presented. We discuss (a) the hill climbing method and (b) 2 trilateration-inspired methods: (b-1) the direction-based approach and (b-2) the least-squares approach. In section 3.4, the comparative evaluation of these 3 simulation approaches is presented. In section 3.5, we conclude the paper and discuss future work.

3.2 Microwave Wireless Power Transfer for Agricultural Sensor System

Since our position estimation method relies on the relationship between distance and transmission efficiency, the location dependency of transmission efficiency, represented by the output voltage of a rectenna, needs to be measured in realistic situations. In this section, we introduce our experimental implementation of a microwave WPT system and present the measurement results of location dependency. The system targets large-scale precision farming as the majority of UAV applications intended for agriculture. The productivity and efficiency of resource usage in the cultivation of grains such as wheat, rice, maize, sorghum etc. needs to improve in order to satisfy the ever-increasing demand for food. The deployment of numerous environmental sensors, such as soil moisture sensors, and the optimization of irrigation should contribute to the enhancement of productivity and the reduction of water consumption. In order to operate sensors in large farm fields, which would be at least over 10 ha, the maintenance cost associated with battery replacement will be a serious issue, more so than greenhouse farming. Thus, our expectation was that our sensor would be used in such scenarios. In fact, we deployed soil moisture sensors in a wheat farm in Hokkaido, Japan, for monitoring melt water from snow; we also planned to deploy sensors at rice paddy fields in India for irrigation management. The targeted field size was decided within the range of 10 ha to 1 km^2.

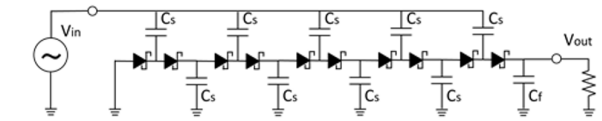

Input frequency: 915 MHz, Number of stages: 5
Stage capacitor Cs: 12 pF, Final capacitor Cf: 1000 pF
Stage diodes: Skyworks Solutions SMS-7630, Load: 1 MΩ

Figure 3.2: Schematic and specification of modified 5 stages Dickson charge pump.

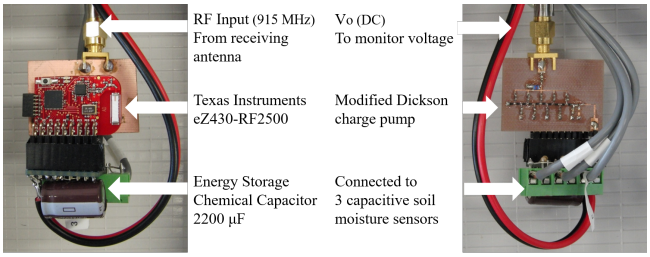

Bottom: Sensor node Top: Charge pump

Figure 3.3: Implementation of battery-less sensor node using TI eZ430-RF2500 with microwave WPT.

3.2.1 System Components

As shown in Fig.3.1, the microwave WPT system is usually composed by an RF power source (T-1), RF amplifier (T-2) and transmitting antenna (T-3), receiving antenna (R-1), RF-DC converter (R-2), energy storage (R-3) and sensor node (R-4). In our experimental implementation, we chose the ROHDE&SCHWARZ SMC100A signal generator as the RF source; a 915 MHz single tone signal was emitted, and amplified to 9 dBm by a MAXIM Integrated MAX2235 RF amplifier functioning as an RF amp; the frequency was used for Radio-frequency identification (RFID). Both the transmitting and receiving antennas were L-COM HG908PCL-NM UHF patch antennas, whose gain was 8 dBi and beam width was 65 degrees.

As the RF to DC converter, we used a modified 5 stages Dickson charge pump [74], which worked as a rectifier and voltage multiplier simultaneously. The Dickson charge pump schematics are shown in Fig.3.2. The charge pump can be implemented at low-cost because it is composed only of capacitors and diodes.

3.2.2 Prototype of The Battery-Less Sensor System

To conduct a feasibility study, we developed a prototype soil moisture sensor node, which implements microwave WPT as shown in Fig.3.3 and Fig.3.4. In this prototype, we used the Texas Instruments eZ430-RF2500 sensor node [53] because of its low power

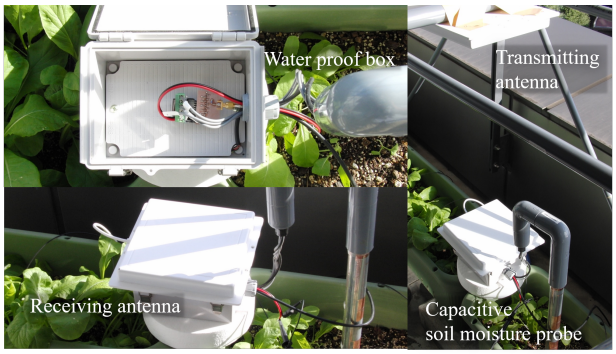

Figure 3.4: Packaging of soil moisture sensing system with battery-less sensor node.

consumption. A 2200 μF chemical capacitor was connected to the sensor node in parallel, as an energy storage medium. The sensor node can measure the capacitance of sensor electrodes by measuring their charging and discharging time. The capacitance has a semi-linear relationship to the soil moisture level represented by volumetric water content. Thus, it works as a capacitive soil moisture sensor. Sensor electrodes were implemented on thin PET film and were identical to our profile probe [P2]. The measurement circuit was switched to eZ430-RF2500 due to the deliverable energy limitation by WPT. The sensor node required 0.235 mJ for each sensing and communication activity. The microwave WPT prototype can transfer several hundred microwatts over a few meters, even if the transmission power is restricted to less than 250 μW, which is the transmission power limit for 900 MHz RFID. Thus, the sensor node can collect data at every second and we confirmed that the prototype can continue sensing sustainably while microwaves were being supplied.

3.2.3 Measurement Setups

As shown in Fig.3.5, we measured the transmission efficiency with a 1 MΩ load, which was connected to a charge pump instead of the sensor node. The output voltage of the charge pump was measured by a tester. The vertical distance between the transmitting and receiving antennae was 100 cm. To measure the location dependency, we moved the transmitting antenna, which was located just above the receiving antenna, horizontally from -80 cm to 80 cm every 10 cm. In order to simulate the situation of the sensor node being deployed at the farm field, the receiving antenna was placed on the plant pot, which was filled with soil as shown in Fig.3.6 (A). Microwaves can be reflected and attenuated by moisture present in crops [75], when the receiving antenna on the sensor is surrounded by crops such as those shown in Fig.3.6 (B). Since we considered the soil moisture profile probe [P2] as the primary target sensor for the WPT system, the situation in which the receiving antenna cannot be placed at a high enough position in order to avoid attenuation by crops was assumed. Additionally, the measurement was

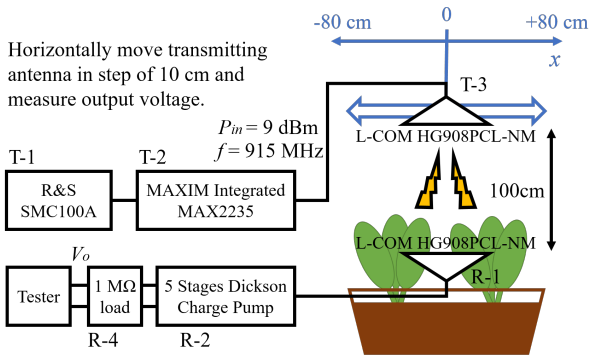

Figure 3.5: Measurement set up for evaluating the relationship between distance and power transmission efficiency.

Figure 3.6: Surrounding environments of receiving antenna. Top: (a), (c) Without crop; Bottom: (b), (d) with crop.

carried out at 2 soil moisture levels (Intermediate: 21.7% and Wet: 27.2%; measured by a Decagon 5TE soil moisture sensor [76]) so that we could observe the effect of moisture in the soil. Hence, the measurement was carried out in the following 4 situations: (a) intermediate soil moisture without crops, (b) intermediate soil moisture with crops, (c) wet soil moisture without crops, and (d) wet soil moisture with crops.

We assumed that the UAV kept hovering at 100 cm while power feeding. The longer vertical distance made the propagation loss larger. Thus, if we would have been able to navigate the UAV accurately enough, the flight height would have then been as low as possible. Popular grains, such as wheat and rice, are mostly smaller than 100 cm; therefore, we considered 100 cm as an acceptable height for such crops. On the other hand, maize and sorghum were made taller than 100 cm. The larger vertical distance was thought to have an easing effect on the dependency of the receiving antenna's position;

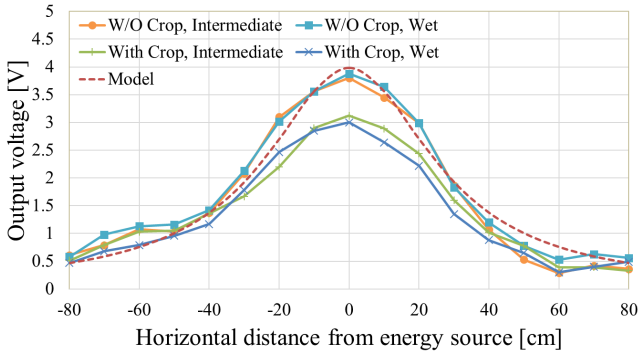

Figure 3.7: Relationship between horizontal distance from sensor node and output voltage of charge pump with various conditions.

therefore, identical measurements with different flight height will be conducted in future work; regardless, this does not alter the bigger picture of location dependency.

3.2.4 Measurement Result and Modeling

Fig.3.7 shows the measurement results. In every situation, the location right above the receiving antenna provided the highest efficiency. An effective zone for power feeding seemed to exist at ±40 cm. While attenuation by crops generally degrades the transmission efficiency, location dependency seemed to have similar shapes in both situations. The effect of soil moisture level change was negligible. Fig. 3.8 shows the result of another measurement that was conducted in order to evaluate the relationship between the receiving power and the position of the transmitting antenna. For energy supply, we used PowerCast TX91501, which has a 915 MHz/1 W RF output, with an 8 dBi patch antenna. Note that PowerCast is powered by a Li-ion mobile battery. The reason why we changed the set-up of the experiment was that the measurements had to be done outdoors, where the ground was covered by short weeds and where measuring instruments such as the signal generator should not be able to endure the dusty environment. We thought that power source differences will not have any effect on the result since the same frequency was used. The vertical distance z between the transmitting and receiving antennae was kept at 100 cm while the horizontal position was changed from $x = 0$ cm to $x = 70$ cm and $y = 0$ cm to $y = 70$ cm. Every measurement was taken 3 times and the result represented their average value. The result showed that there was no significant difference between the x and y direction. In our position estimation method, we need to have a relationship model in order to estimate the distance based on the measured efficiency value.

The relationship would not change dynamically in the short term unless the canopy of plants covered the receiving antenna; therefore, we assumed that the model was mostly static. We used simple approximation, relying on the measured data rather than the defined model based on electromagnetic theories, because any structure in the farm field

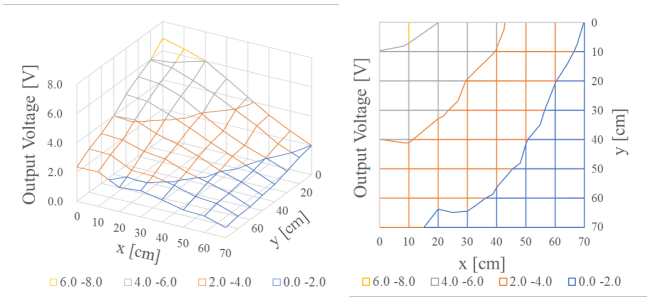

Figure 3.8: 2D Output voltage gradient (Left) and its upper view (Right). x and y are the horizontal distance from the sensor node.

including crops, UAV, and ground surface would affect the microwaves and, therefore, we would not be able to assume free space propagation. In this work, we assumed that the relationship, which is expressed as the following equation, fitted the measured result.

$$V = f(r) = \frac{a}{r^n + b} \tag{3.1}$$

Note that r is the horizontal distance (cm), V is the output voltage (V) of the rectenna, and a, b are constants, which depend on field environment. Parameter n need to be determined experimentally so we tested $n = 1, 2$ or 3 with measurement results under situation (a). Then, we chose an appropriate value by minimizing the errors using the least squares method. Finally, $n = 2$, $a = 3348.83$ and $b = 840.676$ gave the best fit to the measured data. By using this model, distance r could then be calculated as follows:

$$r = f^{-1}(V) = \sqrt[n]{\frac{a}{V} - b} \tag{3.2}$$

Therefore, the UAV can estimate the sensor position based on sensor node feedback.

3.3 Navigation of UAV for Efficient Power Feeding

In this section, we introduce 2 methods of UAV navigation for power feeding. Both methods navigate a UAV to a desired power feeding position. The procedure is described in the diagram shown in Fig.3.9.

First, the UAV tries to move near the sensor node using GPS. It defines an initial point and gets the output voltage information from the sensor node through wireless communication. Then, this is saved as baseline voltage (Initialization). Second, the UAV moves to another point that is assumed to be a better power feeding candidate point. This part plays the most important role in achieving efficient navigation; therefore, the major differences of the 3 approaches occur in this part (Position estimation). Third, the UAV retrieves the output voltage from the candidate point and compares it to the baseline voltage (Measurement). If the measured voltage cannot overcome the baseline, the UAV should return to the previous point (Revert); otherwise, the UAV should stay on the current point since it would have optimized its position. Further, the

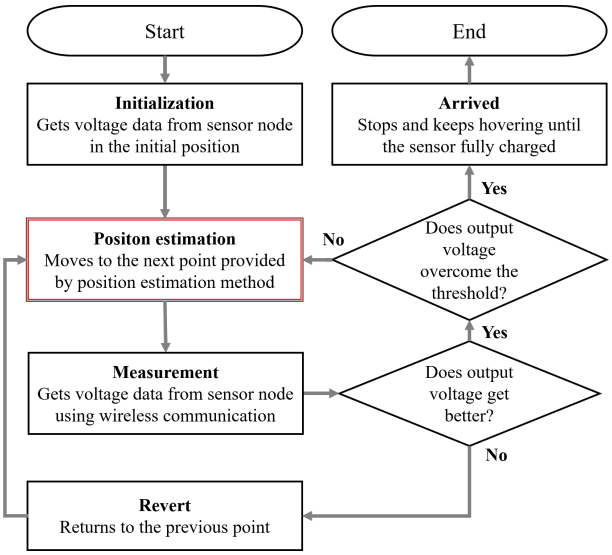

Figure 3.9: Flow chart for the UAV navigation.

UAV confirms whether the output voltage overcomes the threshold, which means that sufficient transmission efficiency has already been earned at this point. Then, the UAV stops moving and remains stationary until the sensor node receives sufficient energy (Arrived). Until that happens, the UAV updates the baseline voltage and iterates until the output voltage becomes higher than the threshold.

In the following part, we discuss how to calculate a more optimal position. There are 2 methods: (a) the hill climbing method and (b) the trilateration-inspired method. We also tried 2 different variations of the trilateration-inspired method: (b-1) the direction based approach and (b-2) the least squares approach. Therefore, 3 approaches were compared.

3.3.1 Hill Climbing Method

The first approach we considered is the hill climbing method, which consists of a UAV randomly moving around as it tries to find a power feeding position that is better than its current position. Since transmission efficiency and the distance to a sensor node have a hill-shaped relationship, as shown in Fig.3.7, the UAV will eventually reach the optimal power feeding position when the initial point is close enough to the sensor node in order for power efficiency changes to be sensed by moving at random. In this method, the UAV chooses the next point randomly at d cm farther from its current position; therefore, position estimation is not applied. This is a simple process, which does not require excessive computation, in addition to being robust to environmental changes. However, it entails a good amount of iteration for a suitable power feeding point to be estimated; therefore, a relatively long period of time is required for feeding enough

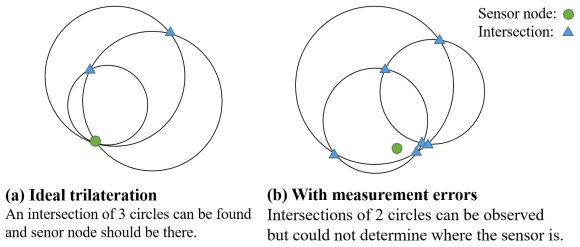

Figure 3.10: Trilateration in ideal case and with measurement errors.

energy to the sensor nodes. The flight time of a UAV is restricted by its battery capacity, which means that the coverage area of the UAV decreases when a longer amount of time is consumed. Thus, a larger number of number of UAVs is required to cover entire farm fields, which leads to increased cost. To avoid this problem, more sophisticated sensor position estimation methods need to be developed.

3.3.2 Trilateration-Inspired Method

As we described in section 3.2.4, the distance to a sensor node can be assumed by equation (3.2). Under the condition that the UAV moves only in the horizontal direction at constant altitude, if the UAV measures the distance at more than 3 different points, the sensor location can be estimated by trilateration. In this approach, 3 circles should intersect as shown in Fig.3.10 (a); however, when distance measurements are not accurate enough, we cannot find the intersection of 3 circles. Nevertheless, the intersection of 2 circles can be found as shown in Fig.3.10 (b). Unfortunately, we cannot expect our distance estimation to be sufficiently accurate for simple trilateration because it contains various reflection effects and attenuation caused by surrounding structures. Hence, we need to figure out an appropriate way of estimating sensor node positions, even if the intersection of 3 circles cannot be observed. In the discussion that follows, the UAV is assumed to move horizontally at constant altitude. In other words, it moves on an xy plane and altitude z is constant.

Direction Based Approach

The first approach was to rely on the heuristic assumption of the sensor node being in the direction where the intersection of 2 circles is most frequently observed. Fig.3.11 shows an example that explains this approach. First, a UAV measures output voltages in order to estimate the distances to a sensor node at 8 points, which are marked as blue squares, on the circle whose radius is d cm and divided into 8 equal parts. Based on the measurement, 8 circles can be drawn and the intersections of 2 circles can then be plotted; these are marked as triangles. Second, the number of intersections is counted in each

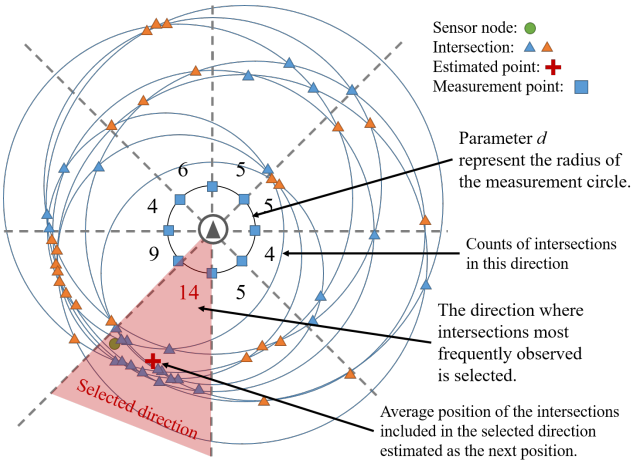

Figure 3.11: Working of the direction-based approach: the direction with most intersections is selected.

direction and the direction including the largest number of intersections is selected as the probable direction; this direction is the one filled with red. Third, the average position of the intersections included in the direction, which is marked as a green circle, is chosen as the next point; then, the UAV will move there and iterate the position estimation until it reaches a suitable power feeding area. The estimated point is not necessarily the same as the actual position of the sensor node, which is marked as a red cross; however, it is accurate enough to shorten the distance to the sensor node within a number of steps that is smaller than the number of steps required by the hill climbing method. While reasonable position estimations can be provided by this approach, one concern is that if a sensor node is near a direction boundary, the distribution of intersections may not be concentrated enough to prioritize directions.

Least Square Approach

Another approach consists of using the least-squares algorithm to estimate the position. In the GPS, when signal from more than 4 satellites is observable, redundant information is leveraged for error correction using the least-squares method [77]. In our case, redundant information is also considered in order to correct measurement errors; therefore, the least squares approach can also be exploited. The advantage of this approach is that it is not limited by the direction boundary issue of the direction-based approach; therefore, this approach can achieve more consistent estimations. When the distances from the sensor node are measured, the position of the sensor node (x_s, y_s) needs to satisfy the following equation:

$$R_i = \sqrt{(x_i - x_s)^2 + (y_i - y_s)^2} \tag{3.3}$$

Note that, i represents the location of measurement; therefore, R_1 is the distance from measurement point 1 to sensor node. In the discussion that follows, measurements are

assumed to be done at m points.

To obtain the position quickly, we used linear approximation so that x_s and y_s were represented as a sum of the appropriate initial value (x_0 and y_0) and correction value (Δx and Δy), respectively.

$$x_s = x_0 + \Delta x$$
$$y_s = y_0 + \Delta y$$

Then equation (3.3) can be expressed by linear approximations as follows:

$$\Delta R_i = \frac{\partial R_i}{\partial x_i}\Delta x + \frac{\partial R_i}{\partial y_i}\Delta y \tag{3.4}$$

The ΔR_i is also expressed as:

$$\Delta R_i = R_i - \sqrt{(x_i - x_0)^2 + (y_i - y_0)^2} \tag{3.5}$$

Therefore, their partial derivatives are:

$$\frac{\partial R_i}{\partial x_i} = \frac{-(x_i - x_0)}{\sqrt{(x_i - x_0)^2 + (y_i - y_0)^2}}$$
$$\frac{\partial R_i}{\partial y_i} = \frac{-(y_i - y_0)}{\sqrt{(x_i - x_0)^2 + (y_i - y_0)^2}}$$

In short, we will call them as α_i and β_i respectively; (3.4) can be written as

$$\begin{pmatrix} \Delta R_1 \\ \Delta R_2 \\ \vdots \\ \Delta R_i \\ \vdots \\ \Delta R_m \end{pmatrix} = \begin{pmatrix} \alpha_1 & \beta_1 \\ \alpha_2 & \beta_2 \\ \vdots & \vdots \\ \alpha_i & \beta_i \\ \vdots & \vdots \\ \alpha_m & \beta_m \end{pmatrix} \begin{pmatrix} \Delta x \\ \Delta y \end{pmatrix} \tag{3.6}$$

When

$$\Delta \boldsymbol{R} = \begin{pmatrix} \Delta R_1 \\ \Delta R_2 \\ \vdots \\ \Delta R_i \\ \vdots \\ \Delta R_m \end{pmatrix}, \boldsymbol{A} = \begin{pmatrix} \alpha_1 & \beta_1 \\ \alpha_2 & \beta_2 \\ \vdots & \vdots \\ \alpha_i & \beta_i \\ \vdots & \vdots \\ \alpha_m & \beta_m \end{pmatrix}, \Delta \boldsymbol{X} = \begin{pmatrix} \Delta x \\ \Delta y \end{pmatrix}$$

Equation (3.6) can be simplified as follows:

$$\Delta \boldsymbol{R} = \boldsymbol{A}\Delta \boldsymbol{X} \tag{3.7}$$

Thus, the correction value can be calculated by:

$$\Delta \boldsymbol{X} = \boldsymbol{A}^{-1}\Delta \boldsymbol{R} \tag{3.8}$$

The initial value x_0 and y_0 are updated using the correction value. Iterating the correction will give a reasonable result; once the correction value gets small enough the calculation will have finished.

However, our estimated distance R_i at position i includes the measurement error ϵ_i. The least squares method tries to minimize its square sum:

$$\Delta \boldsymbol{R} = \boldsymbol{A}\Delta \boldsymbol{X} + \boldsymbol{\epsilon}$$

$$\boldsymbol{\epsilon} = \begin{pmatrix} \epsilon_1 \\ \epsilon_2 \\ \vdots \\ \epsilon_i \\ \vdots \\ \epsilon_m \end{pmatrix}$$

The observation equation (3.9) is shortened by replacing $\Delta \boldsymbol{R}$ and $\Delta \boldsymbol{X}$ by $\boldsymbol{R}_D$ and $\boldsymbol{X}_D$, respectively, as follows:

$$\boldsymbol{\epsilon} = \boldsymbol{R}_D - \boldsymbol{A}\boldsymbol{X}_D \tag{3.9}$$

Then, f will be the square sum that needs to be minimized:

$$\begin{aligned} f &= \epsilon_1^2 + \epsilon_2^2 + \cdots + \epsilon_m^2 = \boldsymbol{\epsilon}^{\mathrm{T}}\boldsymbol{\epsilon} \\ &= (\boldsymbol{R}_D - \boldsymbol{A}\boldsymbol{X}_D)^{\mathrm{T}}(\boldsymbol{R}_D - \boldsymbol{A}\boldsymbol{X}_D) \\ &= \boldsymbol{R}_D^{\mathrm{T}}\boldsymbol{R}_D - 2\boldsymbol{R}_D^{\mathrm{T}}\boldsymbol{A}\boldsymbol{X}_D + \boldsymbol{X}_D^{\mathrm{T}}(\boldsymbol{A}^{\mathrm{T}}\boldsymbol{A})\boldsymbol{X}_D \end{aligned}$$

By minimizing f, we get the partial deviation of $\boldsymbol{X}$ and proceed to calculate the extreme value.

$$\begin{aligned} \frac{\partial f}{\partial \boldsymbol{X}_D} &= -2\boldsymbol{R}_D^{\mathrm{T}}\boldsymbol{A} + 2\boldsymbol{X}_D^{\mathrm{T}}(\boldsymbol{A}^{\mathrm{T}}\boldsymbol{A}) = 0 \\ \boldsymbol{X}_D^{\mathrm{T}}(\boldsymbol{A}^{\mathrm{T}}\boldsymbol{A}) &= \boldsymbol{R}_D^{\mathrm{T}}\boldsymbol{A} \end{aligned}$$

Next, both sides are transposed and a normal equation is obtained.

$$(\boldsymbol{A}^{\mathrm{T}}\boldsymbol{A})\boldsymbol{X}_D = \boldsymbol{A}^{\mathrm{T}}\boldsymbol{R}_D \tag{3.10}$$

Finally, $\boldsymbol{X}_D$ can be calculated as

$$\boldsymbol{X}_D = (\boldsymbol{A}^{\mathrm{T}}\boldsymbol{A})^{-1}\boldsymbol{A}^{\mathrm{T}}\boldsymbol{R}_D \tag{3.11}$$

By using the least squares approach for position estimation, even if some noise and errors are included in the measurement, the reasonable position candidate will be estimated within several corrective iterations.

3.4 Simulation and Result

Comparing the above-mentioned 3 approaches, we tested them by simulating the UAV navigation and power feeding system. The 3 approaches mentioned above were tested

by conducting a simulation of the UAV navigation and power feeding system, for the purpose of performance comparison. In this simulation model, the sensor node charges with energy received from the UAV and stored in its energy storage medium as is, since an end-to-end transmission efficiency model will be used, based on the real measurement mentioned in Section 3.2.4. The energy storage medium should be a super capacitor so that charge-discharge loss may negligible. In addition, the self-discharge of stored energy is ignored as it would be negligible compared to the power supplied during power feeding. The sensor node only consumes the energy stored for sending feedback information to the UAV. The required energy is assumed to be constant and the communication error is assumed not to occur because feedback communication happens only in a few meters and only a single sensor node communicates with the UAV at the same time. The required energy is assumed to be 0.235 mJ, which is the required amount for sensing the output voltage and sending feedback via wireless communication using the Texas Instruments eZ430-RF2500 sensor node. In this simulation, the UAV could accurately move to the destination. We noticed that, in the real world, a UAV may not reach the target location due to wind or other environmental conditions; however, this does not have significant effect on the result of comparison. The following simulations were carried out using Python 2 on Ubuntu 15.10 installed on a ThinkPad X220 (Dual-Core 2.5 GHz CPU) notebook. The Sympy Python package was utilized for formulating the logic of the simulation.

3.4.1 Power Feeding and Measurement Model

As shown in equation (3.1), the output voltage V_o, which the sensor node will observe and use for charging, can be approximated by using the following function of distance x:

$$V_o = f(x) = \frac{3348.83}{x^2 + 840.676} \tag{3.12}$$

However, the received power should contain some variability due to various factors involved in the UAV 's position, microwave propagation, and energy conversion processes. Since accounting for all of these factors would be difficult, we simply added generalized variability to the received power. We assumed that the variability model had normal distribution $N(\mu, \sigma)$. μ represents the mean of the received power $P_r = V_o^2/R$ and can be derived from equation (3.12). σ represents the standard deviation and is defined as half of μ.

In our methods, a UAV reaches a decision based on relative transmission efficiency, by comparison to the best power feeding point; therefore, the definition of efficiency is:

$$\eta = \frac{V_o^2}{V_{max}^2} \tag{3.13}$$

V_{max} was 3.9 V in our measurement; thereby, the efficiency η can be calculated by substituting the measured value of V_o into equation (3.12).

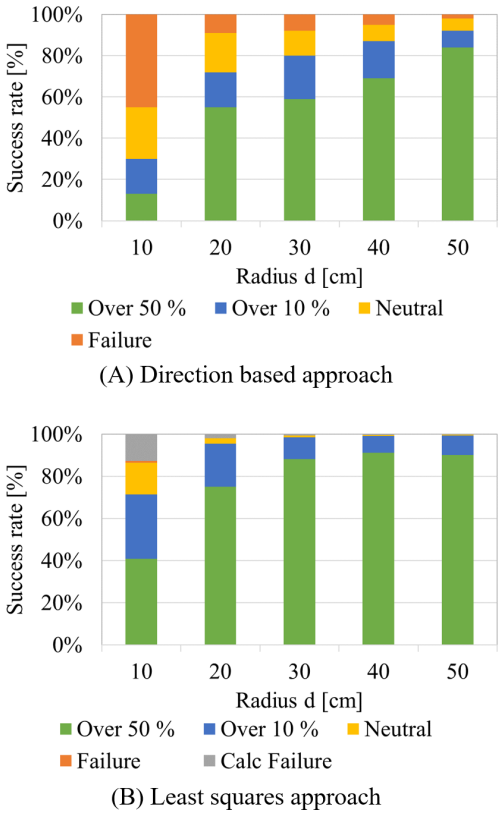

Figure 3.12: Success rates of position estimations for each approach. The target is reaching the desired feeding point where over 50% efficiency is achievable.

3.4.2 Radius Size Evaluation

Our trilateration-inspired methods have a parameter d, which represents the radius size of a sensing circle. In other words, it is measurement density because all measurements will take place on the circle. In general, the measurements that were carried out within a small area did not differ, because distances from sensor nodes did not change much. Therefore, a small d value is not suitable when searching for the optimal power feeding point. Note that the radius d can be decided without regard to GPS navigation accuracy because modern UAVs can measure its relative position change by utilizing sensors (e.g. image sensor, accelerometer and gyro sensor). On the other hand, a large d value, of a few meters, will not make any sense either because transmission efficiency changes drastically within one meter, as shown in Fig.3.7. A reasonable value for d should be determined through simulation. In this simulation, a UAV was dropped 100 cm farther from a sensor node and tried to approach it. Then, it measured the efficiency at the current position and 8 other points on the sensing circle in order to estimate the location of the sensor node using each considered approach. Fig.3.12 shows the position estimation success rate in 100 trials for each d. The green zone, "Over 50%" means

Parameter	Value
Target amount of energy	3.24 mJ
Energy consumption for feedback	0.235 mJ
Waiting time for feedback	1 s
Speed of UAV	10 cm/s
Distance from sensor node	80 to 120 cm (Random)
Step size	$d = 0.1, 0.2, 0.3, 0.4, 0.5$
Threshold to stop exploring	$\eta > 50$ %
Variability model	$N(\mu, \sigma)$, $\sigma = 0.5\mu$
Feeding model	$V = 3348.83/(x^2 + 840.676)$
Time of trials	100 times

Table 3.1: Simulation parameters for feeding time measurement.

the position estimation method's successful estimation of the desired area for power feeding and the UAV approached the area where the transmission efficiency exceeded 50%. The blue zone, "Over 10%", means that the UAV approached the area where the transmission efficiency would have exceeded 10 % but could not reach the desired area. The yellow zone, "Neutral", the UAV moved closer to the sensor node but was unable to achieve a clear improvement of efficiency. The red zone, "Failure", means the UAV moved farther than the initial position where the distance from the sensor was over 100 cm. The gray zone, "Calc Failure", only occurred in the least squares approach. The least squares method could not reach the reasonable value since it would never converge by iteration. In that case, the UAV would be unable to estimate the next position, therefore, reattempting from a non-efficient measurement would be required. A significantly small d value, such as 10 cm, produced many failures and the UAV rarely reached the desired area, in both the direction based and least squares approach. The direction based approach failed more frequently, at any value of d, compared to the least square approach at any d. This means that the direction based approach is unstable and may cause unexpected slowing. On the other hand, the position estimation results obtained by the least squares approach were quite accurate, especially when d was larger than 30 cm. However, with $d = 10$ cm, too many "Calc Failure" were observed. The value of d should be set to value greater than 20 cm, in order to avoid retries and longer feeding time. A larger d produced a better success rate in this simulation, however, a larger d may also cause the UAV to make unnecessary moves, which is inefficient for shortening the power feeding time. Therefore, intermediate d around 30 cm is most appropriate, since the UAV achieves mostly over 10% efficiency in the least squares approach.

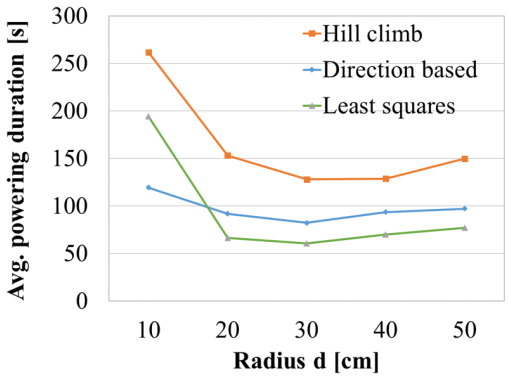

(A) Average performance

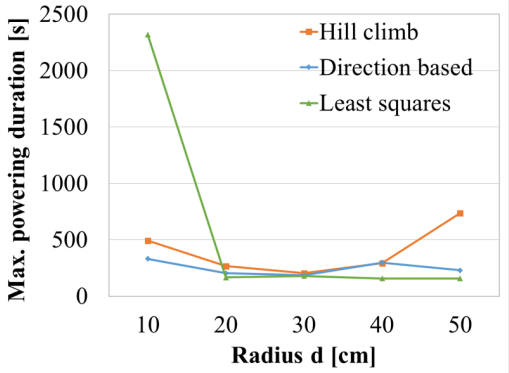

(B) Worst-case performance

Figure 3.13: Feeding time evaluation

3.4.3 Power Feeding Time Evaluation

The eventual goal of position estimation is to shorten the power feeding time; therefore we compared the completion times of the 3 methods. In this simulation, we measured the time needed to supply the target amount of energy to a sensor node. The target amount of energy was set to 3.24 mJ. This was assumed to be adequate in order for the eZ430-RF2500 sensor node to continue sensing data every hour for a day without wireless communication (0.135 mJ x 24 hrs.). In our scenario, the sensor node stores the sensed data locally and sends it to the UAV, which approaches the node for power feeding; therefore, the data would not be uploaded in the typical manner with regard to sensing activity. Note that the large part of agricultural sensing systems, such as soil moisture sensing, does not require frequent sensing, since these environmental conditions do not change radically in a short period of time. Measurements taken at hourly or less than hourly intervals will suffice, and thus, a large amount of energy is not needed for sensing. In this evaluation, the movement speed of the UAV is 10 cm/s and the UAV is required to stay at one measurement position for 1 s in order to retrieve data from the sensor node. Note that the time consumed while moving and measuring was accounted for in the result. The initial position of the UAV is randomly chosen at 80 to 120 cm

farther from the sensor node. We repeated the simulation 100 times for each method with a different value for d. In this evaluation, only the time for the single sensor node was measured because we assumed that another sensor will be located much farther from the target sensor node; therefore, it was considered infeasible to feed power to multiple sensor nodes concurrently. Therefore, the UAV is required to conduct power feeding on a one to one basis. Then, the operation can be simplified as an iterative process of power feeding a sensor node. Note that the interval between soil sensors is typically a few dozen meters, due to soil parameters, such as soil moisture, being the same within the range of a few meters; therefore, high density measurements will not be required most of the time. Additionally, if we consider situations where the sensor nodes are located within a very small area, where it is possible to power feed multiple sensors, the strategy should be revisited. In such a scenario, a feedback fusion mechanism should be introduced. Our proposed method was not designed for high density sensing scenarios.

Next, we gathered the obtained results and determined the average and worst performance. As shown in Fig.3.13, both trilateration-inspired approaches generally outperformed the hill climbing method while the least squares approach had the worst performance when d was smallest (10 cm). The bad performance of the least squares method with $d = 10$ cm is probably due to the large amount of retries triggered by calculation failures. As mentioned, a small d value would not produce meaningful measurements; therefore, it should not be set smaller than 20 cm. According to the average performance results, the best performance for every method, was given by $d = 30$ cm. Note that the hill climbing method with appropriate d should be better than just relying on GPS navigation. If GPS estimates the position with a random error of a few meters, this would be almost equivalent to the hill climbing method with $d =$ several meters, in which the UAV randomly moves in incremental steps of a few meters, while it is controlled by feedback. This should not perform better than hill climbing method with $d = 30$ cm and trilateration-inspired methods and when energy consumption for feedback is not as significant as losing an opportunity for efficient power feeding. For example, if the maximum feeding power is 1 mW, 1% efficiency improvement earns 10 μW gain. According to the radius size evaluations, expected values of efficiency improvement by the trilateration-inspired methods are around 45 % and 31 % with least-squares and direction based approach respectively; and 0.45 mW and 0.31 mW gain are expected. As required energy for a feedback is 0.235 mJ, sending feedback should give larger return than its energy consumption. By comparing the 2 trilateration-inspired approaches, when reasonable d was set, the least squares method achieved the best performance, on average, and also outperformed the other methods in the worst-case scenario. The reason why the direction based method was time consuming, and sometimes struggled to reach the desired feeding point, was related to the boundary issue mentioned in 3.3.2. In conclusion, the least squares approach with 30 cm radius was shown to be the best position estimation method because it achieved the shortest average feeding time. Under this setting, the least squares approach was 52% faster than the hill climbing method and 26% faster than the direction based method, on average. In other words, by using the proposed least squares approach, compared to the hill climbing and direction based

methods, a UAV can deliver a larger number of sensors, by approximately 110% and 35%, respectively, in the same amount of flight time.

3.5 Conclusion

In this paper, we discussed how to navigate a UAV to a desired power feeding area by using sensor node position estimation. First, we defined the model based on measurement process implementing a microwave power transfer system. Secondly, we described the candidate methods for navigation. The hill climbing method is the simplest baseline strategy. Our proposal was to use trilateration-inspired methods and 2 variations of this method were implemented: the direction based approach and the least squares approach.

The former approach relies on a heuristic assumption, which holds that the intersections of 2 circles will be concentrated in the direction of the sensor node. While it can generally outperform the hill climbing method, as we showed through simulation, it can occasionally take too much time for power feeding. The later trilateration based approach was proposed in order to solve the direction boundaries issue of the direction-based approach. Instead of counting intersections, it estimated the location in order to minimize measurement errors, using the least squares method implemented in GPS. It achieved better performance than the direction based approach as long as the size of the measurement circle was appropriately chosen. In our simulation, the reasonable size was 30 cm but revisiting this value is recommended when the power feeding model changes. With this setting, we accomplished power feeding 52% faster than the hill climbing method and 26% faster than the direction based approach. This improvement will contribute to making UAV energy delivery to even more sensor nodes possible, in a single flight and, additionally, to even less UAVs required to cover an entire sensing field.

In future work, we plan to implement the UAV assisted microwave wireless power transfer system and navigation method in order to conduct testing in actual farming fields. By using data from actual UAV operations, we will be able to make more accurate transmission efficiency models and evaluate various factors such as UAV positioning errors. Since UAVs will be exploited for various purposes, reasonable coordination with other tasks, such as seeding, scanning and spraying should be considered; therefore, in future work, we will also discuss how to prioritize tasks that include power feeding for the purpose of achieving synergetic multi-tasking.

Chapter 4

Design of Soil Monitoring Networks and Thin-Film Soil Moisture Sensors

Figure 4.1: 2 types of soil moisture sensors. (Left) Tube shape: SenSprout Pro M series, (Right) Board shape: SenSprout Pro I series

4.1 Introduction

Table 4.1: Comparison of 4 versions of SenSprout Pro sensor nodes

Sensor node	M1	M2	I1	I2
Probe shape	Tube		Board	
Soil moisture	3 depths		2 depths	
Meas circuit	MPR-121	PIC24 CTMU		
GND layout	Shared			Separated
Soil temp.	3 depths		Not available	
Surface temp.	On probe		On board	
Wireless commun	IEEE 802.15.4, 2.4GHz	IEEE 802.15.4g, 920MHz		
Battery	D size batteries x 4	AA batteries x 2		
Packaging	Connected by cables	In single box	Probe is detachable	
Stage	Retired	Discontinued	In production	Prototype

In this chapter, designs of low-cost soil moisture profile probes "SenSprout Pro" series are presented. The first version of SenSprout Pro M1 was developed in 2015 and it updated to the second version SenSprout Pro M2 in 2016. Including feedback through experimental deployments of M1 and M2, SenSprout Pro I1 was developed and finally commercialized as "official" SenSprout Pro by SenSprout Inc in 2017. After the release, we keep working on improvements and update some designs so the latest version is SenSprout Pro I2. Table 4.1 shows summary of these versions.

As shown on Figure 4.1, M series have a tube shape and I series have a board shape. In terms of sensing ability, M series can measures soil moisture, soil temperature in 3 depth and surface temperature and I series can measures soil moisture in 2 depth and surface

temperature. The reason why I series has less sensors and depth than M series is that soil moisture in relatively shallow area gives useful information for irrigation and crop management rather than soil moisture in deep areas and soil temperatures according to feedback from users. To reduce the production cost of sensor system, narrow down the sensor variations and reducing the sensor size is necessary and focused design contributes to make system simple and easy to use. Thus, we decided to cut soil temperature sensors and reduce the number of sensors on updates to I series although extensibility on sensor variations and measurement depth is reserved.

Table 4.2: Comparison of 4 versions of SenSprout Pro gateways

Gateway	GW1	GW2	GW3P	GW3R
Main module	Android phone			Raspberry pi
Wireless commun	IEEE 802.15.4, 2.4GHz	IEEE 802.15.4g, 920MHz		
Sensor data API	API for M series		API for I series	
Applicable sensor	M1	M2	M2,I1,I2	M2,I1,I2
WAN	3G/LTE/WiFi			3G/LTE
Stage	Retired		In production	

In meanwhile, communication specification and gateway design was changed as well. As shown in Table 4.2, we have a major hardware update from GW1 to GW2: switching communication module from 2.4 GHz IEEE 802.15.4 to 920 MHz IEEE 802.15.4g. In GW1 and GW2, Android smartphone worked as gateway to leveraging various ability of smartphones like 3G/LTE connectivity, WiFi connectivity, computational resource, local storage, display, touch interface and so on. However, smartphone is not usually designed to be left outdoor situation for long time and its durability toward temperature and humidity is not enough in some situations so Raspberry pi version is prepared in addition from GW3 series. While switching from GW2 to GW3 series, we also had major software updates on firmware and sensor data API. Thus, GW2 gateways are no longer usable but M2 sensor node can be connected to GW3 gateways by firmware updates.

In following sections, firstly system overview as a wireless sensor networks is presented. secondly, soil moisture sensing mechanism and electrode design are described. Thirdly, detailed design of each version is described with calibration result and some examples of field deployments. More detail of experimental deployments is mentioned in Chapter 5.

4.2 Soil Moisture Monitoring Networks

The developed soil moisture sensor has wireless connectivity and gather data through wireless networks. Figure 4.2 shows the overview of the soil monitoring networks. In this network, sensor nodes periodically measure soil moisture and the other environmental data then upload the data to cloud server through gateway. After that, user can visualize and analyze the data on web or phone apps. The system consists of following components.

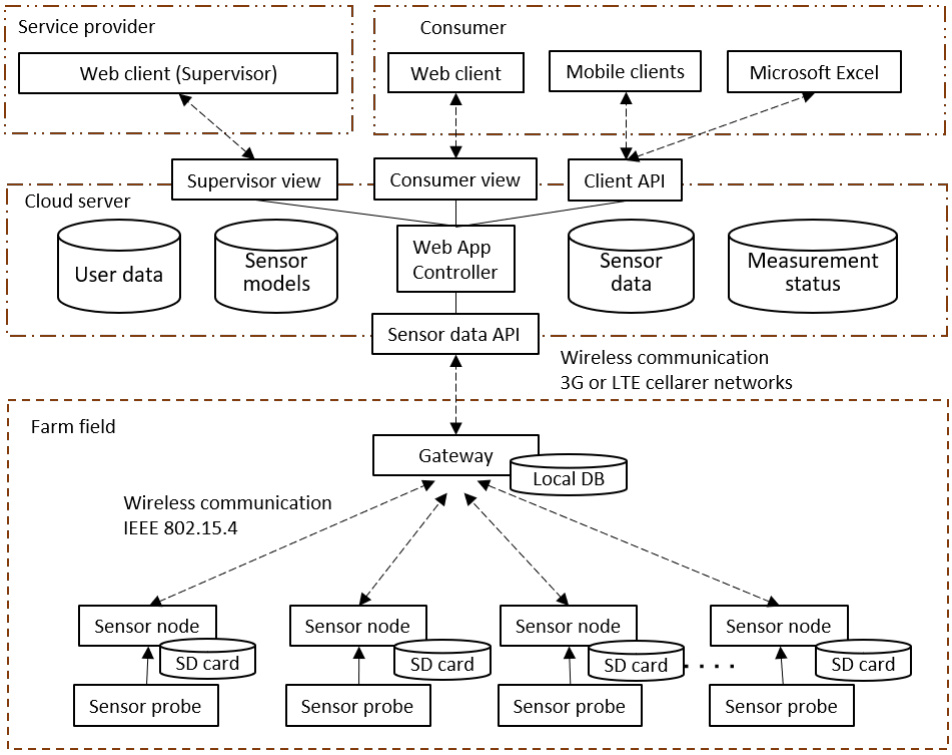

Figure 4.2: System overview of soil monitoring network

1. Sensor node: It has micro-controller unit (MCU), micro SD card, communication module (IEEE 802.15.4 or 15.4g), sensor probe. It owns sensing, temporal data store, uploads of sensor data to gateway. It is driven by batteries.

2. Gateway: It has a Android smart phone or a microcomputer like Raspberry Pi, communication module (IEEE 802.15.4 or 15.4g), mobile network connectivity (leveraging smart phone or having a 3G/LTE dongle). It owns temporal data store, uploads of sensor data to cloud server, and retransmission control. It is driven by either grid power or solar power.

3. Cloud server: It has sensor data API, client API, and view for Web apps. It owns reliable data store and data conversion for consuming. As it is built on cloud service, it has flexibility for scaling the service.

4. Client: Web browser, Android app, iOS app, and Microsoft Excel can work as client to consume the sensor data. It owns data visualization, data analysis, and handling measurement settings with simple user interface.

Sensor nodes and gateway are connected by either IEEE 802.15.4 (2.4GHz) or 802.15.4g (920MHz). IEEE 802.15.4 in 2.4 GHz is globally allowed but its communication range will be limited because attenuation by crops and the other structures are significant. Especially in Japan, the maximum transmission power is restricted to 10 mW although global standard is 63 mW and communication range would not be sufficient. Instead of

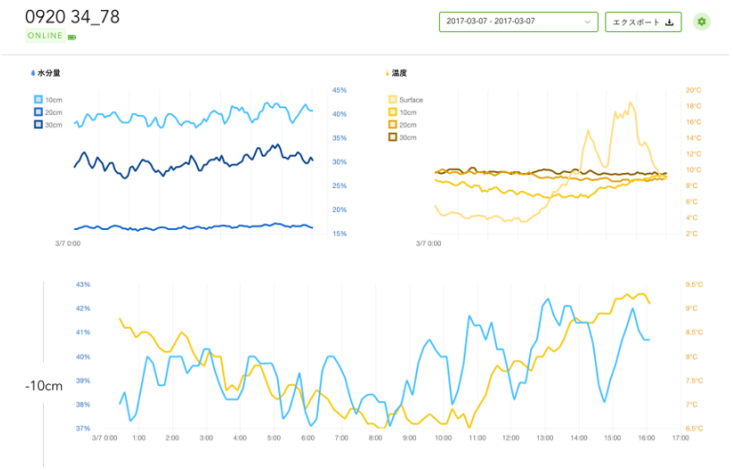

Figure 4.3: Web app for visualizing data

2.4GHz, we use IEEE 802.15.4g in 920 MHz for Japan due to its larger communication range. However, in some countries like India, 920MHz cannot be used for the IEEE 802.15.4g so we keep using 2.4 GHz for such countries. In M1 and GW1 combination, we use TWE-001 STRONG (Tokyo Cosmos Electric Co., Ltd.) communication modules but it was discontinued. From M2 and GW2 combinatino we changed to use WM-Z300 (Sumitomo precision products co., LTD.). For global market, we use XBee-Pro ZB S2B (Digi-international) instead. Considering recent developments on low power wide area (LPWA) communication like LoRa and SIGFOX, a few dozen km can be covered by a single gateway. The LPWA will be popular for agricultural sensing area because its coverage is sufficient for small to medium scale agricultural sensing and its low bit-rate is not serious matter since basically agricultural sensing does not require frequent sensing or real time sensing. Therefore, LoRa version sensor node and gateway will be added to our soil monitoring system in the near future.

The topology of the network is simply star topology in which a gateway directly collected data from all sensor nodes. In maximum 100 sensor nodes can be connected to a gateway. While multi-hop connection is available for some communication module. As initial trial, we have started from the simple topology because we still have flexibility on communication part design including switch to LoRa. Once the gateway gathered the data from sensor nodes, it uploads it to cloud server using sensing data API through mobile data communication. The cloud server stores sensor data and also manages measurements, users and sensor models. The sensor model includes properties of the sensors (e.g. available sensors, measurement depth, and sensor version) and conversion formulas for calculating soil moisture and the other parameters from raw values. On client side, an interactive web app is prepared to visualizing the sensor data (Figure 4.3). Mobile clients are available for Android and iOS as well. Also through export function on web app or directly connecting to API through PowerQuery of Microsof Excel, the sensor data can be imported to Microsoft Excel where users can run more detailed analysis.

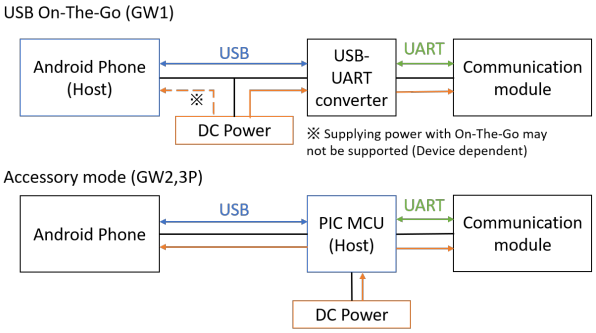

Figure 4.4: Components of Android leveraged gateway

In supervisor view, manufacturer can register sensors and gateways on the system and manage the devices. In order to backup the data, other than the cloud server, both sensor node and gateway locally store the sensor data in its SD card and its local storage respectively. If there are some missing records on the gateway, retransmission operation will run and the missed data will be resend from local storage of sensor node. Note that, due to energy consumption and bandwidth concern, retransmission capacity is restricted so if bunch of data is dropped, it is not promised that all the missed sensor data is resubmitted from sensor node.

4.2.1 Wireless Sensor Networks with Smartphone Reusable Gateways

In the network part, the unique point of the system is leveraging a Android smart phone for gateway. As Raspberry Pi version is prepared, typically microcomputer or micro controllers with 3G/LTE shield are used for the purpose. However, smartphone have been already commodity allover the world and it is available with pretty low-cost. There are various and sufficiently functional smartphones whose price is less than $ 100. Moreover, reused smartphones or relatively old smartphone should be more cheap and probably available with a few dozen dollars. If that is the case, smartphones would be the cheapest device for the gateway. When a user have unused smartphone, it will be reused without spending any cost. Another advantage is its intuitive and familiar user interface. As smartphones are globally used, most of people have already know how to use it; therefore, it is relatively easy to educate users setting up and fixing issues on smartphone based gateway rather than embedded base gateway. Considering expanding system in global scale, mobile communication availability and circumstances are various and it is costly to prepare generally usable hardware for the gateway. Usually locally available cheap smartphones are reasonably optimized for the country and cost effective rather than globally usable embedded devices.

Android OS has some functionality for combining app and embedded devices. USB On-The-Go (OTG) enable a Android phone as a USB host and phone can control the connected USB device. In GW1, we leveraged the USB On-The-Go to control the TWE-

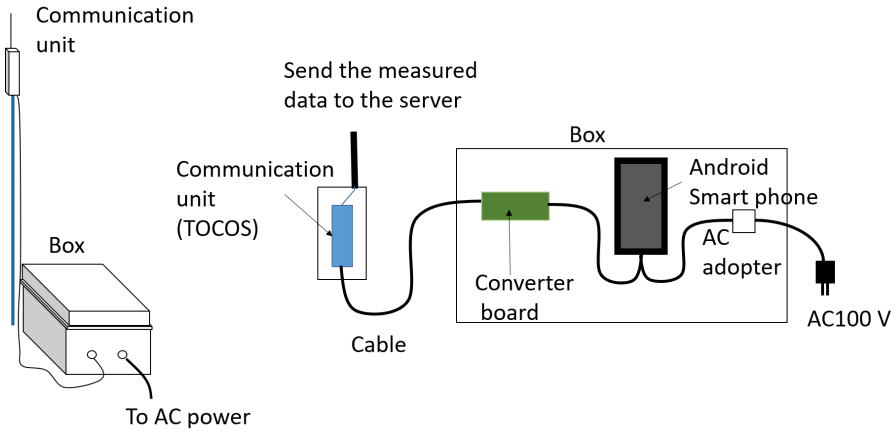

Figure 4.5: Details of SenSprout Pro GW1 gateway

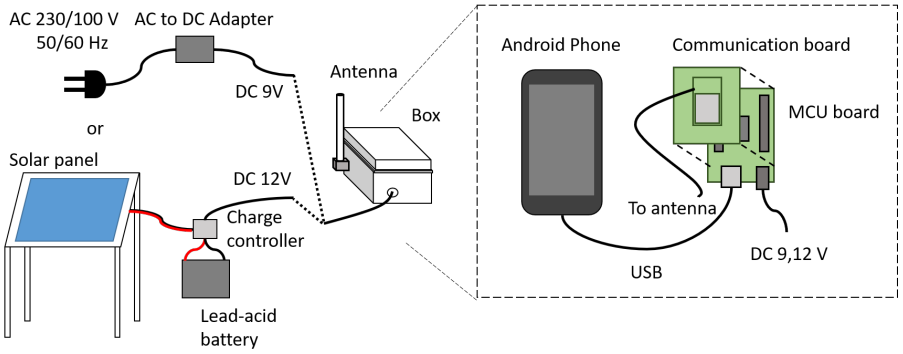

Figure 4.6: Details of SenSprout Pro GW2 gateway

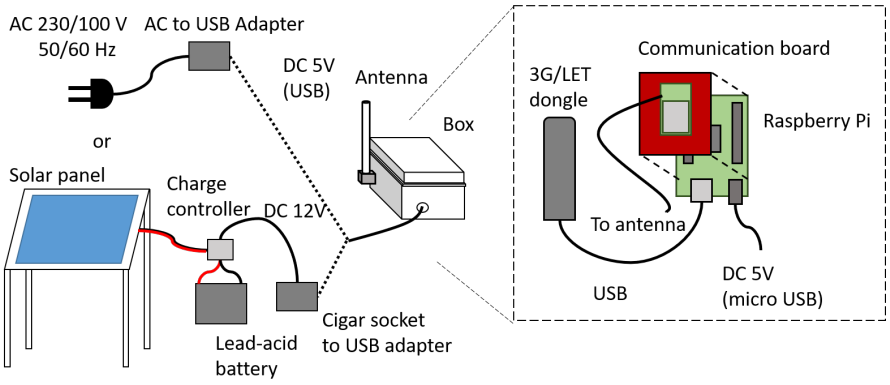

Figure 4.7: Details of SenSprout Pro GW3R gateway

001 communication module through USB to UART conversion as shown on Figure 4.5. While it enable Android to directly connect to communication module, charging Android phone from the USB device while using On-The-Go functionality is not officially allowed and has device dependency. Therefore, we used Nexus 5 (LG Electronics, Seoul, South Korea) for GW1 which seemed working with simultaneous OTG and charging.

Another option is Android's USB accessory mode. In this case, the connected device works as a USB host. In this case, powering and data transfer between connected device and Android phone are enabled simultaneously. However, in this approach additional MCU works as USB host is needed, an Microchip PIC24F Accessory Development Kit for Android is used for GW2 and GW3P as MCU board in Figure 4.6. The accessory mode is relatively old functionality compared to OTG and enabled in the most of currently available Android phones. The Android app for GW1 and GW2 is ordinary Android app which is Java based but the app for GW3P is Android native based app because the main logic for the gateway is in shared native code with GW3R. Thanks to the shared code base, maintenance and updates for GW3 series are simplified.

In the GW3R the smartphone is exchanged to Linux base microcomputer such as Raspberry Pi and Beagle Bone. The advantage of using the microcomputer board is durability to extra heat especially in summer season. In the most of the smartphone, it will be shutdown when its temperature is too high (around 60 °C) because of concern on fires from Li-ion battery. In greenhouse or tropical climate, it is possible that temperature in the gateway box overcome the maximum bar of working temperature of smartphones. By using microcomputer instead, it will be more reliable in quite hot circumstances. As shown in Figure 4.7, the version does not include any Li-ion battery and combination of a microcomputer and a 3G/LTE dongle works as alternative of a smartphone. While power supply requirements is different, other components are almost same to GW3P. Disadvantage of using microcomputer is production cost and compatibility to local mobile communication infrastructure. GW3R rely on 3G/LTE dongle for internet connectivity but such dongle is less common products compared to smartphones. Thus, we would not expect suitable dongle is locally available or there are reusable dongles so it

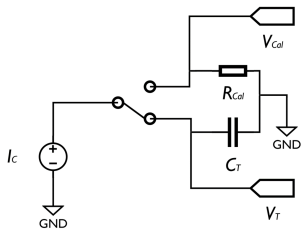

Figure 4.8: Capacitive sensing using constant DC current source

need to be preliminary prepared. In terms of cost, combination of microcomputer board and 3G/LTE dongle is not very competitive quite cheap smartphones. In conclusion, smartphone version (GW3P) and microcomputer version (GW3R) should appropriately selected with consideration about where to deploy and budget requirements.

4.3 Printed Electronics Based Soil Moisture Sensor

The sensor nodes composed by followings

1. MCU and measurement unit
2. Communication module
3. SD card
4. Sensor probe

From M1 to M2, we have many updates on hardware to reduce the board size. For example, in addition to main MCU, M1 sensor node has a capacitive sensing module and a multiplexer but they are merged to a sub MCU in M2. Also SD card is switched to micro SD card in M2. Thanks to the miniaturization, MCU board and communication modules can be in a small package which is mounted on the sensor probe.

4.3.1 Constant DC Current Source Based Capacitive Sensing

Leveraging capacitive sensing module for touch sensors for soil moisture sensing is one of the key idea to fabricate the soil moisture sensor in low-cost. Previously soil moisture measurement has been made in high frequency i.e. 70MHz for accurate measurements [23]; however, it requires high-frequency capacitance measurement circuit which is costly. On the other hand, capacitive sensing techniques are quite commonly used for smartphones, tablets and the other touch enabled devices. Thanks to the rapid growth of the touch interface, capacitive touch IC have been commodity and it became a quite cheap component. Even if measurement frequency (e.g., 50 kHz-3MHz) of the capacitive touch IC is not as high as desired frequency for soil moisture sensing, it should be applicable for practical measurements. Thus, using capacitive touch IC is a reasonable option to enable affordable soil moisture sensor with intermediate accuracy.

Through the all soil moisture profile probe, capacitive sense ability mainly for touch sensing is exploited and its measurement scheme is different from the first prototype mentioned in Chapter 2. The sensor measures capacitance with constant DC current scheme and Figure 4.8 presents its circuit. In this method, a module works as constant DC current source supplies current I_C for a short term T to sensor electrodes which work as a capacitor. Then, the MCU measures appeared voltage V_T. The capacitance of the sensor electrodes C_T can be calculated by

$$C_T = \frac{I_C T}{V_T} \tag{4.1}$$

The capacitance measurement we used for prototype has a concern on influence by resistance changes on connection lines due to oxidization or temperature changes because the measurement rely on time constant $\tau = RC$. In contrast, the constant DC current scheme ensure the supplied current is not affected by line resistance changes. To measure capacitance more precisely, current calibration should be preliminary applied before the actual measurements because constant DC current may vibrate a bit from the setting. For calibration, apply the DC current to the precision resistance R_{cal} and true value of I_C is confirmed through measuring V_{cal}. In this case, I_C in equation 4.1 should be

$$I_C = \frac{V_{cal}}{R_{cal}} \tag{4.2}$$

rather than setting value. Although we collected the calibration current data, the vibration from the setting seems negligible in the most of the time so usually we do not include the calibration result to simplify the capacitance calculation. Generally, the capacitive soil moisture measurements should be done with high frequency to avoid the influence by salinity so the measurement time T which is inverse of measurement frequency is set as short as possible.

4.3.2 Thin Film Sensor Electrodes

The low-cost soil moisture sensor is enabled by printed electronics. Traditional fabrication tools for printed circuit board (PCB) is usually consider small size and it is costly to fabricate oversized PCB. As our sensor intended to measure 10 to 30cm depth by a single probe, probe size will be around 50 cm including margin and above-ground part. It is not applicable size for the most of PCB fabrication process so it would not mass production suitable. On the other hand, printed electronics enables roll to roll fabrication which is pretty efficient to fabricate large electrical circuits on flexible substrates. In roll to roll, all the process shown below is done in mostly automated print and etching machines.

1. Glue plastic film and copper or aluminum foil
2. Print designed artworks with resist ink
3. Apply etching so that metals not covered by ink is removed

4. Remove resist ink

5. Print coating pattern if needed

The fabrication techniques are used for RFID tag fabrication and contribute to make it cheaper. The role size is usually over a meter so it is applicable for our sensor electrodes. Although our production amount have not been enough for getting benefit from roll-to-roll fabrication yet, it should contribute to scaling the sensor productions and delivery in the future. The sensor electrodes for our soil moisture sensor is designed to exploit the potential of the printed electronics.

Since we are relying on capacitance base soil moisture sensing, sufficient size of sensor electrodes need to be reserved because tiny capacitance (e.g. a few pF) is difficult to be measured precisely. As far as measurement frequency is not high (Less than 100MHz), size of the electrodes decides the maximum capacitance which occurs under fully wet condition like in the water. The electrode pattern affects to the minimum capacitance which occurs under fully dried condition like in the air. Detailed pattern such as inter digital capacitor contributes the minimum capacitance larger but the maximum capacitance is not very different from the capacitor composed by 2 plates. Hence, regardless of the electrodes pattern, electrode size is the most important matter for designing the sensor electrodes. In our sensor probe, the electrode height is 25 mm for all models and width is 55, 70 and 35 mm for M1, M2 and I series respectively.

4.4 Prototypes of Soil Moisture Sensor

Although basic design and fundamentals of our soil moisture sensors are not much different in each version but detailed design for each sensors are different and affect to sensor characteristics. We had large hardware updates from M1 to M2 on sensing module and another updates from M2 to I series on sensor probe design. Eventually M1 and I1 have almost no shared components and they required different version of gateway GW1 and GW3 respectively. On the other hand, M2 is still operable under GW3 gateway since its logging part is mostly identical to I series. In following discussion, the design of M1 is explained as a start point and updates on hardware of sensing module are mentioned for M2 . Design changes on probe shape is main topic for I1 and comparison between shared GND design and separated GND design is demonstrated through minor updates from I1 to I2.

4.4.1 SenSprout Pro M1

Sensing Unit Design

As shown on Figure 4.9, the sensor node consists of a MCU board, a battery box and communication unit. The sensor probe is connected to MCU board by 1.5c coaxial cables. Even if the measurement signal is not very high to require coaxial cable but usually coaxial cables have stable capacitance compared to shield cables under temperature

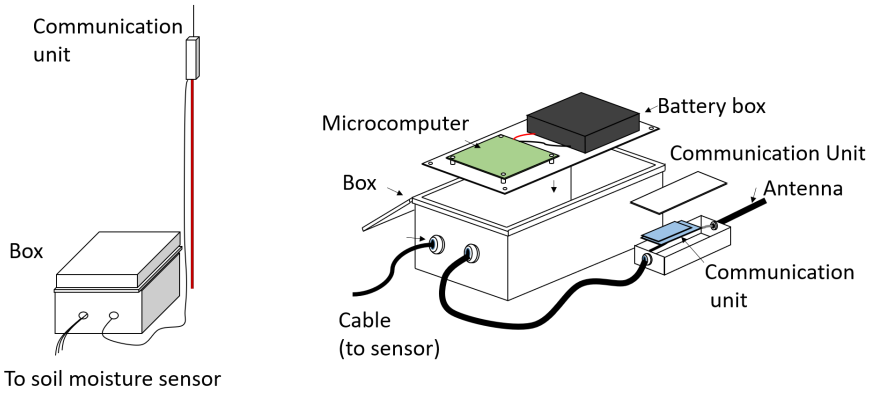

Figure 4.9: Overview of SenSprout Pro M1

changes. The power supply is 6V DC and covered by 4 D cell batteries connected in series. The power consumption of the sensor node is about 1 mW and it will be operable for a year with the batteries. The communication unit contains TOCOS STRONG (Tokyo Cosmos Electric Co., Ltd, Tokyo, Japan) for IEEE 802.15.4 (2.4GHz) communications. The communication range is about 1 km from the gateway. The sensing interval of the sensor is set to every 1 hour so hourly data is uploaded to cloud server.

The main MCU for the M1 sensing unit is LPC1114 (NXP Semiconductors N.V., Eindhoven, Netherlands) and The sensing unit have a capacitive sensing ability provided by a proximity capacitive touch sensor controller MPR121 (NXP Semiconfuctors N.V.). The MPR121 measures capacitance by aforementioned constant DC current scheme. Measurement frequency is set as 62 kHz. Although MPR121 provide 3 measurement frequency options (31, 62 and 125 kHz), we chose middle frequency because of the finest resolution on voltage measurements. Through preliminary experiments, capacitance of the sensor probe will be from 40 to 1000 pF and middle frequency is the best choice in this range. As mentioned before, higher frequency is better for soil moisture measurement to avoid influence by soil electrical conductivity and soil temperature [23] but differences of the influence between 62 kHz and 125 kHz is not significant. Therefore, the priority of resolution of voltage measurement is higher than mitigating the influence.

We developed the thin-film soil moisture probe shown on Figure 4.10 for M1 sensor node. The probe has 4 temperature sensors (Surface, 10, 20, and 30 cm) and 3 soil moisture sensors (10, 20, and 30 cm). Note that, the surface temperature sensor set 2 cm above the ground surface indication line. The copper pattern shown on Figure 4.11 is fabricated on PET film without coating and thickness of the copper is 30 μm and the PET substrate is 40 μm. For temperature sensors, NTC thermistor temperature sensors (NCP18WF104J03RB, Murata manufacturing Company, Ltd., Kyoto, Japan) are putted on the pads created on each measurement depth. Each soil moisture sensor consist of two wide bars whose width and length are 25 and 55 mm respectively. The gap between the two bars is 1mm. The bars work as a capacitor and its capacitance reflects permittivity of touching medium such as soil. The wires connected to each sensor is gathered at the

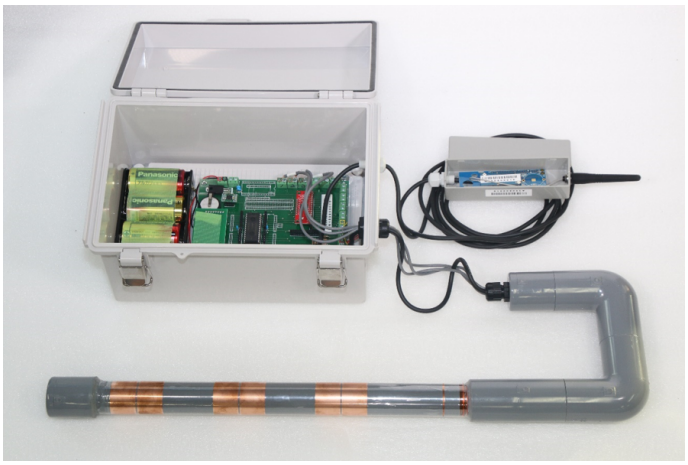

Figure 4.10: Soil moisture sensor SenSprout Pro M1

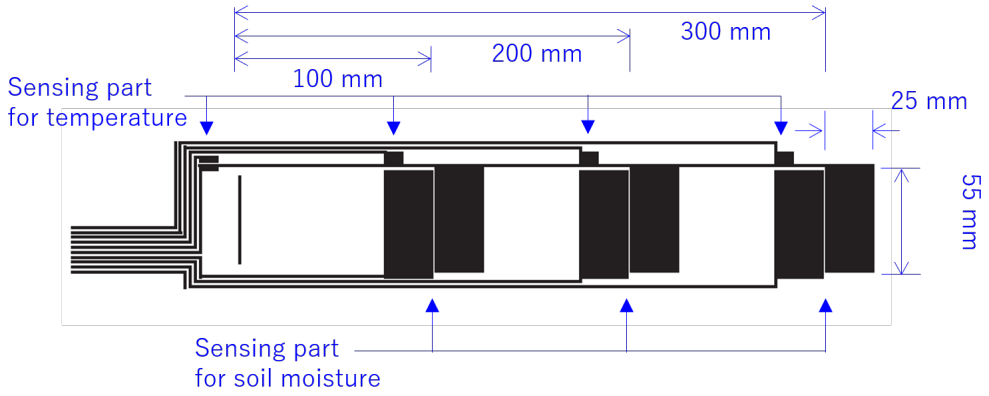

Figure 4.11: Sensor electrodes design for M1 probe

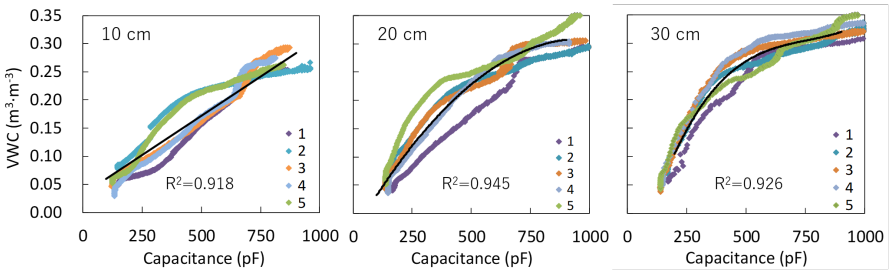

Figure 4.12: Sensor calibration result for M1 probe

end of the film with 2.54 mm pitch so that it is easy to attach a connector for flexible circuit film. The sensor film is rolled on a PVC pipe whose diameters are 32 mm (outer) and 25 mm (inner), then, covered by a 50 μ m (after shrinking) PET heat shrinking for waterproofing. The bottom edge of the PVC pipe will sealed with silicon sealant.

Sensor Calibration

Volumetric water content (VWC) is most common format for indicating soil moisture level. Its definition is water volume per unit soil volume and its unit is m^3m^{-3}. Therefore, the measured capacitance need to be converted to VWC. Usually, empirically obtained equation of relationship between permittivity and VWC is applied such as the Topp's equations [10]. For the developed probe, we developed our own empirical equations by a calibration experiments. For M series, we assumed that reference sensors indicate mostly true value and our sensors are calibrated by comparison between the reference sensor and capacitance value. In the calibration experiment for M1 probe, 5TE (Decagon Devices, Inc., Pullman, WA, USA) are chosen as a reference. The developed probe was placed in a 50 cm long column whose diameter is 10 cm and its bottom is closed by fabric membrane. The gap between column and sensor probe is filled by soil sample which was collected in greenhouse in Ibaraki prefecture, Japan and the soil was packed with a bulk density of 0.8 Mg m^{-3}. The soil sample typically considered as a kind of Andosols and is organic matter-enriched volcanic ash soil. 5TE sensors were inserted from side wall of the column at depths of 10, 20 and 30 cm which were aligned to developed sensor. After that, the column was placed in a container, which had around 5 cm ponded water. The ponded water was infiltrated into the soil from the bottom due to capillary force. The water level is manually kept to be at 5 cm during the experiment until the capacitance at the 10 cm depth was stable. The infiltrated process was repeated 5 times with the same sensor. According to preliminary verification for individual differences of sensors, the variability of sensor is negligible and iterating the process with the same sensor is no problem. The approximate equations for the three depths were estimated by the least square method from the relationships between the capacitance of the developed sensor and VWC measured by 5TE.

Figure 4.10 show the calibration results and the colors and numbers indicate the

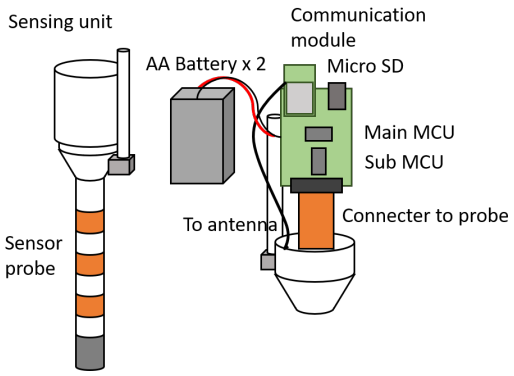

Figure 4.13: Overview of SenSprout Pro M2

repeated count. The black lines are the estimated equations through polynomial approximation.

As we could not determine which curve gave best result, we calculate approximate equations from all data. Considering the shape of curves, a linear function (4.3), a quadratic polynomial (4.4), and a cubic polynomial (4.5) are applied to 10 cm, 20 cm and 30 cm depths, respectively. The estimated equations are following where θ is VWC (m^3m^{-3}) and C (pF) is measured capacitance.

$$\theta = 2.8 \times 10^{-4} C + 3.2 \times 10^{-2} \tag{4.3}$$

$$\theta = -3.7 \times 10^{-7} C^2 + 7.1 \times 10^{-4} C - 3.5 \times 10^{-2} \tag{4.4}$$

$$\theta = 8.8 \times 10^{-10} C^3 - 2.0 \times 10^{-6} C^2 + 1.6 \times 10^{-3} C - 1.4 \times 10^{-1} \tag{4.5}$$

The coefficients of determination, R2, for 10 cm, 20 cm, and 30 cm depth were 0.918, 0.945, and 0.926, respectively. The 95% confidence interval for each derived equations were 0.050 m^3m^{-3}, 0.031 m^3m^{-3}, and 0.022 m^3m^{-3} for 10, 20, and 30 cm depth.

Each depth has a different curve shape because wiring part and shared ground part on the other depth affects to capacitance and their effects are varied in each depth. As the significance of the effect depends on the length of wires so the 10 cm sensor which have shortest wire has almost liner curve. On the other hand, sensors in 20 and 30 cm depth has more complex characteristics which need to be express with higher-order polynomials. The complexity may cause problem on measurement accuracy and ideally the capacitance and VWC should have semi linear relationship so that was considered as an issue for M series probe.

4.4.2 SenSprout Pro M2

Sensing Unit Design

For the M1 sensor node, sensing unit and probe are separated and connected by cables. Connecting cables is troublesome and have risk to be cut by farming activity or animal

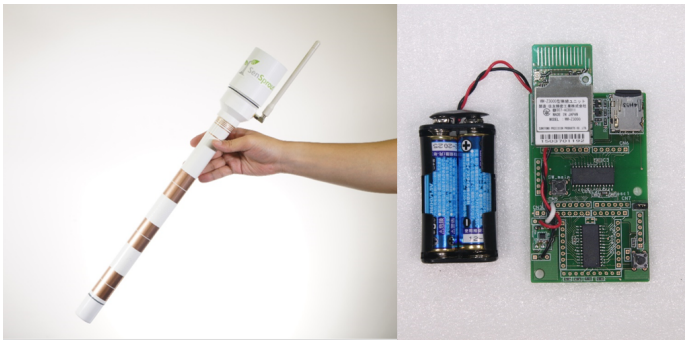

Figure 4.14: Soil moisture sensor SenSprout Pro M2

attacks. Long cables may pick up some noise or their slight characteristic changes may be reflected on the measurement result. Considering the issue, the sensing unit and probe should be unified like Figure 4.13. Minimizing the number of components and shrinking the PCB size were required to unify the sensing unit to the probe. Energy consumption was another issue on M1 sensor node. 4 D cell batteries seem too much for driving a sensor for a year. As sensors are in sleep mode in the most of the time, energy consumption in sleep mode need to be reduced to expand the battery life. Wireless communication range also need to be expanded. In M1 probe, receiving antenna need to be on line-of-sight from transmitting antenna to ensure the communication range. Thus, long antenna pole is mandatory but it also requires additional labor for sensor deployment. To simplify the installation process, antenna is attached to the box and sensor nodes should work without having antenna pole when the distance from gateway is not very far. The main reason why the antenna need to be on line-of-sight is we used 2.4 GHz microwave which is easily absorbed by water and attenuation by crop is significant.

Considering these problem, the following improvements were applied in M1 to M2 update.

- Switching MCU from LPC to PIC24 XLP
- Eliminating MPR121 and leveraging PIC's charge time measurement unit (CTMU)
- Switching communication module from 2.4 GHz IEEE 802.15.4 to 920 MHz IEEE 802.15.4g
- Unifying probe and sensing unit as shown on Figure 4.14 left

The first improvement was simply switching to the MCU which have lower energy consumption. PIC24 (Microchip Technology Inc., AZ, USA) is one of the most common 16 bit MCU and eXtreme Low Power (XLP) technology is introduced for some PIC24 series MCU. From M2 sensor node, PIC24FJ64GB002 is used and its supply current in deep sleep mode is 20 nA in minimum and 500 nA with real time clock/calender (RTCC). That is one of the lowest energy consumption for 16 bit MCU. Supply current

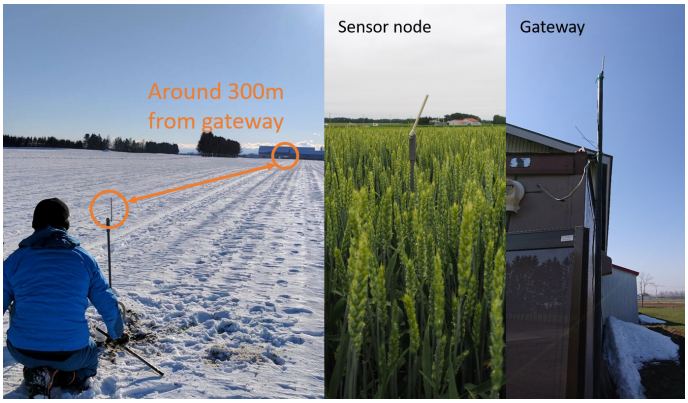

Figure 4.15: Adding antenna on the pole contributes to expand communication range

of LPC1100 series in deep sleep mode is 6 μA so it is more than 10 times larger than the PIC XLP enabled MCU. Thanks to reducing energy consumption, 2 AA batteries are enough for driving the sensor for a year when measurements happen on hourly basis. In addition to that, some of PIC24 have charge time measurement unit (CTMU) which works as constant DC current source. Thus, constant DC current scheme for capacitance measurement is enabled solely by a PIC MCU. The CTMU supplies 80 μA for 0.075 μs to charge up the electrodes and the capacitance voltage is measured. Thus, first 2 improvements were given by switching to PIC24.

Also communication module was changed to WM-Z3000 (Sumitomo Precision products Co., Ltd., Hyogo, Japan) which is compliant to IEEE 802.15.4g known as a physical layer of Wi-SUN standard. IEEE 802.15.4g using 920 MHz which is know as platinum frequency bands and has desirable characteristics for mobile wireless communication. Attenuation by crops is relatively not significant compared to 2.4 GHz and it should have better communication range. Thus, antenna pole is not necessarily prepared if the required communication range is not very long and crop size is not large. However, adding antenna on the pole should help to expand the range and ensure the communication reliability. For example, when the probe is deployed in snowy area like Hokkaido, Japan, antenna pole is prepared and the receiving antenna was remained to be out of snow and crop as shown on Figure 4.15. In this case, the maximum communication range was reached to around 300 m. Thanks to the design changes on hardware, the PCB size was reduced (Figure 4.14 right) and the sensor node became cable less design which is easy to handle during the installation.

Probe Design

The sensor electrodes design for M2 was not much updated from M1 probe as various hardware changes were applied on sensing unit and we needed to evaluate them at first. The main change from M1 design is the width of the soil moisture sensors which is expanded to 70 mm to enhance sensitivity of the sensor. Other than that, there were

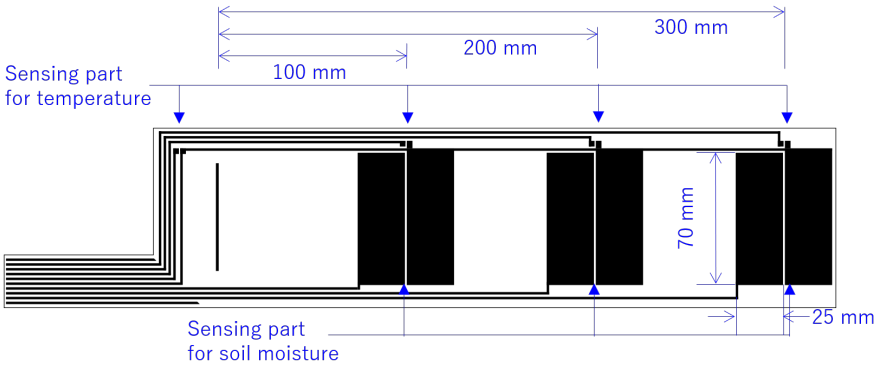

Figure 4.16: Sensor electrodes design for M2 probe

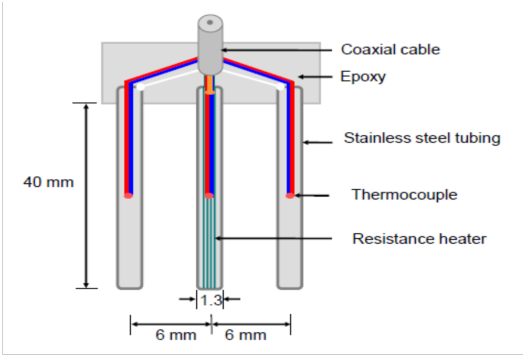

Figure 4.17: Design of thermo-TDR sensor used for calibration

minor layout changes but they were not affect to the measurement result. In M1 probe, end of the PVC pipe is closed by a bit larger cap than the pipe. The diameter difference between the cap and the body pipe larger hole need to be digged to install and it is difficult to pull the sensor from soil after measurements. Thus, we eliminated the gap by changing the diameter of the cap while it requires some additional labors.

Sensor calibration

The same approach was taken for M2 probe in which rely on a reference soil moisture sensor. In this calibration, TDR100 (Campbell Scientific Inc., UT, USA) with 3-needle thermo-TDR sensor (Figure 4.17). Note that the sensor is used as a simple TDR sensor so the thermocouples and resistance heater were not used for this measurements. TDR sensors should gave more accurate result than 5TE. The conversion from permittivity measured by TDR to VWC is rely on Topp's equation [10]. In this experiments, settings was almost same as calibration experiments for M1 probe but drying process was taken rather than infiltrating process. In this process, after filling the sample soil between column and sensor, water was added to sample soil until saturation then left until it

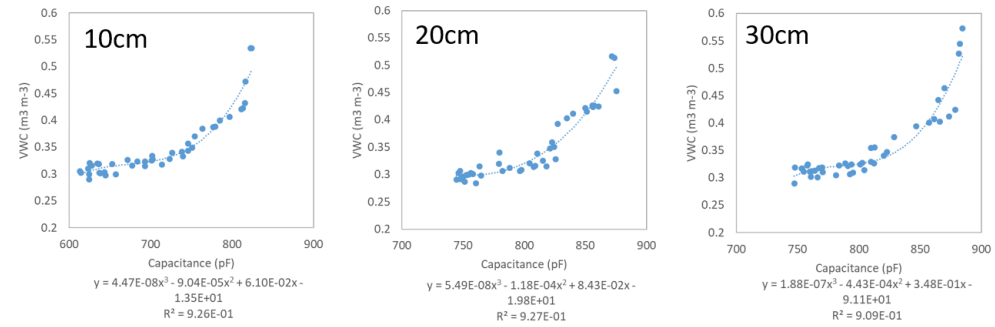

Figure 4.18: Sensor calibration result for M2 probe

dried up with periodical measurements. Even if infiltrating process is quicker than drying process, unevenness of soil moisture will be occur since soil moisture move is not very fast. Therefore, there is a concern that soil moisture around reference sensor is not same as soil moisture around target sensor although both moisture is measured in the same time. In drying process, soil moisture is gradually changing and soil moisture in same depth would be uniform. The issue of drying process is it requires quite long time for measurements as we need to wait the soil is dried up for about a month. Moreover, in room temperature, it is difficult to make soil extremely dried (a few percent in VWC) so it cannot be calibrated in dry region. However, wet region is relatively important for agriculture rather than dry region so it is practical to focus on wet region.

Figure 4.18 shows calibration result of the M2 probe and the estimated equations are following where θ is VWC ($\mathrm{m^3 m^{-3}}$) and C (pF) is measured capacitance.

$$\theta = 4.47 \times 10^{-8} C^3 - 9.04 \times 10^{-5} C^2 + 6.10 \times 10^{-2} C - 1.36 \times 10^{1} \tag{4.6}$$

$$\theta = 5.49 \times 10^{-8} C^3 - 1.18 \times 10^{-4} C^2 + 8.43 \times 10^{-2} C - 1.98 \times 10^{1} \tag{4.7}$$

$$\theta = 1.88 \times 10^{-7} C^3 - 4.43 \times 10^{-4} C^2 + 3.48 \times 10^{-1} C - 9.11 \times 10^{1} \tag{4.8}$$

The coefficients of determination, R2, for 10 cm, 20 cm, and 30 cm depth were 0.926, 0.927, and 0.909, respectively. The 95% confidence interval for each derived equations were 0.054 $\mathrm{m^3 m^{-3}}$, 0.068 $\mathrm{m^3 m^{-3}}$, and 0.101 $\mathrm{m^3 m^{-3}}$ for 10, 20, and 30 cm depth.

These equations are not applicable in dry region like around 0.1 VWC since it may cause negative VWC. In wet region, the sensed capacitance was not very stable as the capacitance is linear to inverse number of measured voltage and influence by quantization errors were expanded in higher capacitance. According to the calibration result, soil moisture sensor in different depth has different characteristics. Basically deeper sensor tended to have higher capacitance. That is reasonable because soil moisture sensor in deeper area has longer connection line and capacitance appeared on the line were included in the measured capacitance. The approximated equations are not desirably fit to the original curve in over 0.4 in VWC so calculated result in this region would not be reliable.

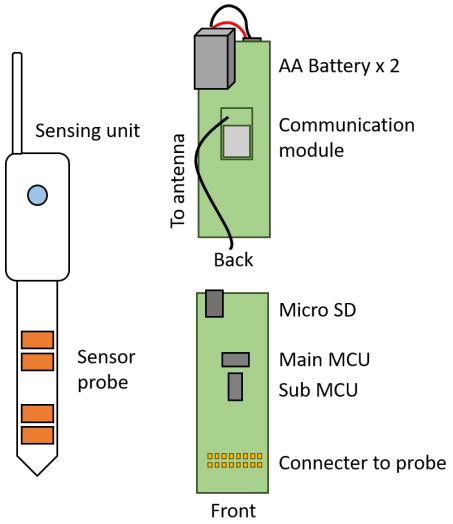

Figure 4.19: Overview of SenSptour Pro I series

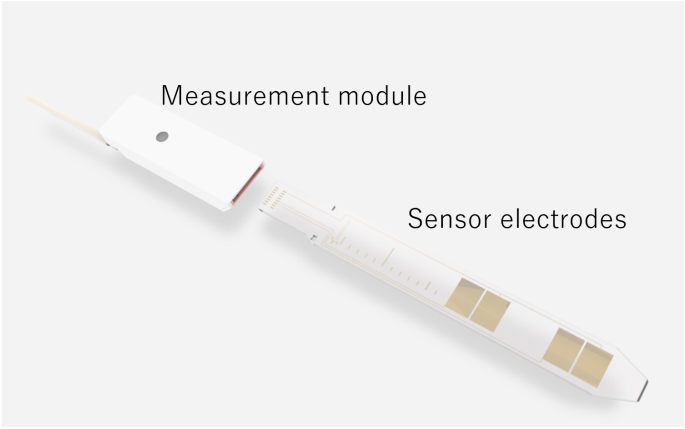

Figure 4.20: Detachable probe for I series

4.4.3 SenSprout Pro I1

Sensing Unit Design

Other than the probe shape and connector to probe, MCUs, wireless communication module, and the other components are not changed from M2 sensor node although its chassis design and PCB layout are changed as shown on Figure 4.19.The connectors are selected to enable exchanging probe without opening the chassis.

Probe Design

The tube shape probe is convenient using with earth auger and the other drill machine to digging the hole but there is inevitably gap between the sensor electrodes and hole.

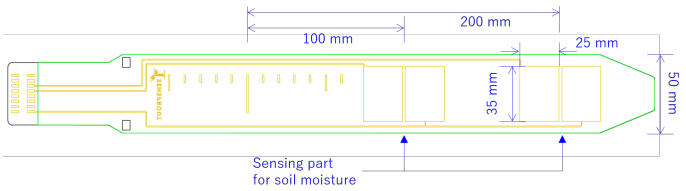

Figure 4.21: Sensor electrodes design for I1 probe

Since sampling volume of our sensor probe is not large, the sensor electrodes need to stably fit to soil. Also density of the soil touched to the sensor electrodes should be aligned to the density of surrounding soil as volumetric water contents will be different when the soil density is changed. However, it is difficult to fill soil in the gap with appropriate density and it highly depends on installation process and who install the sensor. Considering the problem we explored best practice for installing the sensor. For example, filling the mad in the hole before the installation and putting the probe can make sure the contact to soil but it changed soil structure and moisture level from original. On the other hand, if we focusing on greenhouse farming for leaf vegetables, shorter measurement depth is acceptable and it would be possible to directly put board shape structure to around 20 cm depth to soil without digging a hole if it is preliminary rotary-tilled. Therefore, we revisited the probe shape and switched to board shape and shortened the length of the probe so its measurement depth is now 10 and 20cm in default. Probably there are needs to measure soil moisture in deeper area from fruit farmers and grain farmers who focusing on tall crops like maize, solgum and sugar cane as their root will be reached deeper than 20cm; however, it is desirable to have a handy alternative for farmers who caring shorter crops like baby leaf, spinach, lettuce and the other leafy green vegetables. As the board shape probe can be inserted directly to soil, it will not damage soil structure, it keeps mostly original soil density and it is relatively easy to ensure the electrodes appropriately touched to soil. As shown in Figure 4.20, the probe is designed to be detachable and measurement depths are selectable by exchanging the probe. Currently, 10, 20cm is selected as a default. The variation of the probe will be expanded according to the feedback from farmers. Additionally, there are risks that probe would be damaged by scratches with stones and degraded by solar radiation and heat cycling so the probe should be considered as a consumable component and easily exchangeable.

The basic design of the sensor electrodes (Figure 4.21) is not very different from M series but sensor panel width is shortened to 35 mm considering the shape changes of the probe. In addition to that, lines and pads for thermistors are eliminated because in I series there is no soil temperature sensors. The main reason why we eliminated the temperature sensors is production cost. From the I1 probe, almost all the processes for probe production are machine operations rather than manual procedures. The probe is made by just gluing fabricated film with resist coating to 5 mm PET board and cutting outlines so it is much simplified from M series by its shape changes and elimination of

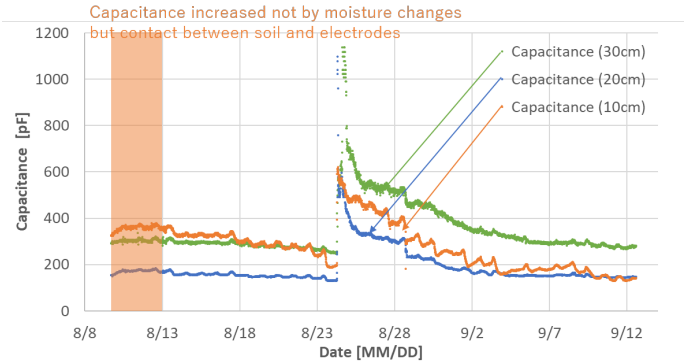

Figure 4.22: Capacitance measured by M2 probe (10 cm, 20 cm, 30 cm)

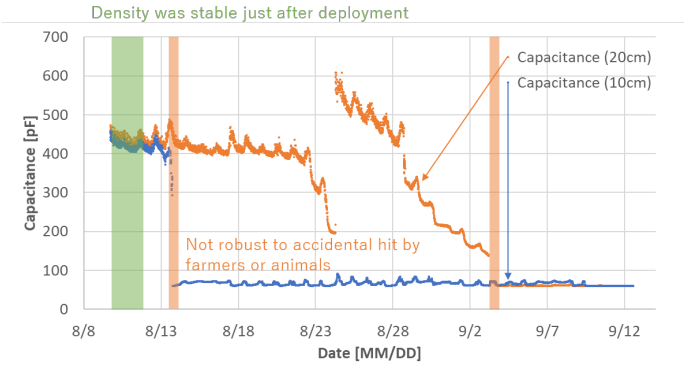

Figure 4.23: Capacitance measured by I1 probe (10 cm, 20 cm)

temperature sensors. Also, attaching thermistor on the board has concern on direct installation because the surface of the board is no longer flat. Since the sensor probe can be exchanged a probe having temperature sensors so it was decided to be skipped in the default design.

Figure 4.22 and Figure 4.22 show comparison between a M2 sensor and I1 sensor installed in the same green house and same time. The experiments have run in the farm field of Union-farm (Omitama, Ibaraki, Japan) from August 8 to September 13, 2017 and the soil is Andosols. While these sensors were installed in the same house, it was not necessarily have same soil moisture but relative soil moisture changes will be identical. In this comparison, raw capacitance is used as calibration curves of M2 and I1 are different. Note that daily vibrations on soil moisture was not reflect actual soil moisture changes but influence by board temperature of the sensor which will be eliminated using board temperature data. Figure 4.22 is soil moisture data measured by M2 probe which has tube shape. As mentioned before, it is difficult to fill the gap between the soil and hole preliminary digged for tube shape probe. Thus, in the beginning of measurements, slight increase of capacitance is observed which is not actually caused by soil moisture change

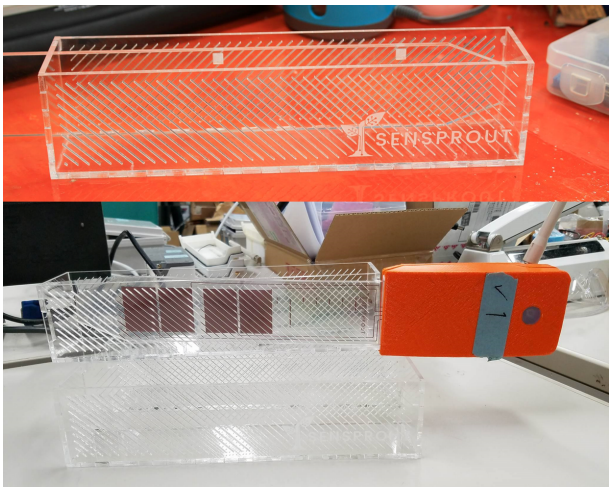

Figure 4.24: Container for calibration with drying process and inserted I1 sensor node

but density changes around sensors. The effect continues for a few week. Indeed, in this term, while no irrigation applied until August 24, capacitance increased from August 9 to August 13. However, after that, it reasonably captured soil moisture changes including saturation in shallow area and soil moisture transfer to deeper area after irrigation. Figure 4.23 is soil moisture data measured by M1 probe which has board shape. The probe is directly inserted after rotary-till and seeding. Thanks to direct insertion, the sensor immediately got stable contact with soil and increase of capacitance observed for M2 was not appeared. On the other hand, the board shape has less stiffness compared to tube shape and may bow if someone hit the sensor node. The lack of stiffness may cause lost of contact with soil by making a gap between soil and electrodes. It is possible that farmers or animals hit the sensor during measurements so I1 would have weakness on robustness. Adding some support structures or jig on probe is discussed toward the problem and it would be avoided by providing appropriate installation and management guide to users. Comparing of relative changes on capacitance of 20 cm depth, the board shape probe identically work to the tube shape probe. Even if there are several challenges on board shape like stiffness, benefit of the board shape is relatively large compared to disadvantages and it should worth introducing. Detachable sensor probes and simplification on production process is quite important to reduce the cost of sensor probe by fully leveraging the volume efficiency of printed electronics.

Sensor Calibration

From the I series, calibration process was dramatically accelerated because of the size change of the probe. The total length of a 10, 20cm probe and sensing unit is around 50 cm which can be put in a dry chamber. In order to accelerate drying process, the just size container was made as shown in Figure 4.24. In this container, the probe is inserted from a slit on the side wall and soil sample is filled to face the sensor electrodes. Around

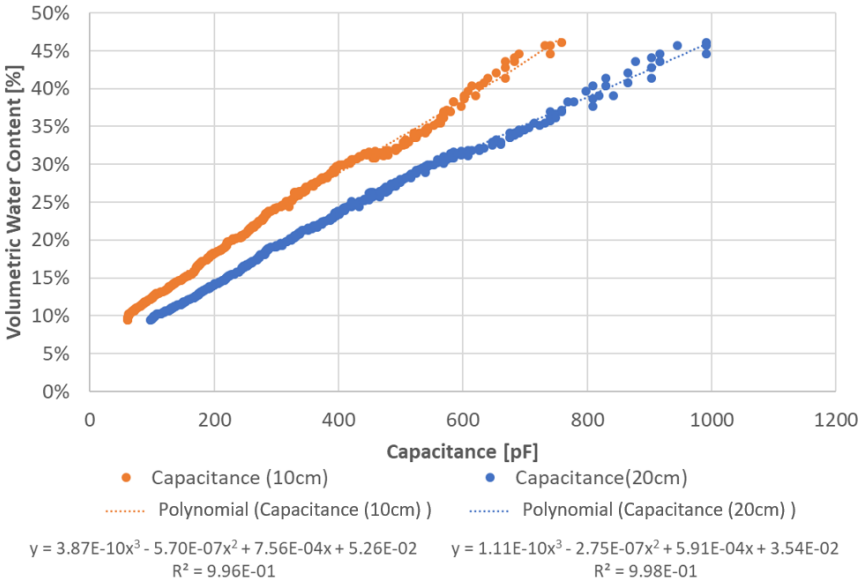

Figure 4.25: Calibration result for SenSprout Pro I1

470 cm^3 soil can be filled in the package. Opposite side of sensor probe does not face to soil sample but it should be fine because the sensor probe has quite limited sampling volume and did not respond to the water on the opposite side in the preliminary tests. A lot of slits are made on the wall to accelerate drying soil. By drying the soil in the package with 50 °C, the soil moisture can be handled from saturation to air-dried only in 5 days.

Thanks to reducing the probe size and required soil amount, ground truth VWC can be calculated from weight of the soil. In this experiment, the package was putted on a scale and the soil weight was continuously monitored in every 10 minutes. Also soil moisture measurement by the developed sensor was also running in every 10 minutes. Using preliminary measured dried weight of soil, amount of water in the soil can be calculated from current weight since the most of weight change is caused by evaporation of water in the drying process. The VWC estimation must be more accurate than using reference sensors.

Figure 4.25 shows a calibration result with Andisols. The dry density of the sample soil is 2.44 g/cm^3. The I1 sensor cannot respond to low VWC (less than 10%) because the capacitance of electrodes is stuck to 60.3 pF under the moisture level. Note that the capacitance is same as when the probe is left in the air. On the other hand, capacitance measurement no longer very stable when the capacitance is greater than 1000 pF due to quantification errors on AD conversion. Therefore, in calibration, measurements point where either sensor has the capacitance less than 60.3 pF or greater than 1000 pF were eliminated. Then, the measurable range of soil moisture is around 10 to 45 % in VWC. The estimated equations are following where θ is VWC (m^3m^{-3}) and C (pF) is measured

capacitance.

$$\theta = 3.87 \times 10^{-10} C^3 - 5.70 \times 10^{-7} C^2 + 7.56 \times 10^{-4} C + 5.26 \times 10^{-2} \quad (4.9)$$

$$\theta = 1.11 \times 10^{-10} C^3 - 2.75 \times 10^{-7} C^2 + 5.91 \times 10^{-4} C - 3.54 \times 10^{-2} \quad (4.10)$$

The coefficients of determination, R2, for 10 cm, and 20 cm depth were 0.996, and 0.998, respectively. The 95% confidence interval for each derived equations were 0.010 m^3m^{-3}, and 0.0082 m^3m^{-3} for 10, and 20 cm depth. The approximation was much better than M series because of improvements of calibration process. The I series sensor has semi-linear characteristic and it is desirable for soil moisture sensor and it was achieved by shape changes. The remaining issue is that difference between sensors for 10 cm and 20 cm are significant and still approximated equations need to be prepared for each depth. Considering expanding variety of sensing depth by leveraging detachability of the probe, universal conversion equation is preferred because calibrating all sensors for each soil types requires too much labor to scale. That was room for improvements in I2 updates.

4.4.4 SenSprout Pro I2

Sensing Unit Design

From I1 to I2 update is not apparently large but is important for accuracy improvement. Basic design and components are same as I1 even if some simplification and miniaturization are under discussion. The changes are probe design and software for measurement. In short, ground pattern design is changed from shared to individual. According to the probe design change, the CTMU setting for holding time was changed from 0.075 μ second to 0.225 μ second while input current is kept as 80 μA. It is 3 times longer than M2 and I1 but actually the setting was not tuned to board shape probe designs as it was set for the tube shape design. To maximize the resolution of voltage measurement, sufficient charging time needs to be selected considering the size of the sensor electrodes. Since width of the sensor is shortened from 70 mm to 35 mm, the maximum capacitance of the electrodes would be almost half from M2 design. Shape changes from tube to board would affect to reduce the capacitance as well. In addition to that, ground separations introduced in I2 also make the capacitance smaller. Combining these factors, we need to change the CTMU setting.

Probe Design

10, 20cm is default for I1 sensor node but 5, 15 cm 4, 10 cm are added as alternatives in I2. In the I2 update, we narrowed down the target depth to shallow area because, in Japan, greenhouse farmers are most interested in sensor devices and irrigation optimization and our main partners focus on leaf green vegetables whose root length is not very long. In I series, changing measurement depth is not costly so longer probes will be prepared afterword. Note that the 5, 15 cm probe and 10, 20 cm probe is almost same

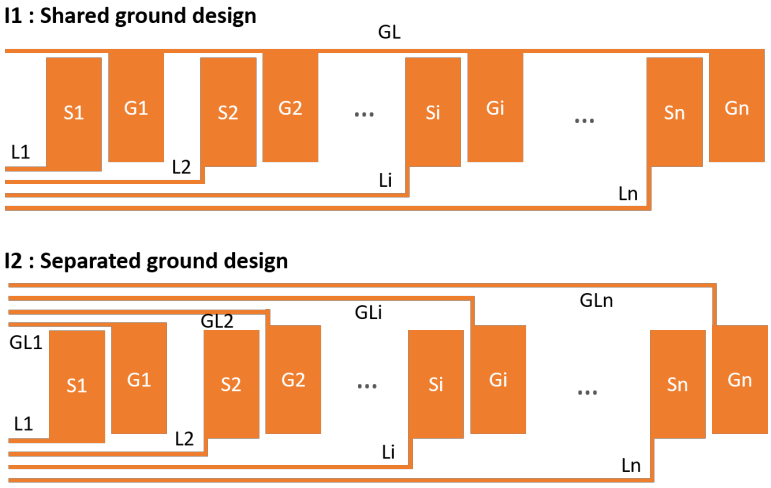

Figure 4.26: Shared ground design and separated ground design

and it is possible to use 10, 20 cm probe as equivalent of 5, 15 cm probe by installing the 10, 20 cm probe 5 cm shallow from the default indication of surface level.

From I1, the most important change in I2 updates is separating the ground patterns for each depth. Even if ground patterns on different depth are far from the sensor in target depth but it affected to measurement result. In low frequency measurement, the capacitance of the soil moisture sensor is basically depends on the size of the electrodes rather than distance from ground pattern. Therefore, considering the shared ground design as shown in Figure 4.26 measured capacitance C_i is

$$C_i = \sum_{k=1}^{n} (C(Si, Gk) + C(Li, Gk)) + C(Si, GLs) \tag{4.11}$$

when the capacitance appeared between sensor Si and ground pattern in Gk is expressed as $C(Si, Gk)$ and capacitance appeared between line Li and ground pattern Gk is expressed as $C(Li, Gk)$. Although influence by $C(Li, Gk)$s can be mitigated by making the line as thin as possible, $C(Si, Gk)$s are not negligible as the size of bar is not small. As capacitance between the other depth is included on the measurement result, soil moisture in another depth will affect to the measurement. The effect is complex and cause differences on calibration curves in each depth.

In separated ground design, measured capacitance C_i is

$$C_i = C(Si, Gi) + C(Li, Gi) + C(Si, GLi) + C(Li, GLi) \tag{4.12}$$

If the line width is thin enough, $C_(Si, Gi) \gg C(Li, Gi) \simeq C(Si, GLi) \gg C(Li, GLi)$ and only the capacitance between the sensor and ground in the same depth is observed. By introducing separated ground pattern, differences on calibration curve will be mitigated. Capacitance caused by lines is also eliminated by adding line only patterns and subtracting the measured capacitance of the line patterns [P31] but it requires too many number of ports so currently just separating ground is reasonable option in this time.

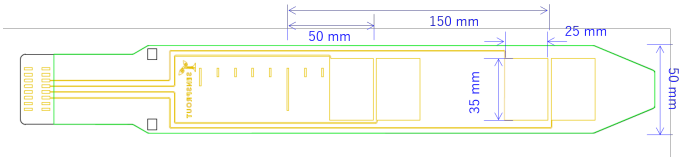

Figure 4.27: Sensor electrodes design for I2 5cm-15cm

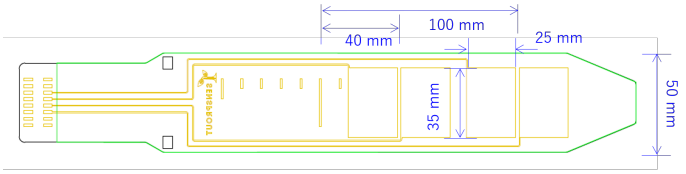

Figure 4.28: Sensor electrodes design for I2 4cm-10cm

As we reduced number of sensors from M2 to I1 update, we have enough number of spare ports on MCU to separate grounds. The MCU has 8 ports for measurements so if we take ground separated design, 4 channels of soil moisture sensors are available in maximum. Figure 4.27 and Figure 4.27 show probes for I2 with separated ground design. Their measurement depth are 4,10cm and 5,15cm, respectively. Width (35 mm) and height (25 mm) of the sensor bar are not changed from I1 design.

Sensor Calibration

Calibration have been done with identical setup for I1 with updated CTMU settings. The sample soil is Andisol sampled from a greenhouse in Mashiki, Kumamoto, Japan. It is also organic matter-enriched volcanic ash soil so this is not much different from the samples used for calibration of M1 and M2. Its dry density is from 1.88 g/cm^3 for 5,15 cm and 1.84 g/cm^3 for 4,10 cm. For the I2 probes, drying process from saturation to air-dried were repeated 2 times to confirm the repeatability.

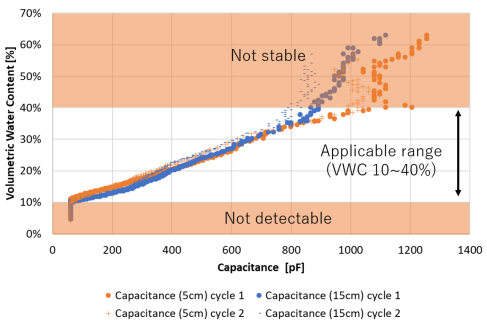

Figure 4.29: Iteration of calibration for I2 5cm-15cm

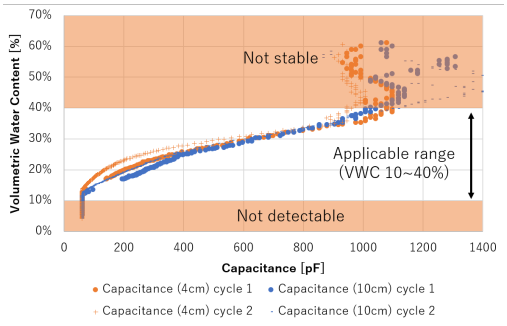

Figure 4.30: Iteration of calibration for I2 4cm-10cm

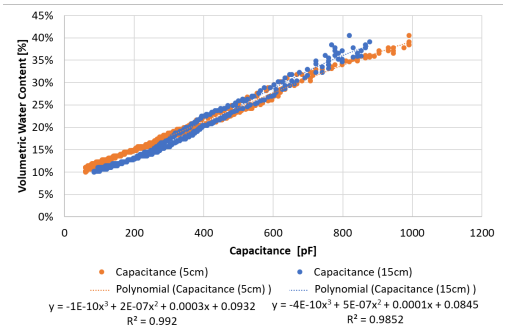

Figure 4.31: Calibration curves for I2 5cm-15cm

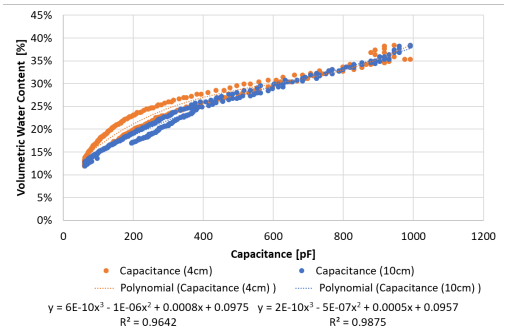

Figure 4.32: Calibration curves for I2 4cm-10cm

Figure 4.29 and Figure 4.30 show all the plot in the calibration experiments. As mentioned for I1, under 60.3 pF is not detectable and over 1000 pF is not reliable as it is difficult to do stable measurement in the area. According to the result, measurable range is from 10 % to 40% Differences between first cycle and second cycle were not significant for 5,15 cm probe but some differences can be observed on 4, 10 cm probe. That may be because density of sample soil was changed in the second cycle as the calibration is based on the assumption that the density and structures of the soil should not change during the measurement; however, there was potential to cause density and structure change by pulling water for the next cycle but more detailed investigation is needed to figure out what was caused the differences. Anyways, the differences on the cycle is not very serious matter for calculating the approximated equations .

To get approximated equation, the plots out of measurable range were filtered out and the filter result are shown on Figure 4.31 and 4.32. The estimated equations for 5, 15 cm probe are following where θ is VWC (m^3m^{-3}) and C (pF) is measured capacitance.

$$\theta = -1.11 \times 10^{-10}C^3 + 1.59 \times 10^{-7}C^2 + 2.52 \times 10^{-4}C + 9.32 \times 10^{-2} \quad (4.13)$$

$$\theta = -3.55 \times 10^{-10}C^3 + 5.32 \times 10^{-7}C^2 + 1.47 \times 10^{-4}C + 8.46 \times 10^{-2} \quad (4.14)$$

The coefficients of determination, R2, for 5 cm, and 15 cm depth were 0.992, and 0.985, respectively. The 95% confidence interval for each derived equations were 0.012 m^3m^{-3}, and 0.016 m^3m^{-3} for 5, and 15 cm depth. Expected improvement, reducing differences between sensors in the other depth, was achieved by introducing the separated ground design. The characteristics of the sensor in 5 cm and 15 cm are quite similar except highly wet range. Since capacitance is linear to inverse value of measured voltage, small differences on voltage are emphasized on capacitance.

When including plots from both of the depths and calculating common approximated equation, the equation is

$$\theta = -3.70 \times 10^{-10}C^3 + 5.46 \times 10^{-7}C^2 + 1.15 \times 10^{-4}C + 9.82 \times 10^{-2} \quad (4.15)$$

The coefficients of determination, R2, was 0.979 and the 95% confidence interval were 0.016 m^3m^{-3}, and 0.019 m^3m^{-3} for 5, and 15 cm depth. The result seems competitive toward individual approximated equations. If the similarity of characteristics is

promised, an approximated equation made for a sensor is reusable for the sensors in the other depth. When we provide more longer probe like for 40 cm depth, it will not be able to be in the dry chamber and it is difficult to quickly get calibration result. As a calibration result for 5 and 15 cm is likely applicable to a sensor in 40 cm depth, calibration with the actual long probe is not mandatory. It should contribute to simplify and accelerate calibration process.

The estimated equations for 4, 10 cm probe are following where θ is VWC (m^3m^{-3}) and C (pF) is measured capacitance.

$$\theta = 5.88 \times 10^{-10}C^3 - 1.05 \times 10^{-6}C^2 + 7.58 \times 10^{-4}C + 9.75 \times 10^{-2} \quad (4.16)$$

$$\theta = 2.34 \times 10^{-10}C^3 - 4.91 \times 10^{-7}C^2 + 5.41 \times 10^{-4}C - 9.57 \times 10^{-2} \quad (4.17)$$

The coefficients of determination, R2, for 5 cm, and 15 cm depth were 0.964, and 0.987, respectively. The 95% confidence interval for each derived equations were 0.025 m^3m^{-3}, and 0.014 m^3m^{-3} for 5, and 15 cm depth. For 4, 10 cm probe, differences between these 2 sensors are larger than the 5, 15 cm probe. That is probably because gap between sensors are too close to work individually and the sensors and it may be sensitive for condition changes around the gap. It may degrade linearity of calibration curve as well. For such short interval sensor probe, common approximated equation would not be applicable but such kind of short interval will not be taken for long probe which cannot be in the dry chamber.

4.5 Expansion to Capture Other Soil Parameters

Although soil moisture is the most attractive parameter for soil monitoring but farmers would like to know various parameters such as electrical conductivity, pH, soil temperature, water level and matric potential. Leveraging the detachable probe mechanism, the sensing unit can accept the other type of sensors without changing firmware because PIC CTMU is directly applicable for both capacitance and resistance measurement. Electrical conductivity and temperature can be measured by resistance measurements with stainless electrodes and thermistor, respectively. Soil moisture, water level, and matric potential is enabled by capacitive sensing as water content in the material affects to permittivity and it appears as capacitance. A prototype of low-cost matric potential sensor was developed exploiting soil moisture sensor.

4.5.1 Capacitive Soil Matric Potential Sensor with Gypsum Plates

The low-cost soil matric potential sensor is composed by electrodes fabricated on thin PET film and gypsum plate covering the electrodes. As same as soil moisture sensor, PIC24 MCU measures capacitance that represents volumetric water content (VWC) of the gypsum plate and the matric potential can be calculated using correlation between potential and VWC which is preliminarily measurable. Matric potential is the potential energy of water in soil and crucial factor for plant water relations. Thus, matric potential

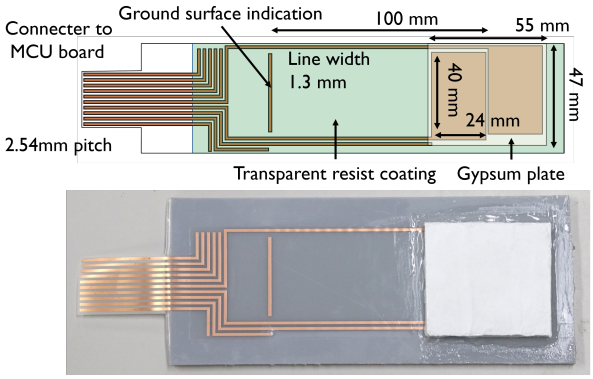

Figure 4.33: Overview of the potential sensor

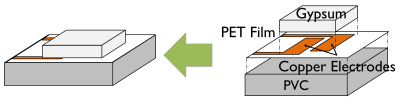

Figure 4.34: Cut model of the potential sensor

sensors are expected to play an important role in precision farming. The advantage of using matric potential rather than VWC is that the matric potential is not affected by soil types and no calibration is required. On the other hand, it is not intuitive metric and not very easy to understand its definition for ordinary farmers. In order to measure matric potential, tensiometer is usually used as it is simple and low cost; however, tensiometer requires periodical refill of deaerated water which is troublesome and it cannot be used under frozen temperature. Considering the disadvantage resistive measurement base potential sensor like 200SS WATERMARK Sensor (The IRROMETER Company, Inc., CA, USA) or capacitive sensing base matric potential sensors like MPS series and TEROS 21 (METER Group, Inc., WA USA) are commercialized. Both of them covering electrodes with ceramics having various size of pore as a porous solid. When the porous solid is putted in the wet soil, the larger pores easily filled by water but some smaller pores are not filled with water as the water is stuck in the soil. If surrounding soil become wet and has higher water potential than the porous solid, water will be moved to porous solid to fill the pores until balancing. In contrast, if surrounding soil is dried and has lower potential than the porous solid, water in the porous solid is extracted and moved to soil until balancing. Therefore, measuring amount of water in the porous solid enable to estimate water potential of surrounding soil.

However, current potential sensors are not very practical and affordable for farmers. Resistive sensing base potential sensor have issues on durability as the electrodes are damaged by repeating measurements. Even if it is inexpensive, requiring frequent replacement is not desired. Capacitive sensing based sensor does not have such problem but it is not provided with affordable prices. As a result, it have not been very common in practical fields.

We developed a potential sensor probe which is compatible to soil moisture sensor as shown in Figure 4.33. Since there are huge demands on soil moisture sensors, the compatible potential sensor will have benefits by volume efficiency on sensing unit production. As the proposed sensor is composed only by cheap materials and VWC measurement mechanism is leveraged, we believe a one-package soil VWC + matric potential sensor node can be implemented within affordable price for farmers.

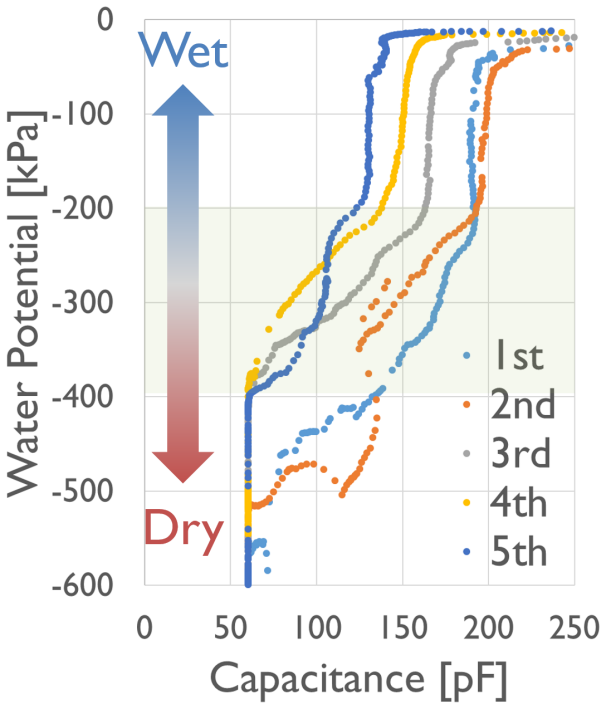

Figure 4.35: Relationship between capacitance and matric potential

VWC and capacitance have semi-linear correlation since water has much larger relative permittivity (around 80) compared to soil particles and gypsum so the VWC can be calculated from capacitance of electrodes facing to target. PIC24 MCU includes Charge Time Measurement Unit (CTMU) for capacitive sensing. We use the capacitive sensing for measuring VWC of soil and it is applicable to measure VWC of gypsum as well without any modification. Matric potential of soil can be calculated since the VWC of gypsum represents the potential of surrounding soil.

The sensor is composed by 3 layers as shown in fig 4.34.

1. 5 mm PVC board as a basement
2. PET film with copper electrodes fabricated by etching and coated with resist for waterproof (PET 50 μm and Copper 12 μm)
3. Gypsum plate (powder-water ratio 11:10).

We set our sensor and a Decagon MPS 6 potential sensor (Decagon Devices, Inc., WA, USA) in the same box filled with black soil and dried it in a dry chamber (from about 30% to 5% in VWC) 5 times. Measured water potential and capacitance have positive correlation from -400kPa to -200kPa which means our sensor should work as a potential sensor in this range. However, in the iteration of the measurements, relationship between capacitance and matric potential is changing. That is due to hysteresis of the soil and the result in 1st and 2nd times would not be very reliable. More iteration would be needed to evaluate the characteristics of the potential sensor and durability of the sensor. Currently

the fabrication is highly depends on the hand works and individual differences between sensors would be significant. As a next step, mass produced porous solids should be explored to enable consistency on the sensor fabrication.

4.6 Summary

In this chapter, design of the soil monitoring networks are discussed. The basic concept of the sensor is leveraging common capacitive touch module for soil moisture measurements. The measured data is uploaded to cloud server and delivered to users for visualization and analysis. Wireless communication between sensor node and gateway is rely on 2.4 GHz IEEE 802.15.4 or 920 MHz IEEE 802.15.4g. In the gateway, cheap or reused smartphone is exploited as a low cost computing device with mobile internet connectivity. The soil monitoring networks have frequent updates so 4 version of gateways (GW1, GW2, GW3P, and GW3R) and 4 version of sensor nodes (M1, M2, I1, and I2) have been developed. Detailed design of each versions were described one by one. Updates from M1 to M2 included various improvements on circuit design, wireless communication module, energy consumption, and packaging. Updates from M2 to I1 had drastic change on probe shape. Updates from I1 to I2 is apparently small but important for measurement accuracy and enabling common calibration setting. After the I2 updates, the developed sensor probe acquire almost desired characteristics. The approximated equation is fitted to the measurement result and its 95% confident interval is improved from around 0.05 (M1 and M2) to around 0.002 (I2) m^3m^{-3}. The possibility of applying the common approximated equation to all sensors is presented in the calibration result of I2 sensor node. It should contribute to simplifying the calibration process. Of course there are several candidates for next improvements like introducing line capacitance elimination; however, in this time, we should carefully triage the remaining issues from the perspective of cost-effectiveness. As the development reached a milestone, continuing field deployments and prioritizing remaining issues based on real feedback will be needed before deciding the next update plan. At least, expanding variation for more deeper depth, development of jig for easy and quick installation, and collecting approximated equations for VWC estimation with various soil type are in for next update.

On the other hand, adding variations on detachable probes are important to enhance the ability of the soil monitoring networks. A prototype of soil matric potential sensor have been developed leveraging capacitive sensing but EC sensor is the next target.

In terms of the cost-effective ness, the cost of a sensor node will be approximately $200 US dollars and it sale price could be around $300 US dollars. The sale price of a gateway will be also around $300 US dollars. Since the sensor and gateway includes wireless communication abilities and can measure soil moisture in multiple depths by a single probe. This is much inexpensive than the currently available soil moisture sensors for research purpose. There is potential to reduce the price when it is in mass production because of efficient production using printed electronics. Eventually, the soil monitoring

system will be delivered with affordable price for farmers and suitable for large scale deployments.

Chapter 5

Experimental Deployments of Soil Monitoring Networks

5.1 Introduction

The developed soil monitoring system is deployed allover the world to proof its usability, reliability, and practicality in various environments. All M1, M2, I1, and I2 sensors introduced in chapter 4 experienced field deployments. In this chapter, several case studies of field deployments are picked up.

1. Long term operation
   (a) Grain farming (Obihiro, Hokkaido, Japan)
2. Irrigation optimization and automation
   (a) Greenhouse farming (Omitama, Ibaraki, Japan)
   (b) Fruits farming (Hyderabad, Telangana, India)
   (c) Grain farming (Hyderabad, Telangana, India)
3. Extreme conditions
   (a) Tropical climates (Benoda, MH, India)
   (b) Frozen soil (Sinhidaka, Hokkaido, Japan)

The purpose of presenting cases in category 1 is proofing the long term operability. The most of the deployments were finished in a few months but sensors were remained in fields around 8 months for 1a and the the deployments continues over 2 years. Therefore, they are suitable for evaluate durability and reliability of sensors. In 1a, M1 and M2 sensors were used.

Cases introduced in category 2 are more practical and focus on figuring out how farmers should use the soil moisture sensors for irrigation optimization. In Japan, greenhouse farmers are interested in irrigation managements while grain farmers are not very attracted. Open field culture in Japan is basically rely on natural rain and they do not have any irrigation equipments so there is no easy way to control soil moisture. Therefore, a practice in greenhouse farming (2a) is presented. Note that M2 sensors are used for 2a.

On the other hand, in India, irrigation is crucial even for open-field culture because India is under monsoon climate. In the area, there is almost no rain in dry season but in rainy season, tons of water is delivered by quite frequent rains. Irrigation is necessary for rabi crops which are mainly grown in dry season. Irrigation is not very important for kharif crops which are mainly grown in rainy season as rain can be expected but may required in some cases. 2b was for irrigation amount optimization for mango trees and 2c was for evaluation on relationship between irrigation amount and growth of maize. Irrigation methods were drip irrigation and ridge irrigation for 2b and 2c, respectively. The exploited sensors are M2 and I1 sensors for each cases.

In category 3, we tackled to deploy sensors under tough condition in terms of temperature and communication quality. In 3a, M2 sensors went through both rainy season and dry season in tropical climate. The maximum surface temperature was 47 °C and

Figure 5.1: Deployments in Obihiro. The target crop is winter wheat (Right) and Chinese yam (Left bottom)

the relative humidity should be kept around 100 % through rainy season. In contrast, M2 sensors also experiences extremely low temperature in 3b which was -15 °C. In this field the soil was frozen over 30 cm so the sensors were no longer able to capture soil moisture but its melting can be confirmed through soil temperature measurements.

5.2 Long Term Operation

5.2.1 Grain Farming (Obihiro, Hokkaido, Japan)

Hokkaido area is kind of a special region in Japan because it is the only place where large scale farming is commonly practiced. Japanese food supply is highly rely on the crops harvested in this area although it is in subarctic zone and has quite cold winter which is not suitable for growing crops. The farmers in this area are interested in introducing technologies for modern farming. For example, some of them have a real time kinetic (RTK) GPS base station to improve GPS accuracy and enable precise navigation of tractors and leverage unmanned aerial vehicles (UAVs) to monitoring their farms. Of course agricultural sensing is attractive for them to optimize farming activity, assess risk of disease, and predict harvest amount. They mostly focus on outdoor culture and it is usually rain-fed cultivation. Even if they do not have irrigation system, understanding

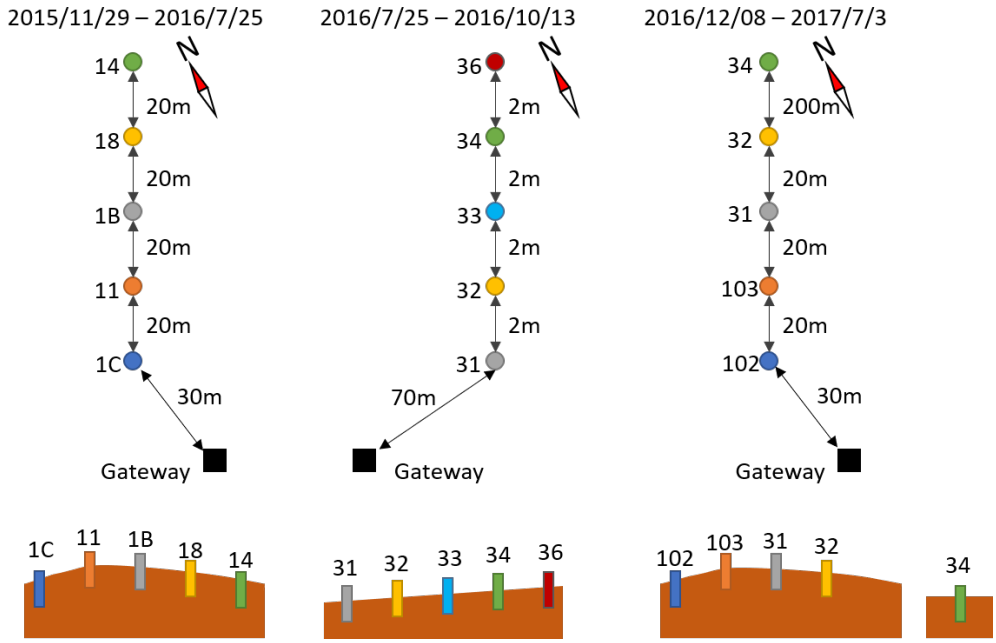

Figure 5.2: Setting of deployments in Obihiro, Hokkaido, Japan from 2015 to 2017

soil condition through sensor data is still important to improve farming productivity. Considering the background, we started to deploy prototype of soil monitoring network in 2015 at Ikemori farm (Obihiro, Hokkaido, Japan). The initial motivation was monitoring snow melting and ground water moving during the melting process which is not measurable by remote sensing. Thus, the sensors were deployed in end of November or beginning of December on a wheat field. The cultivation of the winter wheat is usually in middle of July. Besides, the partner farmer worked on Chinese yam from July to October so the sensors were moved to the field of Chinese yam which was next to the wheat field until the next sawing of the wheat. Therefore, we had following 4 deployments in the fields (Figure 5.1).

1. From 2015/11/29 to 2016/7/25 for winter wheat with 5 M1 sensor nodes and a GW1 gateway
2. From 2016/7/25 to 2016/10/13 for Chinese yam with 5 M2 sensor nodes and a GW2 gateway
3. From 2016/12/8 to 2017/7/3 for winter wheat with 5 M2 sensor nodes and a GW2/GW3P gateway
4. From 2017/7/3 to 2017/10/13 for Chinese yam with 5 M2 sensor nodes and a GW3P gateway
5. From 2017/10/24 to present for winter wheat with 2 M2 sensor nodes and a GW3P gateway

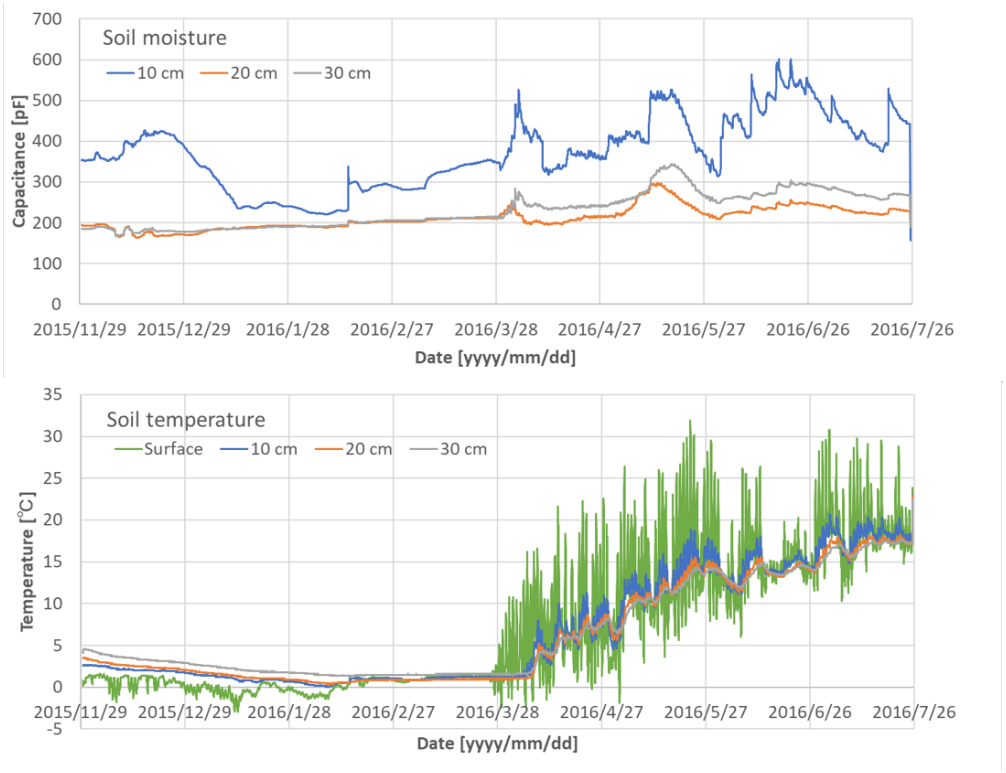

Figure 5.3: Soil moisture and soil temperature measured by M1 sensor node (Node 14)

Although we had updated from M1 to M2 but the the monitoring has been continuing for 2 years in total. The most used M2 sensor nodes have been working for 1 and a half year so it is suitable for evaluation the durability and practicality in long term operation. Soil sample was collected in the field and M2 sensor was calibrated with the soil while calibration for M1 sensor was skipped since the update to M2 was expected.

Figure 5.2 shows where the sensors were deployed in each deployments. Unfortunately, node 33 and 36 were damaged during the second deployment so they were exchanged by 102 and 103. In the third deployment, 34 tried maximum communication range so it was far from the other nodes. It was able to communicate for a month, even if it was 300 m far from gateway; however, in mid of winter, its antenna is covered by snow and lost communication. Meanwhile, the data was safely stored in local SD card.

Figure 5.3 shows a data from M1 sensor node through the first deployment. As it was not calibrated, soil moisture is represented with raw capacitance. It kept working under the snow through the winter season and succeeded to capture soil moisture changes caused by snow melting from late March to beginning of April. After that, soil moisture changes by precipitations were captured on 10 cm soil moisture data.

As shown in 5.4 Soil temperature data is also interesting to know when the melting of snow and frozen soil is ended. During the winter, the surface temperature sensor is covered by snow and until it was faced to air, its temperature will be kept around 0 to 2 °C. So the snow covering the sensor 14 was cleared in around 3/27. Soil temperature

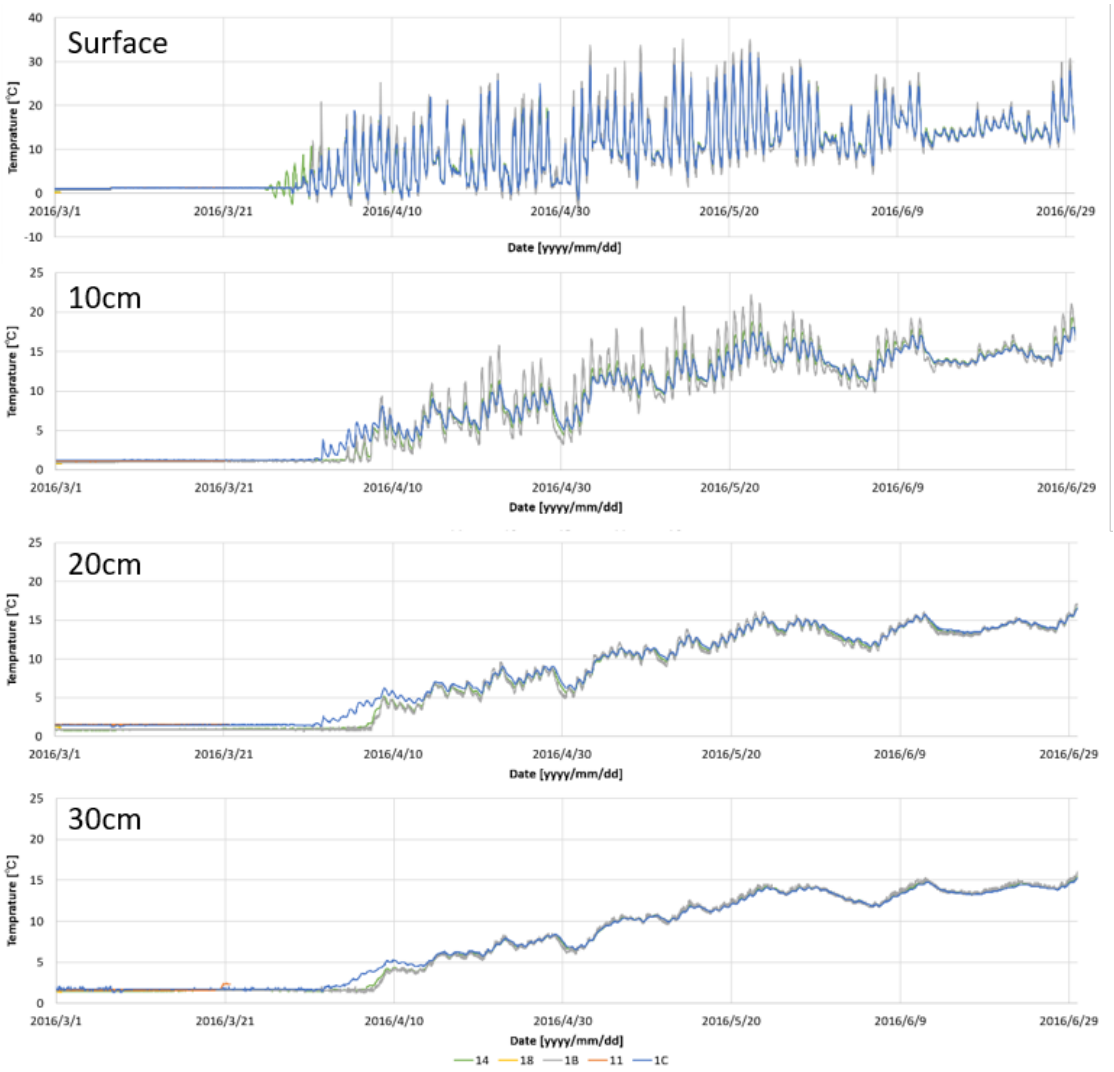

Figure 5.4: Temperature in Obihiro collected by M1 sensor nodes

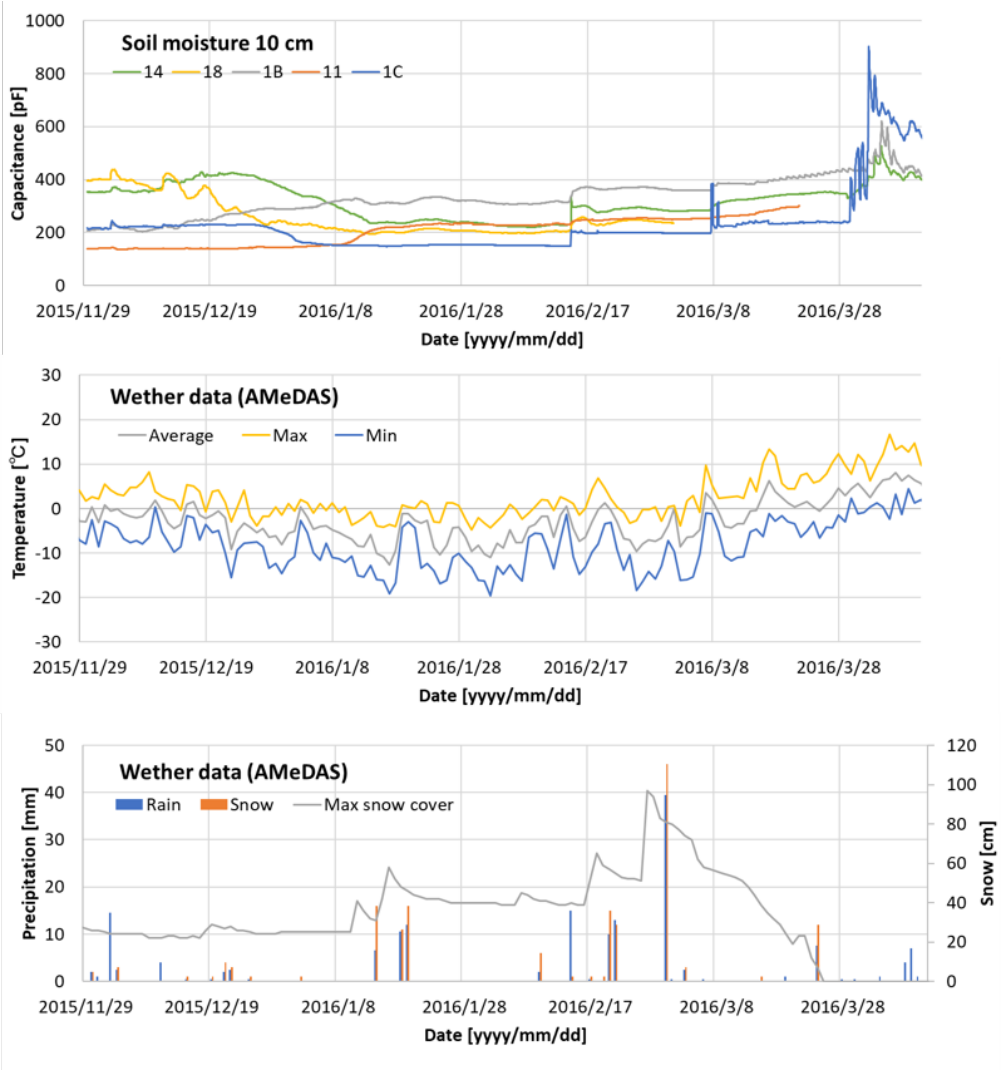

Figure 5.5: Relationship between soil moisture changes and wether conditions

is start moving from 4/6 which had about 10 days delay from melting of snow. In 2015, these area experienced huge snow in early winter which rarely happens. As thick snow covered soil before temperature was going down, freezing depth of soil was shallow than average. Therefore, the snow melting was the primary factor to determine when the temperature changes started. Comparing these nodes, melting of snow firstly occurred around node 14 but soil temperature changes happened from node 1C and for the others, it happened in mostly same timing. 1C was on the slope facing to south-west so it was easy to capture solar heating compared to others. That is why 1C experienced earlier melting.

Figure 5.5 shows relationship between soil moisture changes and weather conditions. The weather data for Obihiro area was retrieved from AMeDAS which is operated by Japan Meteorological Agency. In 2/14, sudden soil moisture change was observed while

the sensor should be under the snow and it was too early for melting of snow; however, according to the weather data, there was unseasonal rain in 2/14 rather than snowing. Thus, some of snow should melt due to the rain and the supplied water was infiltrate to the soil and the water moves were captured by the soil moisture sensors. Comparing the temperature data and when the snow started melting, The minimum temperature seems to be a key factor to accelerate the melting. The minimum temperature came in to plus in 3/30 which is almost near to the day melting observed. Also we can see a sudden soil moisture changes on node 1C in 3/7 and 3/8. These 2 days were relatively warm and the minimum temperature was around 0 °C so it also supports the assumption.

Year to Year Comparison

Thanks to deploying sensors almost in same location in 2015 and 2016, year-to-year comparison can be applied. As mentioned before the winter from 2015 to 2016 there was a lot of snow than usual and the winter from 2016 to 2017 was closer to average. Usually Tokachi area including Obihiro does not has many snow but has quite low temperature; therefore, soil freezing is significant and freezing depth would reached a few dozen cm in maximum. In winter from 2015 to 2016, soil was not fully frozen even in 10 cm as soil temperature was not be in minus while minus soil temperature was observed December and February 2017 which indicate soil freezing depth was reached to 10 cm. Comparing the temperature data, snow seemed to be cleared much earlier in 2017 as the surface temperature is start moving from 3/21 which is around 1 week ahead to 2016.

In addition to that, air temperature in March and April 2017 was much higher than March and April 2016. Interestingly, while 2017 had warmer climate, the day when the soil temperature start moving is almost same. It started moving from 4/5 in 10 cm. In 20 and 30 cm, it was more aligned except node 1C. However, there were quite cold days around 2017/4/10 and it depressed soil temperature. Indeed, that was a beginning of farming seasons and farmers in this area usually focus on planting potato. Appropriate soil temperature for planting potato is over 5 °C due to avoid some disease caused by bacteria which is active in low temperature. Traditionally, farmers just estimate the soil temperature from air temperature based on their experiences. However, it was tricky when it had vibrated temperatures like 2017. Since there were warm days on the end of March, they tended to assume soil temperature had been reached to appropriate level but actually not yet. Even worse, it was unseasonal heavy snow on 4/12 and soil temperature was remained to be low.

Thanks to monitoring the soil temperature data through the system, the farmer supporting us for the deployments postponed planting of potato due to concern on insufficient soil temperature, while the most of neighbors had been planted. After that, the area covered by snow and planted potato faced the risk of disease. Even if the soil monitoring system was not originally intended to be used for decision making on planting, it was valuable for deciding the schedule based on the actual data rather than experiences and sense.

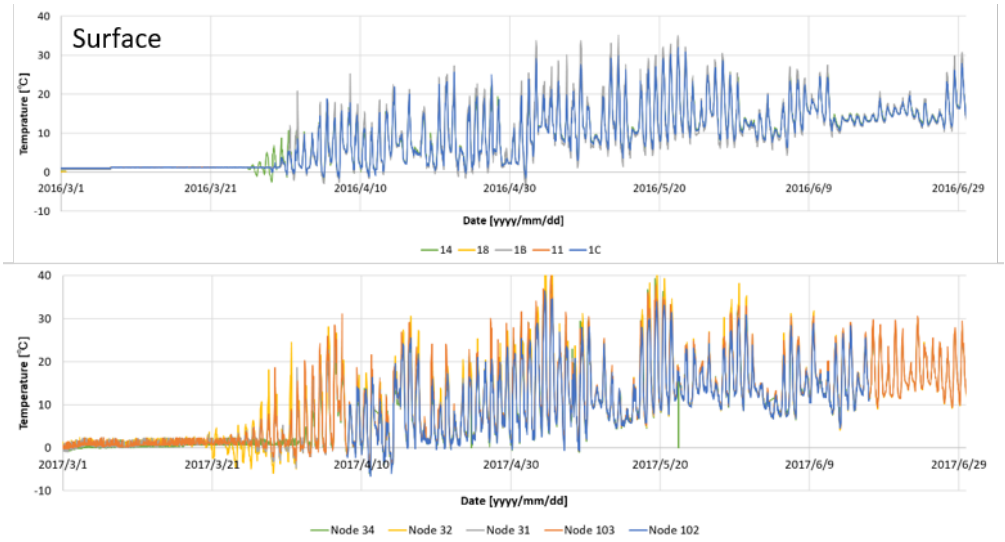

Figure 5.6: Year-to-year comparison on surface temperature

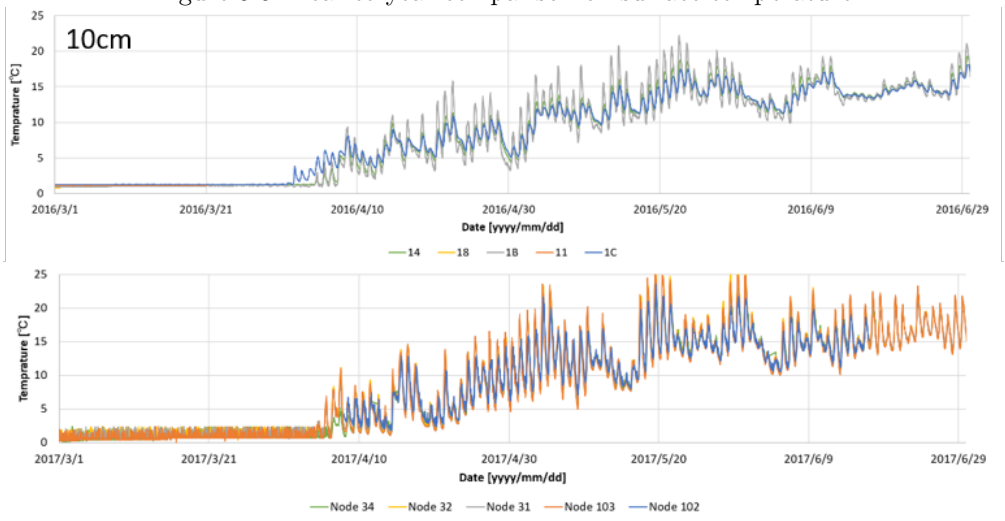

Figure 5.7: Year-to-year comparison on soil temperature in 10 cm depth

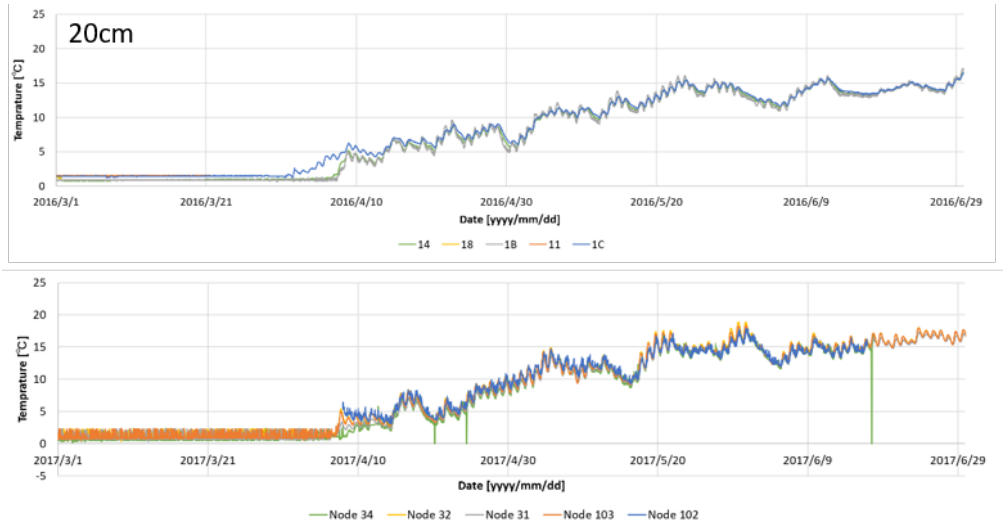

Figure 5.8: Year-to-year comparison on soil temperature in 20 cm depth

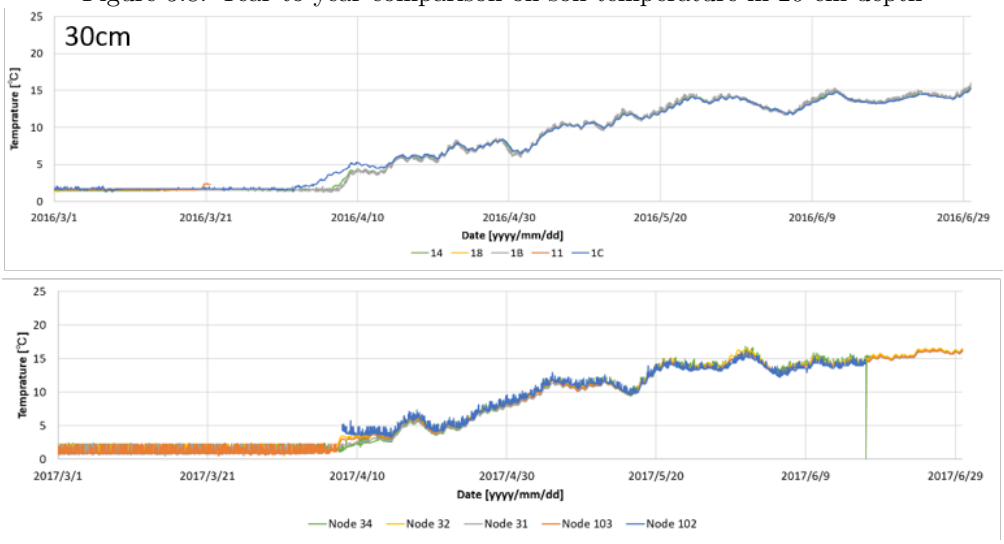

Figure 5.9: Year-to-year comparison on soil temperature in 30 cm depth

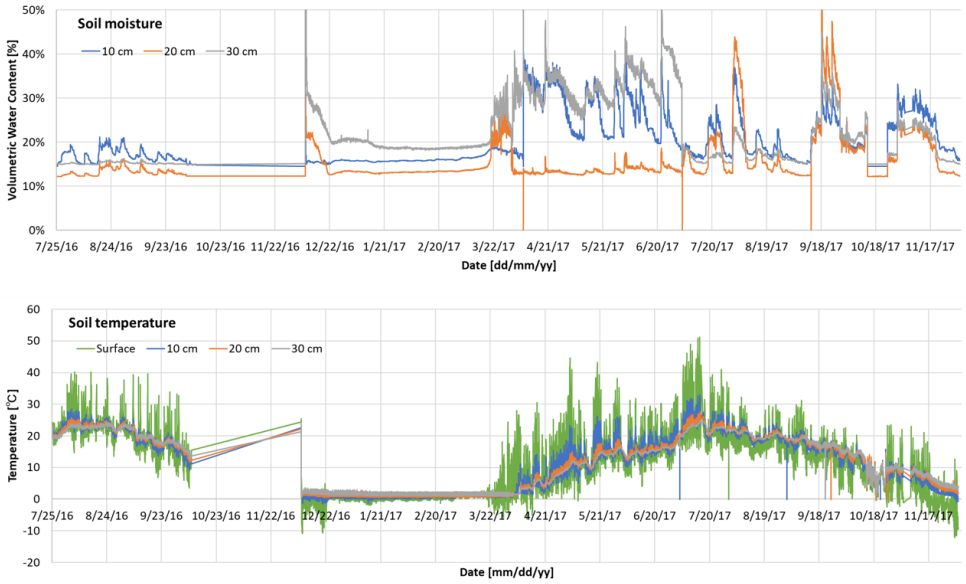

Figure 5.10: The longest operation of M2 sensor (Node 32). From 2016/07/25 to 2017/12/03

Continuous Deployments with M2 Sensor Nodes

While a firmware update to support GW3P was applied to M2 sensor nodes in April 2017, they are keep working over a year. The M2 sensor have a useful life of a year so it has been already in out of operating life. In addition to that, they have experienced freezing temperature during the tough winter which should shorten the operating life. Of course batteries are periodically changed twice in December 2016, July 2017. While the battery life is estimated to a year, we need to exchange battery before winter because working range of alkaline battery is typically from 5 °C to 45 °C but the sensor will be operated under 5 °C for this area. Under too low temperature, alkaline batteries cannot supply sufficient power and it will shorten the battery life. Therefore, we use lithium batteries instead although they are much expensive than alkaline batteries.

5.11 shows the soil moisture data in the second deployment targeting Chinese yam. Chinese yam has quite long root, which can reach around a meter, and its growth and health would be related with soil moisture. Before planting the yam, deep trenches were made using a trencher pulled by a tractor. Thanks to the trenching, the density of the covering soil where yams are planted is extremely low. Thus, it is quite easy to insert the probe but it was difficult to make sure the soil is appropriately faced to sensor electrodes. As a result, some of the sensors (36,32,31) would under estimating the soil moisture. However, relative changes of soil moisture were captured and differences of soil moisture in each depth can be observed.

Figure 5.12 shows the soil moisture data collected in deployment happened in the winter from 2016 to 2017. In the experiment, initial soil moisture level was a bit high because we tried to put mad in the digged hole before inserting the soil moisture probe

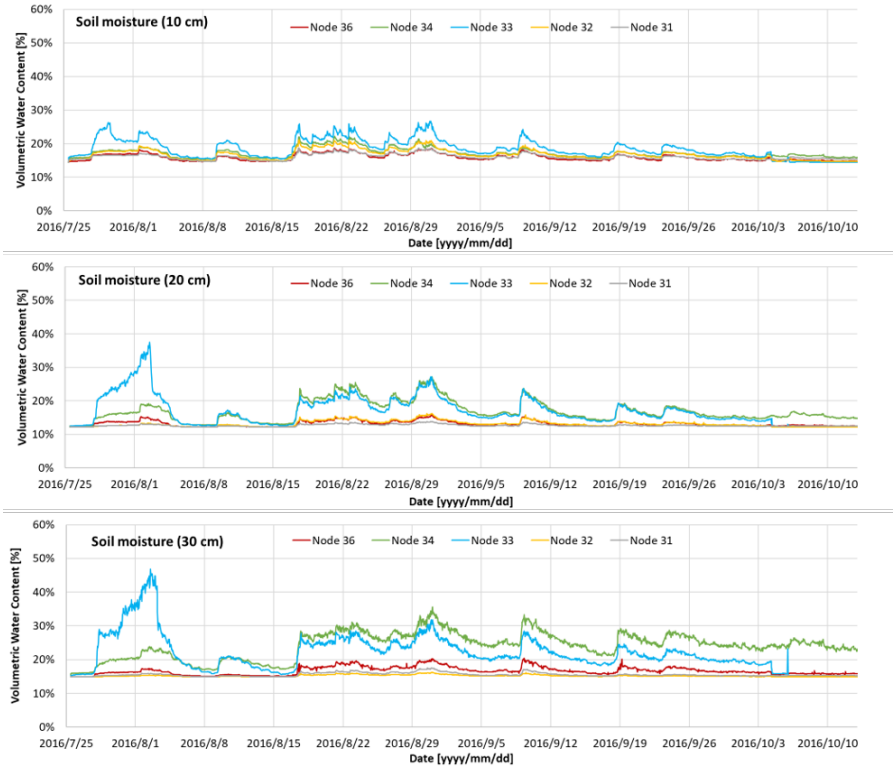

Figure 5.11: Soil moisture collected by M2 in the deployment from 2016/7/25-2016/10/13

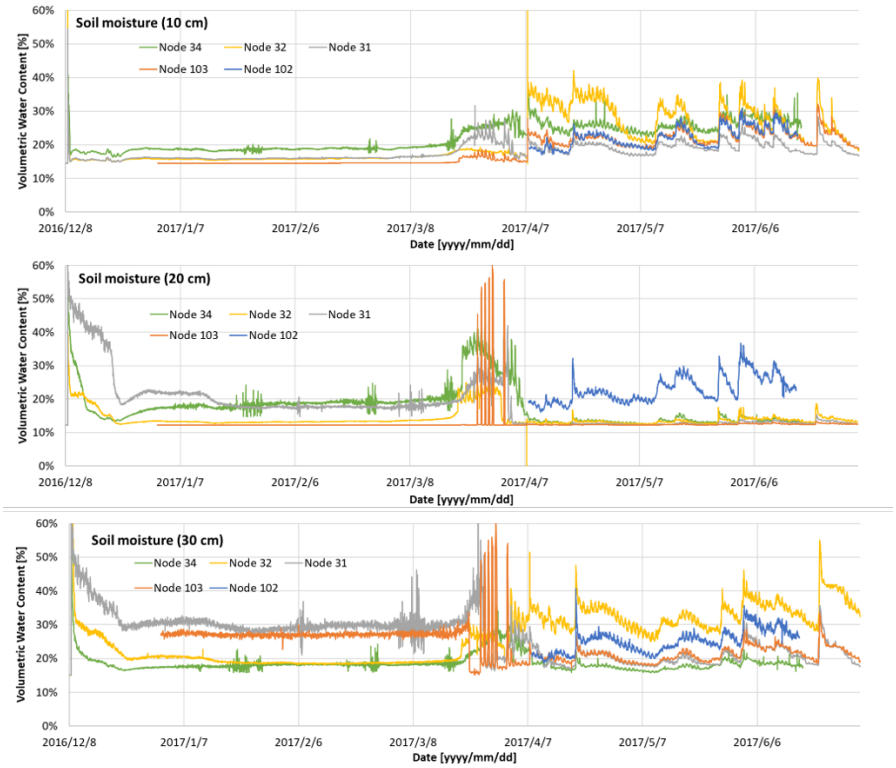

Figure 5.12: Soil moisture collected by M2 in the deployment from 2016/12/8-2017/7/7

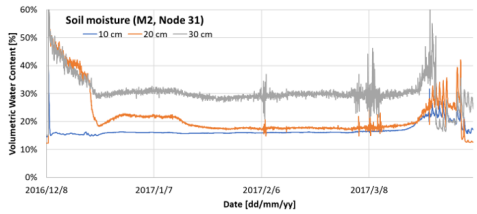

Figure 5.13: Soil moisture capture by M2 sensor node (Node 31)

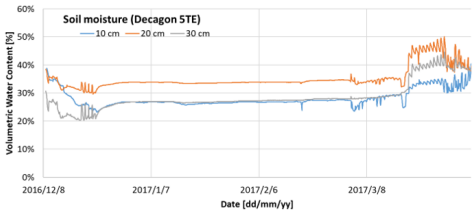

Figure 5.14: Soil moisture capture by 5TE

to make it easier to fit to the soil. It took a few weeks until the added water was spread. It kept working though a winter as well as M1 sensor node. Note that package of sensor node was miniaturized in M2 update and it was fabricated by fused deposition modeling (FDM) based 3D printer with ABS; therefore, it was not promised to be waterproof and we had some concern on it. However, it safely worked though the whole measurement period. The sensors should gave valuable information about the soil moisture changes, moving, and unevenness due to melting snow and precipitations.

At last, Figure 5.13 and Figure 5.14 shows comparison between commercialized sensor M2 and 5TE (Decagon Device Inc., WA, USA). Note that the 5TE was also calibrated with the sample soil collected in the field. While probably M2 over estimating soil moisture in 30 cm, the result on 10 and 20 cm is competitive to 5TE. Not only capturing relative changes but also the absolute value is not very far from measured result by 5TE. To measuring 3 depth, 3 5TE and 1 EM50 data logger were required and their total cost will be around $2000 US dollars without having wireless connectivity. Cost of our M2 sensor will be around $200 US dollars so it would be 10 times cost-effective and it has wireless connectivity to uploading data to cloud. Data logger with internet connectivity is sold as EM50GX by Decagon as well but required cost is $2000 US dollars for logger only. In addition to that, the unified and cable-less design is much easy to install for measuring soil parameters in multiple depth.

5.3 Irrigation Optimization and Automation

5.3.1 Greenhouse Farming (Omitama, Ibaraki, Japan)

Settings of Experiments

In greenhouse farming, water supply to crops is totally rely on irrigation so the most of greenhouses have sprinkler to supply water. However, water pressure is not uniform and amount of supplied water is varied. Basically sprinklers near water source have higher pressure and sprinklers far from the source have lower pressure. Thus, amount and quality crop will be varied due to the uneven soil conditions even if they are grown in the same greenhouse. The variability on crops has caused huge loss on food production since consumers always request aligned crop size and ensured quality. Precise soil

Figure 5.15: Settings of the deployment for garland chrysanthemum in Omitama, Ibaraki, Japan

moisture control is considered as a key factor to improve yield ratio. The amount of water supplied from a sprinkler is adjustable on its nozzle manually but it is not easy to adjust all the nozzle with appropriate settings without having any quantified data on soil moisture level. Therefore, they already have a way to adjust a irrigation in sufficient granularity but actually do not have a way to optimize it base on the data. Union-farm is a productive agricultural production corporation located in Omitama, Ibaraki, Japan and has various knowledge and deep understanding on organic farming. Main crops are komatsuna (Japanese mustard spinach), spinach, lettuce, mizuna (Japanese mustard green), shungiku (garland chrysanthemum), Moroheiya (mulukhiyah), Kushinsai (kongxincai, water morning glory), chingensai (bok choy) and tomato.

The leading farmers in Union-farm has already understood that unevenness of soil moisture would cause variance on crops but the soil moisture level have never been quantified due to lack of affordable solutions on soil moisture monitoring. We have collaborated with Union-farm from 2015 and we are continuing experimental deployments until now. Updates on sensor system was immediately introduced once it has been ready for field deployments. In 2015, M1 sensors were supplied to them in 2015 and replaced by M2 sensor in 2016. Currently, the M2 sensors are replacing by I1 sensors. The total number of deployed sensors should be over 100.

In this section, one of a long-term deployment for garland chrysanthemum is presented. Note that garland chrysanthemum is also known as edible chrysanthemum and it is used as a leaf vegetable. The deployment started in October 20, 2016 and ended in April 11, 2017 so it was almost 6 months. The location of sensors are presented on Figure 5.15. A GW2 gateway and 6 M2 sensor nodes were deployed and each plot had 2 sensor nodes. Note that 3 Decagon 5TE were also installed in the each plot for comparison.

1. Plot 1 (Front): Relatively wet. Node 93 and 94 were installed.
2. Plot 2 (Center): Intermediate condition. Node 95 and 96 were installed.
3. Plot 3 (Back): Relatively dry. Node 97 and 98 were installed.

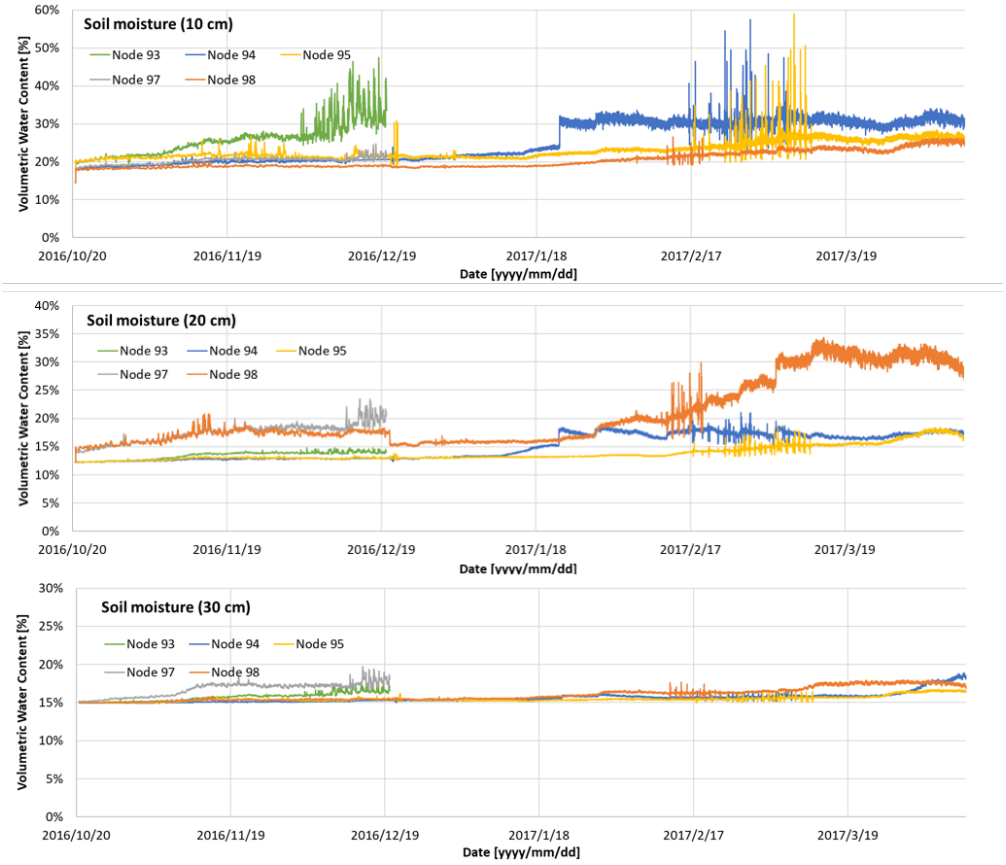

Figure 5.16: Soil moisture data in a greenhouse (Omitama, Ibaraki, Japan) captured by M2 sensor node from 2016/10/20 to 2017/4/11

As far as the sensor node are placed in the same line and in the same greenhouse, differences of solar radiation and temperature would not significant. Thus, the main factor affecting to crop amount and quality would be soil moisture. As shown on the photo on Figure 5.15, in this greenhouse, mulching was applied to keep soil temperature during the winter. Weekly irrigation is applied but the amount of irrigation is not large because the soil is covered by mulching materials which block evaporation from ground surface. The major factor to reducing the soil moisture was crop evapotranspiration.

Measurement Result

5.16 and 5.17 shows the soil moisture and temperature measured by M2 through the season. It was very unfortunate that data collected by Node 96 was lost due to trouble on local SD card. Node 93 and 97 faced some trouble during the maintenance in December 20. Node 94 did not collected data from 12/12 to 12/20 because it turned off due to low battery level in December 12 and the batteries were replaced in December 20 then it returns working.

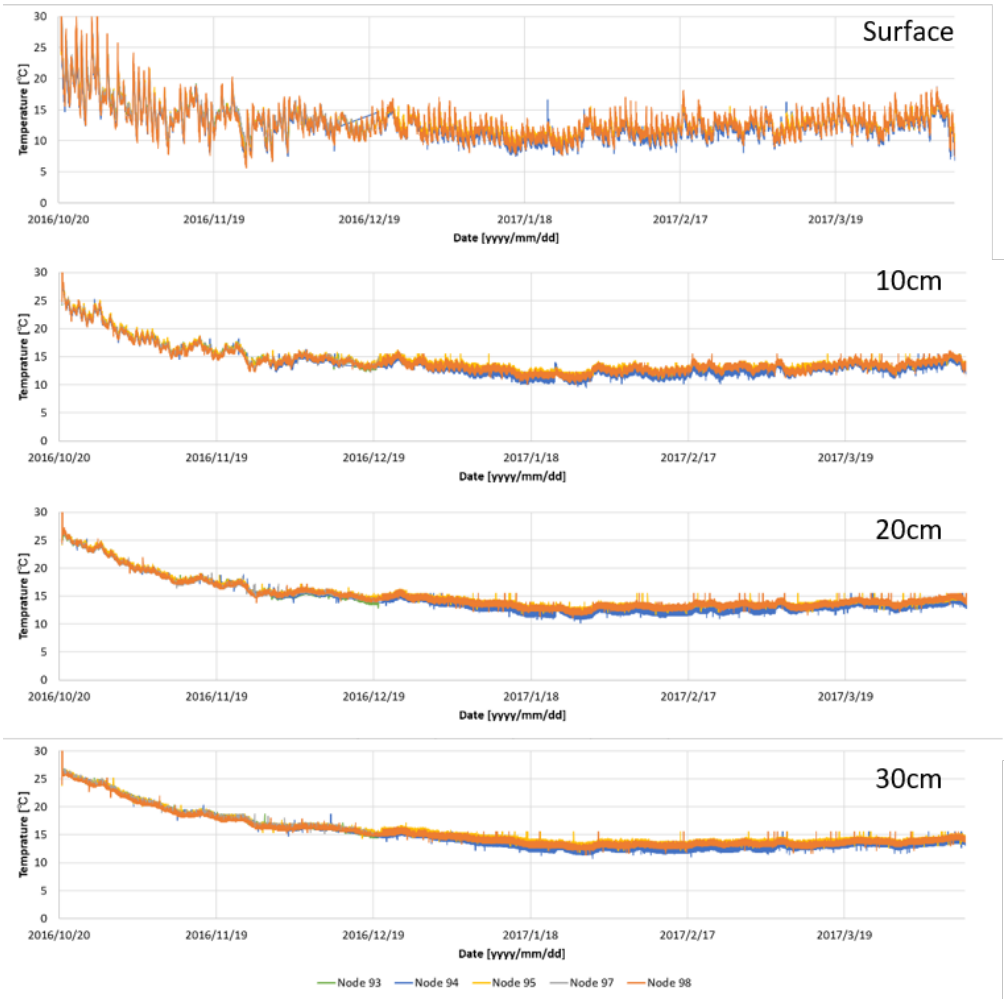

Figure 5.17: Temperature data in a greenhouse (Omitama, Ibaraki, Japan) captured by M2 sensor node from 2016/10/20 to 2017/4/1)

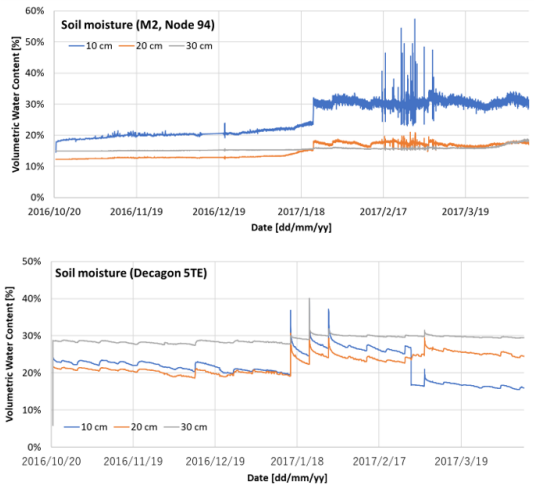

Figure 5.18: Comparison between M2 and 5TE on soil moisture sensing

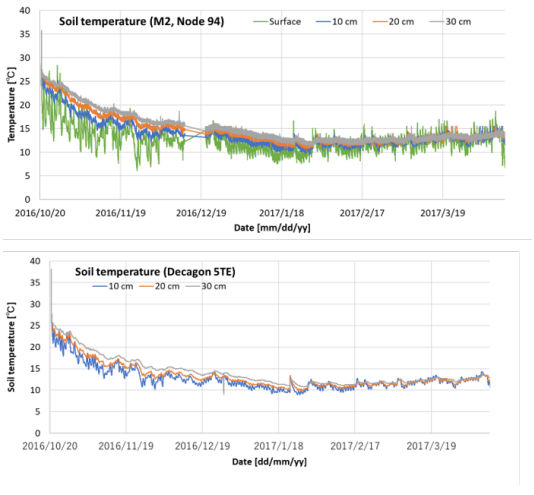

Figure 5.19: Comparison between M2 and 5TE on soil temperature sensing

However, at least a sensor kept working in each plot so it is possible to compare the plots in the most of the measurement term. Shallow area tended to have higher moisture level but that may not reflected actual soil moisture especially in 30 cm. The dynamic range of soil moisture in 30 cm seems too small and it would be caused by insufficient density of soil surrounding the sensor electrodes. Node 94, 95, and 98 experienced jaggy noise from February to March. As they happened for all depth in the same time, it would be accidental unstable measurements. However, it was not very clear why the trouble were happened for all sensors. The temperature data was not very difference on each plot. Node 94 always indicated the lowest temperature in the all depth, so it is suspected that temperature sensor of Node 94 was biased to be under estimating.

Comparison with 5TE

Comparison with 5TE was also applied in the deployment as shown in 5.18 and 5.19. Node 94 is selected as a representative and the data of 5TE was collected from a 3 5TE buried around the Node 94 so it should be almost same ideally. As mentioned before, soil moisture on 30 cm of M2 sensor was not working well on the situation and failed to capture the slight soil moisture changes appeared on 5TE; however, it is difficult to capture as soil moisture in 30 cm was mostly constant and our M2 sensor was not very responsive to such a small change in wet region. Also 10 cm and 20 cm did not capture soil moisture changes until middle of January because insufficient filling of soil between sensor probe and digged hole. The gap between sensor probe and the hole is usually filled by soil when irrigation or rain happened; however, in this experience, the soil surface was covered by mulching materials and the gap was not filled without strong irrigation. According to the 5TE data, there are relatively large amount of water was supplied in Jan 15, Jan 22, and Jan 29. Thanks to the irrigation, the gap between soil and the

probe was filled and start responding irrigation. After that, soil moisture in 10 and 20 cm seemed to be appropriately captured while there were high frequency noise. Note that such kind of noise can be mitigated by taking moving average so it is not a serious matter. On the other hand, 5TE also experienced lost of contact with soil in February 28 when maintenance and harvest of sample crops happened. Probably, someone hit the cable of 5TE during the tasks and 5TE in 10cm was moved from its original position. Of course, density of soil was changed and it was not consistent from the measured data before Feb 28. As M2 data indicated, the soil moisture level in 10 cm was kept higher than 20 cm but 5TE underestimate the soil moisture due to the trouble. It imply that contact between soil and sensor is universal problem of soil moisture sensor. We need to mitigate the risk of accidental hits by someones during the measurement not to move the sensor and change condition of measurement. Even if the M2 sensor cannot capture the small moisture changes by weekly irrigation but succeeded to capture major trends of the soil moisture.

Soil temperature data seems identical for both sensor but M2 sensor indicated a bit higher than 5TE regardless of possible under estimation on Node 94. Difference between 2 sensors is around 1 °C. That maybe caused by the tube shape. A PVC pipe is used for M2 body and inside the pipe is vacant so the air in the pipe may be a little warmer than the soil. However, it was uncertain what causes the difference because the measured result would be affected by individual differences or bias of temperature sensor and related components.

Comparison on Plots

Figure 5.20 is soil moisture for each plot. While soil moisture data in 30 cm depth was almost in same level in all plots due to the lack of sufficient contact between soil and sensor probe, data in 10 cm depths were corresponding to assumption on the soil moisture level. On the other hand, from February to March, soil moisture in 20 cm overcome in 10 cm in plot 3 while soil moisture in 10 cm had not increased much. Compared to the other plot, the soil moisture in 20 cm plot 3 overcame the other plots and had highest moisture level. Even in plot 1, soil moisture in 20 cm was kept less than 20 % but its around 30 % in plot 3. The reason why that was happened on the plot 3 is not very clear but we could say there was soil moisture change in 20 cm depth.

Figure 5.20 is temperature data for each plot. Plot 1 seems a little colder than the others but it would not be significant. Irrigated water, which was originally underground water, was warmer than air temperature in winter. Thus irrigation increased soil temperature and it was clearly appeared in January on plot 1. In this greenhouse, groundwater was used not only for irrigation but also remaining temperature. The greenhouse double structure and by spraying warmer groundwater to inner greenhouse, the temperature was kept around 13 °C even if in midwinter. Note that outside air temperature of February in this area is usually around 10 °C in maximum and around 0 °C in minimum. The temperature adjustment by groundwater is crucial to growing crop in winter without having boiler.

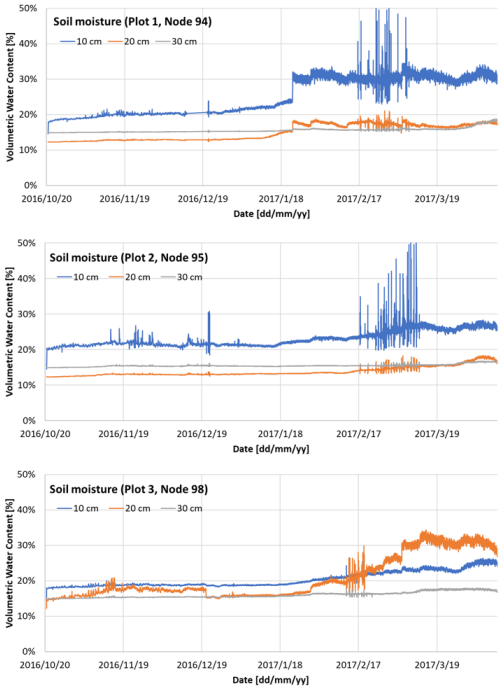

Figure 5.20: Soil moisture comparison between plots in Omitama, Ibaraki, Japan

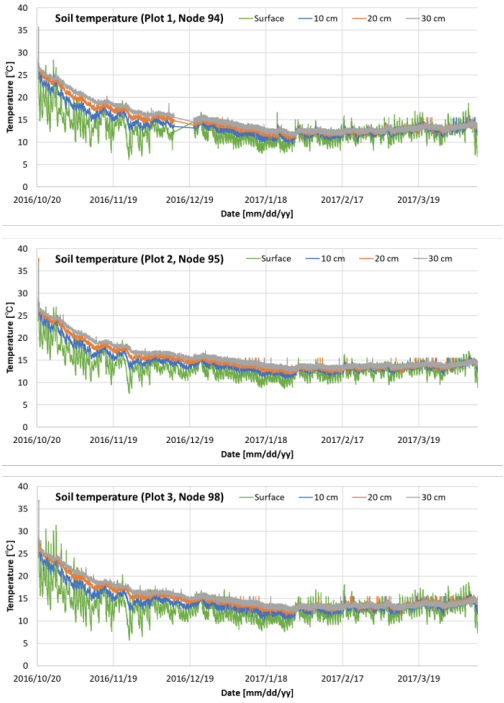

Figure 5.21: Temperature comparison between plots in Omitama, Ibaraki, Japan

Effects to Crops

During the deployments, there are 5 times of harvest and we have collected crop data as well as sensor data. Some kind of garland chrysanthemum accept iteration of growing and picking. During the experimental period, there were 5 times of harvests (Nov 16, Dec 20, Jan 25, Feb 28, and Apr 11). In each harvest, 14 sample crops are picked up around where the sensors were installed. The length of the crops are aligned in picking up and weights of crops were measured. Heaviest 2 and lightest 2 were eliminated as outlier so there were 10 valid samples for each plot. After measuring weights, nitrate nitrogen, and sugar content of samples were measured.

Figure 5.22 shows the weight differences on each plots, no significant differences were appeared on Nov 16, Jan 25 but statistically significant differences were observed between plot 1 and 3 in the other harvests. Especially there were relatively large differences in Dec 20 and Apr 11 and interestingly that were opposite result. It means that plot 1 had advantage in early stage (October to December) but plot 3 would be under better circumstances in late stage (February to April). As mentioned before, basically plot 1 have larger soil moisture level through the deployment but plot 3 have larger soil moisture (20 cm) in the late stage. Probably the soil moisture differences caused the result. In terms of aligning the crop weight, Nov 16 and Jan 25 are desired result so remaining the condition would be important. On the other hand, response to soil moisture would be different between early stage and late stage. As the root length should be longer in

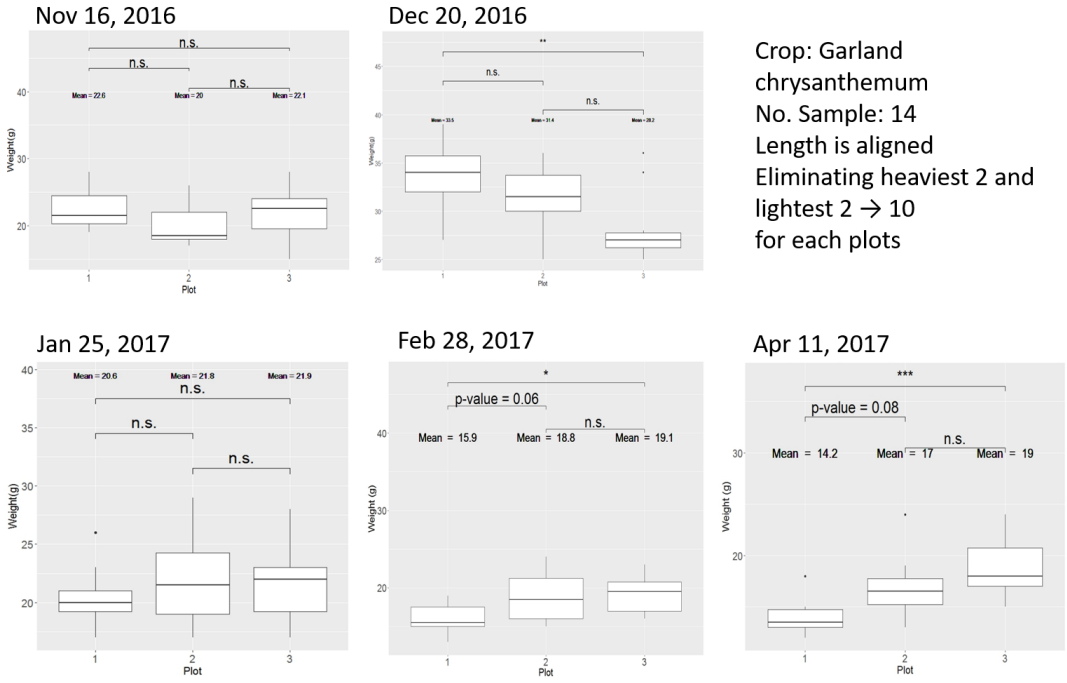

Figure 5.22: Crop weight comparison for 5 times of harvest

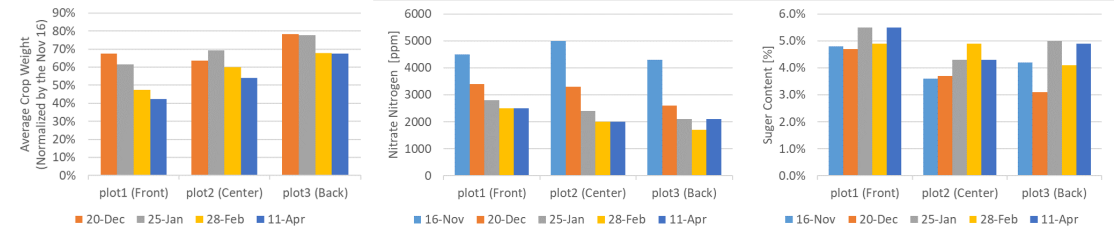

Figure 5.23: Normalized average weight, nitrate nitrogen, and sugar content comparison for 5 times of harvest

late stage, soil moisture in deep area would be important in the late stage rather than shallow area because plot 3 exceeded plot 1 on crop weight, while plot 1 has sufficient soil moisture in 10 cm. It would be difficult to control soil moisture in deeper area but if possible it will contribute to stability on crop size in the late stage.

Figure 5.23 shows nutrition data of the harvested crops in each plot. As the average weight was decreasing by repeating harvests so normalized average weight will informative to the nutrition evaluation. The average weight is normalized by the average weight of crop in Nov 16.

Nitrate nitrogen means stored amount of nitrogen in the crop as nitrate salts. As base fertilizer was applied before sowing, the soil was nitrogen rich and plants retrieved and stored nitrogen in the early stage. After that gradually consuming the stored nitrogen so it is reasonable that the crop has lower nitrate nitrogen level in late stage. There was not significant differences between plots but increase of nitrate nitrogen observed in plot 3 at the last harvest. As soil moisture level in deeper was increased in the late stage at plot 3, some remained nitrogen in soil would seep into water then it might be moved to plants through water. The condition change of fertilizer would affect to difference of crop amount as well.

Sugar contents are constant to be in relatively higher level in plot 1. Probably crops at plot 1 were under desirable circumstances in the early stage. However, high sugar content in the late stage would be due to concentration of chemicals to relatively small crop amount. The crop amount in Apr 11 was just 42 % of the amount in Nov 16. As the crop was shrunken, sugar content should increase as well as plot 2 and 3. In other word, sugar content data for plot 2 and 3 are reasonable. Decrease of crop amount is not significant for these plots so sugar content was increased in the late stage. However, the sugar content in plot 3 was varied in each harvest so its quality were not very stable.

In conclusion, plot 2 (center) would gave the best result in these 3 plots. As farmer adjust environments by focusing on the center part of the greenhouse, it was intended result; however, clarifying what kind of environmental data could affect to the crop amount and quality is important to get desired harvest even in the edges of the greenhouse by introducing more precise controls.

5.3.2 Fruits Farming (Hyderabad, Telangana, India)

Settings of Experiments

While precise irrigation control is only required in greenhouse in Japan, data driven irrigation is attracting huge attention in dry region like India. India has monsoon climate in which rainy season and dry season are clearly separated. In dry season, irrigation is mandatory to growing crops including fruit tree. Traditionally surface irrigation or ridge irrigation is the most common irrigation method but some advanced farmers and research institute start using drip irrigation system which efficiently deliver water to root area of plants. The irrigation tube is prepared and water is dripped to crops. Some of Indian farmers are exploring high-valued crops to effectively earn money and fruits started to

Figure 5.24: Solar powered GW2 gateway and a M2 sensor node deployed in the mango field

be their target as fresh fruits such as citrus, pomegranate, guava, and mango are sold with higher price compared to grains and beans. Especially India dominates mango production and it made almost half of mango in the world.

In this deployments, the target crop is mango and it was grown with drip irrigation. International crops research institute for the semi-arid tropics (ICRISAT) is an international non-profit organization owning scientific research. ICRISAT, India Hyderabad supported the experimental deployment to figure out appropriate irrigation level which can balance crop amount and quality. There is an assumption that restricting water supply results higher sugar content but harvest will be depressed due to strong water stress. Thus, they would like to collect soil moisture data through continuous monitoring although they periodically measured soil moisture using neutron probe. They thought sampling interval is not sufficient but neutron probe is not suitable for continuous monitoring. Combining data from our sensor and their neutron probe, on-site calibration is possible by using neutron probe as reference. It is troublesome to export soil sample as it must through quarantine as an exception. Note that importing soil from foreign country is basically prohibited by law in the most of country including Japan while exceptions can be applied in some specific cases. Thus, it should be difficult to do calibration in lab by bringing back the soil and the soil moisture data shown in the experiments is just raw capacitance while on-site calibration with neutron probe have not been finished yet.

As shown in Figure 5.24, in this deployment, GW2 gateway was powered by solar panel with acid-lead batteries. Deployed sensors were M2 sensor nodes and it was covered by plastic bag to avoid heavy rains.

Figure 5.25 shows where the sensors were deployed and irrigation level for 3 plots.

1. Irrigating least amount of water. Having node 17 and node 24
2. Irrigating moderate amount of water. Having node 19 and 18
3. Irrigating most amount of water. Having node 21 and 20

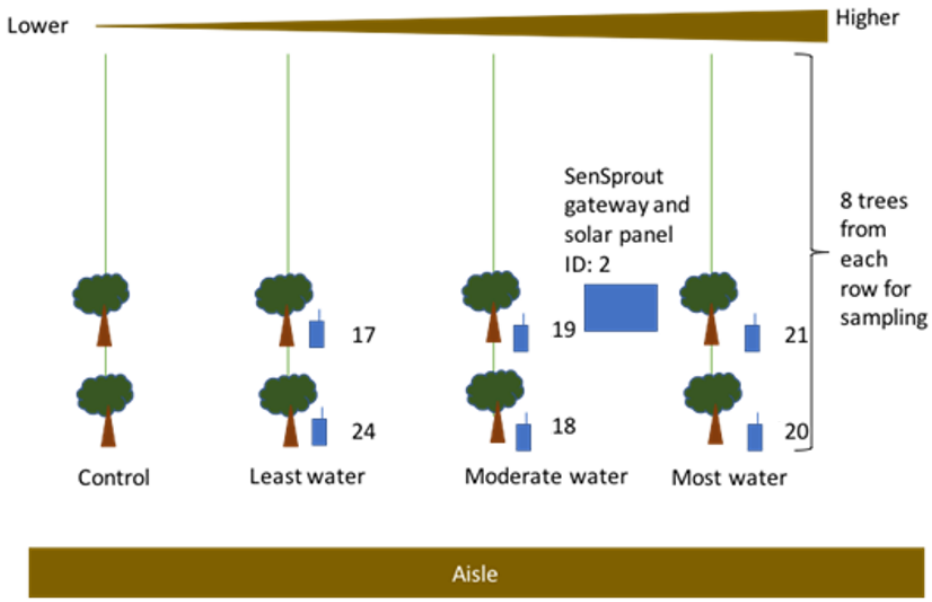

Figure 5.25: Overview of deployments in ICRISAT, India, Hyderabad

Total 6 M2 sensor nodes are deployed and each plot had 2 sensor nodes. The deployment started January 24 2017 and continued until beginning of July. In India, usually mango trees bear their fruits from March and mature them through experiencing some rains in late April to beginning of May. The harvest happened before staring the rainy season which is middle of June. During the dry season appropriate irrigation is required. The irrigation applied in weekly basis and had started from January and ended in April.

Measurement Result

As shown in Figure 5.26, weekly irrigation was correctly captured though node 21 which locating in the plot 3. The soil moisture was gradually increasing through the irrigation. It means the irrigation supply more water than consumed by evaporation from ground surface and evapotranspiration of crops. In every irrigation, supplied water was reached to 30 cm. Once irrigation was finished in the April, soil moisture in 10 cm depth is immediately start decreasing but soil in deeper area keep higher moisture level for several weeks.

Surface temperature started increasing from March and soil temperature follow it with some delays. Temperature differences between night and daytime was not significant probably because the sensor is installed under a mongo tree and the sensor was not exposed to direct sunlight.

Figure 5.27 shows all the soil moisture data collected in the deployments. Node 19, 20 and 24 seems too responsive to soil moisture changes and had relatively large jaggy noise so they are not suitable for comparison of plots. When we checked the deployed sensor in November 2017, the heat shrink film was damaged and it would no longer waterproof.

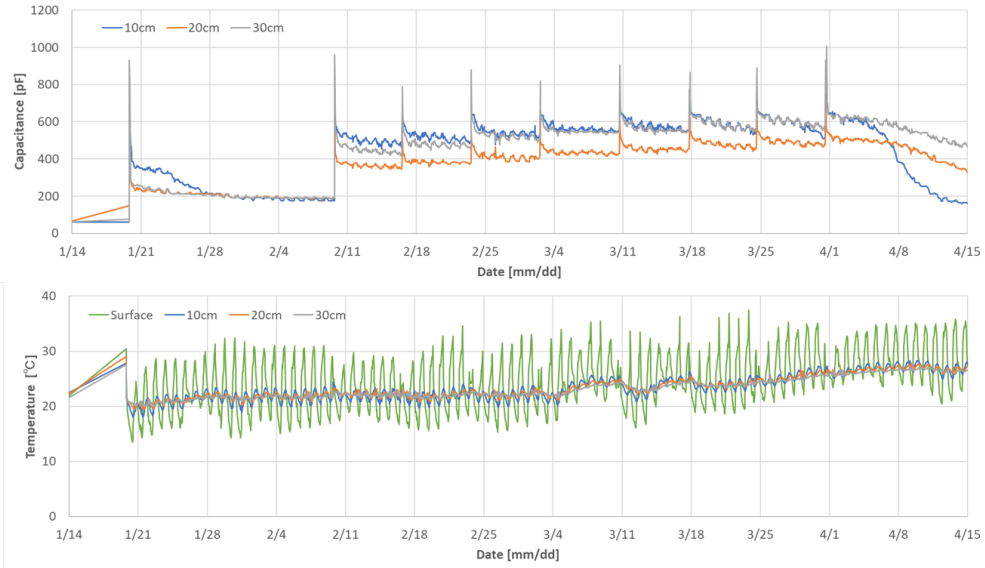

Figure 5.26: Soil moisture and temperatures measured by M2 sensor node (node 21) in Hyderabad, Telangana, India

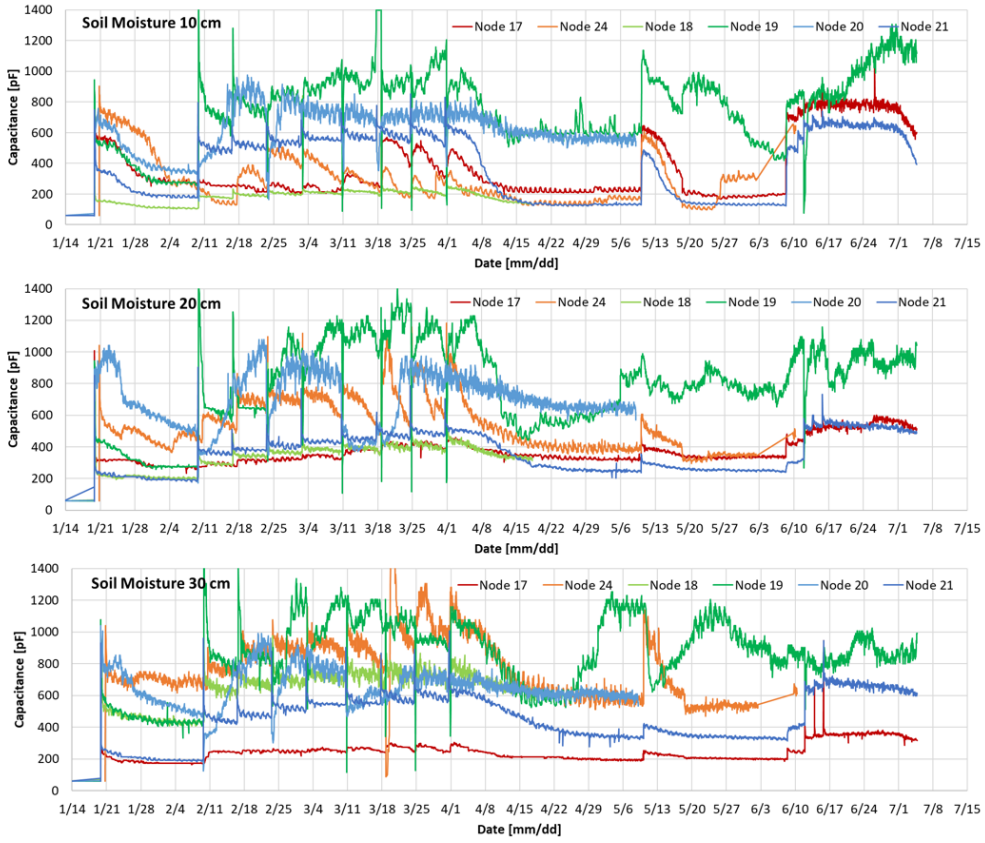

Figure 5.27: Soil moisture data of all deployed sensors in Hyderabad, Telangana, India

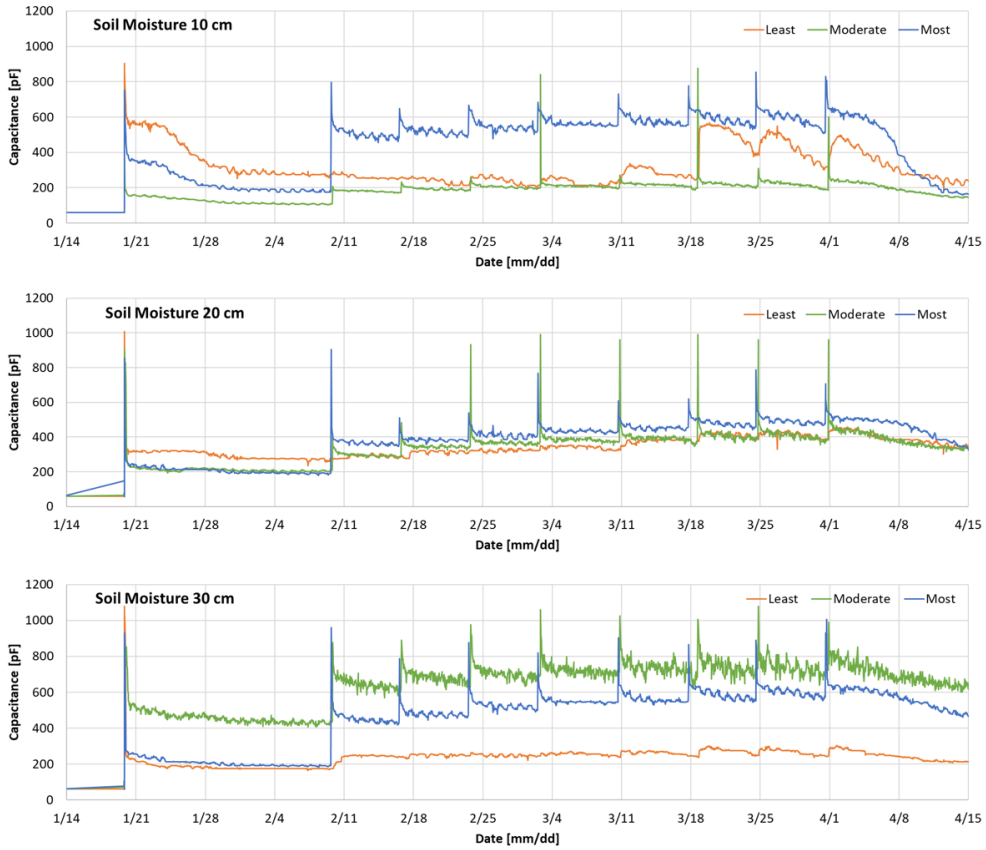

Figure 5.28: Comparison of 3 plots having different irrigation levels in the mango field

If that was the case, water may infiltrate inside the heat shrink film and directly hit sensor electrodes then the sensor would respond too much than it is designed. Node 18 was stopped in April 18 and Node 24 was stop working on June 2 due to insufficient battery voltage. These 2 using alkaline batteries as usual but the others are using lithium battery to make it durable to high temperature so they were not stopped through the deployment.

Comparison on Plots

Figure 5.28 shows the comparison of 3 plots. The plot 1, 2, and 3, were represented by node 17, 18, and 21, respectively. In plot 2 and 3, irrigated water was reached to 30 cm but soil moisture change in 30 cm was not clear in plot 1 because the irrigated water was immediately absorbed by soil in shallow area and rarely reached to 30 cm. Thus, in plot 1, water was kept in shallow area and it was also appeared on soil moisture in 10 cm depth. After March 18, soil moisture in 10 cm was increased while it was not reached to 20 and 30 cm.

In soil moisture 10 cm, Plot 2 was exceeded by plot 1 through the whole period even if larger amount of water should be supplied. That was probably due to insufficient contact

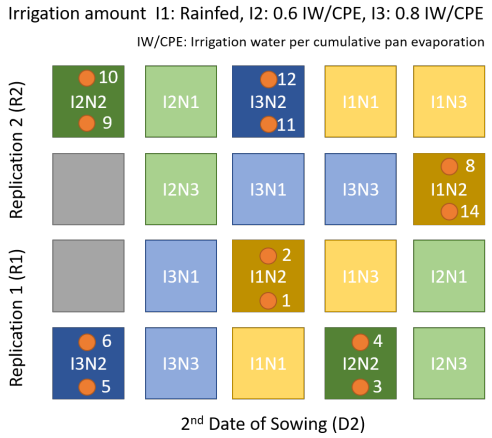

Figure 5.29: Plot settings for the experiment in the maize field and sensor locations

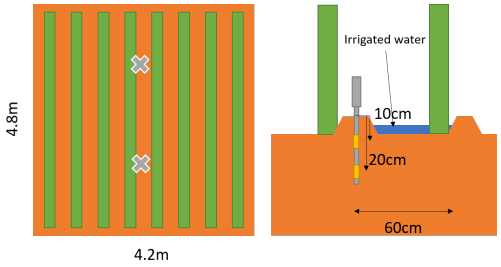

Figure 5.30: I1 sensor node setups in the each plot

Figure 5.31: Deployed I1 sensors in the experimental field in PJTSAU, Hyderabad, Telangana, India

with soil and probe. The soil in this field seemed to be shrunken when it was dried up so there was a risk to making gap between soil due to the shrink. While gradual soil moisture increase was observed in 20 cm for plot 3, the other plots almost remained to be in the same level. That was reasonable result as it can be expected by the experimental setup. In soil moisture 20 cm, the order of soil moisture level was plot 3 > plot 2 > plot 1 after the irrigation started. Therefore, these sensors should appropriately capture the soil moisture level.

5.3.3 Grain farming (Hyderabad, Telangana, India)

Settings of the experiments

The University of Tokyo, Indian Institute of Technology (IIT) Hyderabad, IIT Bombey, and Professor Jayashankar Telangana State Agriculture University (PJTSAU) are work-

ing for enabling efficient crop management by agricultural sensing, remote sensing, and optimization of irrigation. There is an experimental field in Hyderabad and plots with different irrigation strategy and nitrogen level are prepared. Soil moisture and weather data are collected by agricultural sensors including our soil moisture sensors. Meanwhile crop growth is monitored by remote sensing and image processing with UAV. The target crops is maize for the deployment.

Iterative experiments are planned in the maize field in both rainy season and dry season. Crops mainly grown under rainy season is called kharif crops and crops mainly grown under dry season is called rabi crops. Rabi is considered as primary season for this experiments since irrigation should play important role. The experiment in kharif is considered as secondary but still valuable for testing sensor systems.

The deployment was started in August 9, 2017and finished in late October so it was in kharif season. 12 I1 sensor nodes and a GW3R was prepared for deployments but unfortunately the GW3R had connectivity issue on 3G mobile network and also attenuation by maize crops was significant than expected. Only a few sensor nodes can communicated with the gateway. Therefore, although it was a hard decision, we have decided to leave the sensor with offline mode. The data shown below are collected from local microSD cards collected from sensor nodes in the next visit happened November 2017.

Figure 5.29 shows what plots are prepared for the experiments. In this experiment, 3 sowing date, 3 replications, 3 nitrogen levels, and 3 irrigation level are prepared. We deployed sensors in D2 group whose sowing date is July and in 2 replication R1 and R2. Also we have narrow down the target to N2 nitrogen level so target plots were

1. D2R1I1N2: I1 Rain-fed, Node 1 and 2 was installed
2. D2R1I2N2: I2 0.6 IW/CPE, Node 3 and 4 was installed
3. D2R1I3N2: I3 0.8 IW/CPE, Node 5 and 6 was installed
4. D2R2I1N2: I1 Rain-fed, Node 14 and 8 was installed
5. D2R2I2N2: I2 0.6 IW/CPE, Node 9 and 10 was installed
6. D2R2I3N2: I3 0.8 IW/CPE, Node 11 and 12 was installed

Note that IW/CPE ratio means irrigated water per cumulative pan evaporation so irrigation amount is I3 $>$ I2 $\gg$ I1. As shown in 5.30, plot size is 4.8 x 4.2 m and there are 8 ridges whose interval is 60 cm. The sowing interval is 20 cm. Ridge irrigation is applied manually in which water are supplied through water channel between the ridges. The sensor probes were inserted on the top of the ridge and its measurement depth is 10 and 20 cm from the top of the ridge. The deployed sensors were shown on Figure 5.31.

Comparison on Plots

Figure 5.32 presents soil moisture data collected by I1 sensors deployed in R1 plots. Also precipitation data and occurrence of rain and thunderstorm provided by Weather

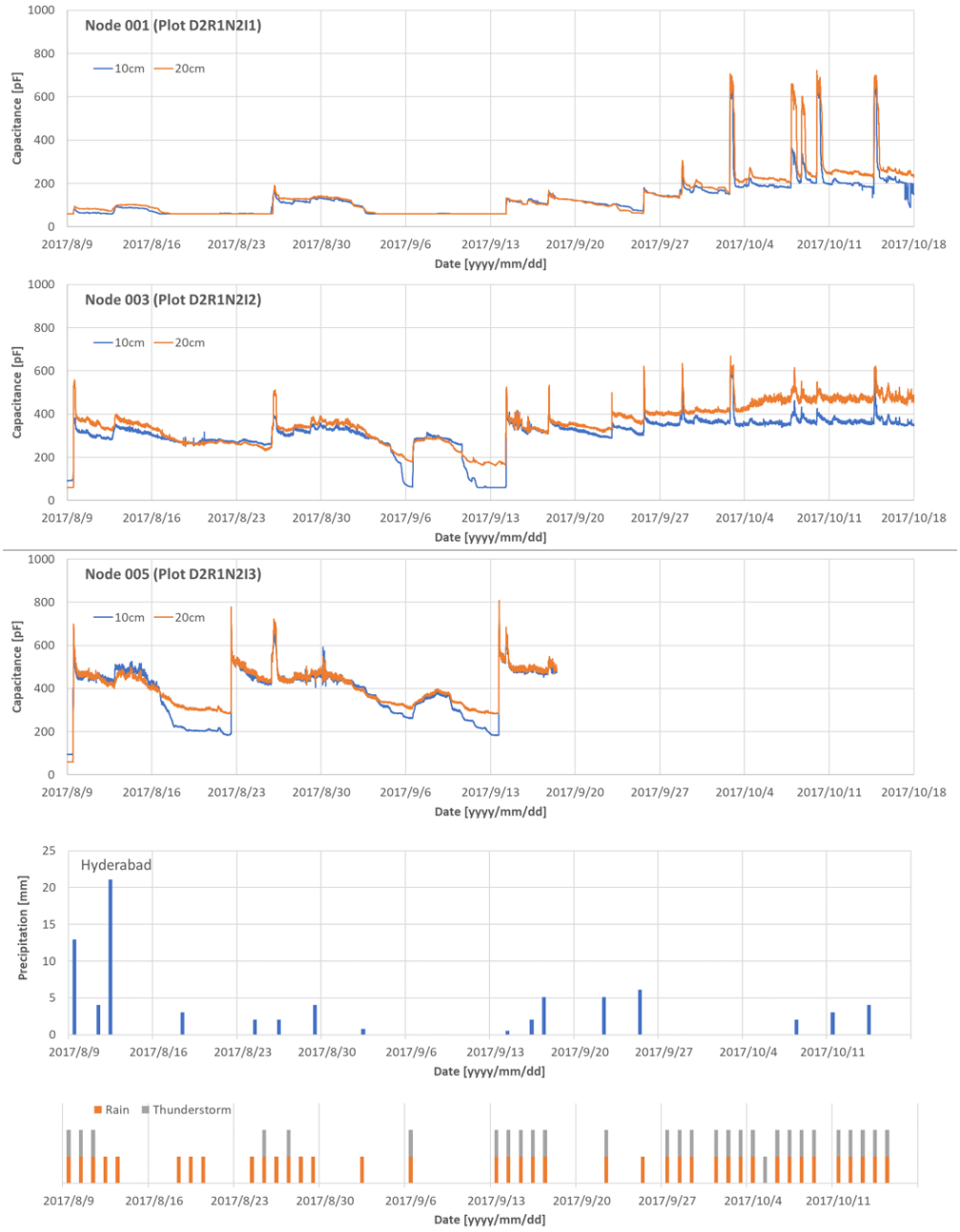

Figure 5.32: Comparison on 3 plots having different irrigation level in R1 group

Underground service (https://www.wunderground.com/). As the sensor node have not been calibrated with the soil sample in the field, raw capacitance was used for soil moisture indication. For I1, I2, and I3 represented by node 1, 3, and 5, respectively. The other sensors seems not providing reliable result due to unstable contact between soil and probes. The expected soil moisture difference according to the plot settings were observed. In I1 plot, the soil moisture level is initially quite low. In contrast in I3 plot, soil kept sufficient water and never dried up even in 10 cm depth. I2 has intermediate level so soil in 10 cm was dried up around 9/6 and 9/14 while soil in 20 cm have remaining water. As it was in kharif, there were frequent rain and soil moisture changes by precipitation were clearly appeared in I2 and I3 plots; however, in I1, the water supplied by rain seemed to be quickly infiltrate by dried soil. Once sufficient water was supplied thunder storms around 9/27, it started to responding to precipitation. Note that the case that having rain and thunderstorm but no precipitation amount was recorded would mean there were hit-or-miss rain and thunderstorm. Thus, actual precipitation amount would be different from the representative data. Other members are working on deploying precipitation sensor in this field so when the collected data is ready for use, more detailed analysis will be enabled. Node 5 down in Sept 18 which was just about a month later from the deployment. That was strange that the battery still have remaining power when it stop working. Probably more investigation is required.

Figure 5.33 presents soil moisture data collected by I1 sensors deployed in R2 plots. For I1, I2, and I3 represented by node 14, 9, and 12, respectively. The other sensors seems not providing reliable result due to unstable contact between soil and probes. Compared to R1 group, these sensors would not accurately capture soil moisture. For example, node 9 is just responding to precipitations but soil moisture level was not reflected on the data. For node 14, it was difficult to fit the sensor probe to dried soil and intentionally supply some water to improve the contact. Thus the initial soil moisture level seemed to be high while it was in the most dried plot so soil moisture in the first 2 week would not be aligned to the surrounding soil. If such process was needed for fitting, the amount of water should be restricted not to affect the measurement result. Node 12 also struggled to get appropriate contact with soil in the first half but after 9/13 it started working well. Combining node 5 and 12, the soil condition in I3 plot can be estimated during the whole experiment period.

5.4 Extreme Conditions

In this section, the case studies deploying sensors in extreme conditions are explained. As mentioned in some experiences in India, operating sensor system under tropical climate is challenging due to its high temperature and high solar radiation level. Also operating sensor system under subarctic climate was also difficult especially when the soil is frozen. We have tackled to the such tough conditions to proof robustness and durability of the developed soil monitoring network.

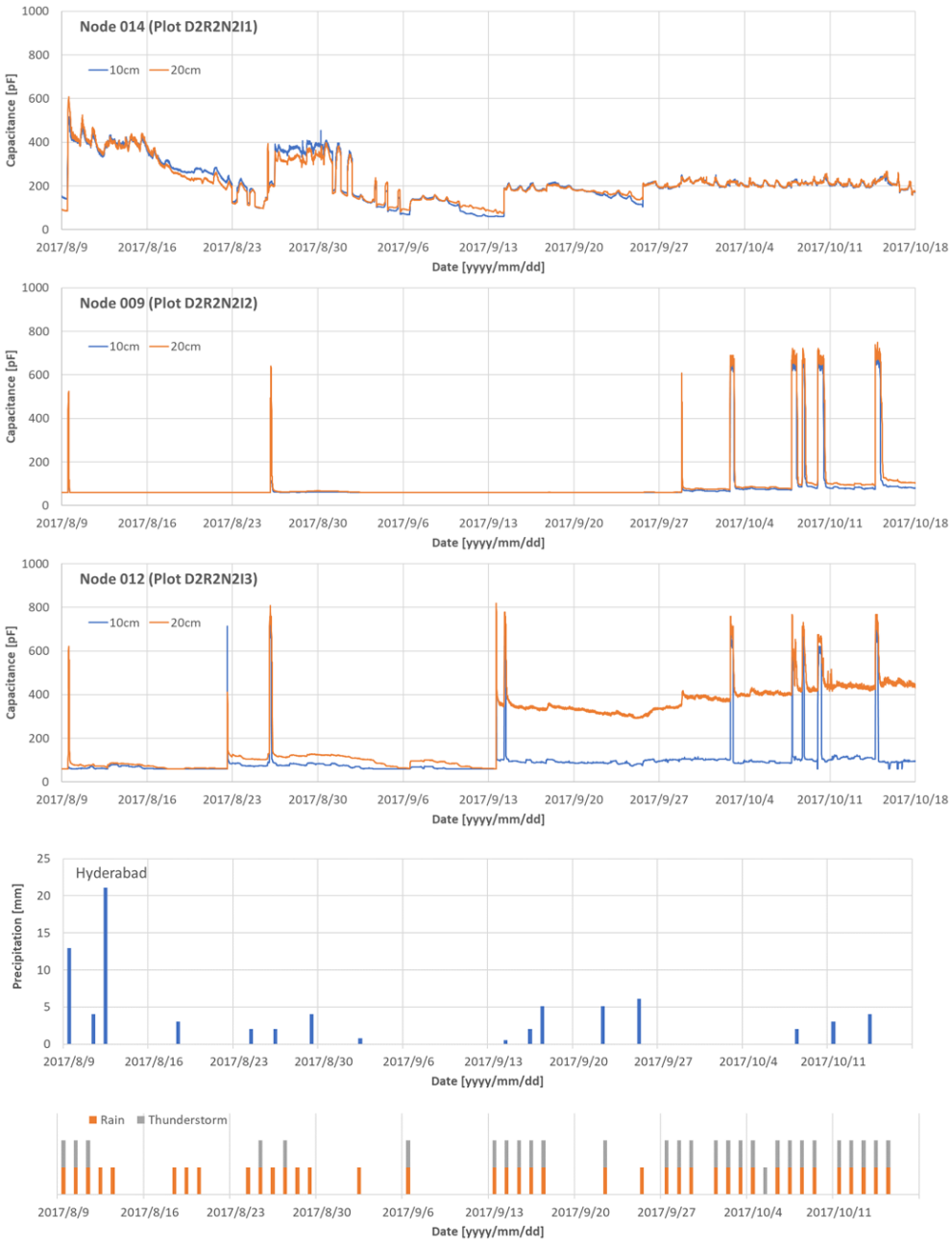

Figure 5.33: Comparison on 3 plots having different irrigation level in R2 group

Figure 5.34: Orange field in Benoda, Maharashtra, India. Deployed GW2 gateway and M2 sensor node

5.4.1 Tropical Climates (Benoda, Maharashtra, India)

As a part of collaborative work with IITB, the developed sensor system was deployed in citrus fields in Benoda. Benoda is a small village near Warud which is around 100 km far from Nagpur. Warud has huge production of oranges and the oranges harvested in this area were exported to all over the India and Nagpur orange is famous in India. Therefore the deployment happened in orange fields. The motivation of introducing soil moisture sensor in the orange field is different from the other deployments in India. That is for blocking infection of disease of orange trees called gummosis. Once an orange tree infected to gummosis, it will gradually weaken and eventually die in the worst case. The cause of gummosis is a bacteria in the soil and infection likely happens when the soil is saturated with water and flood happened. The flood transmitting the bacteria and carrying the disease. Thus, unnecessary flood should be avoided by restricting irrigation to reserve a space to absorb water in the soil. Relationship between irrigation level and risk of infection should be figured out for prevention of gummosis.

The orange field have drip irrigation so precise control on irrigation was possible. IITB already deployed several soil moisture sensors but more dense measurements were preferred but budget was limited and they requests cost effective soil moisture sensors which we developed. The initial field test have done in February 2016 with a few M1 sensor nodes and GW1 but no long-term deployment happened in that time. The second trial happened in August 2016, 8 M2 nodes and 2 GW2 gateways in 2 different fields. In December 2017, we have visited the field for maintenance and updates so the data is collected from micro-SD card to fill the blank in collected data through wireless networks.

Figure 5.35 shows soil moisture data collected by M2 sensor nodes. The experiment started at the beginning of August and closed in middle December. The sensors experienced frequent rains in August and September but once dry season was started. Soil

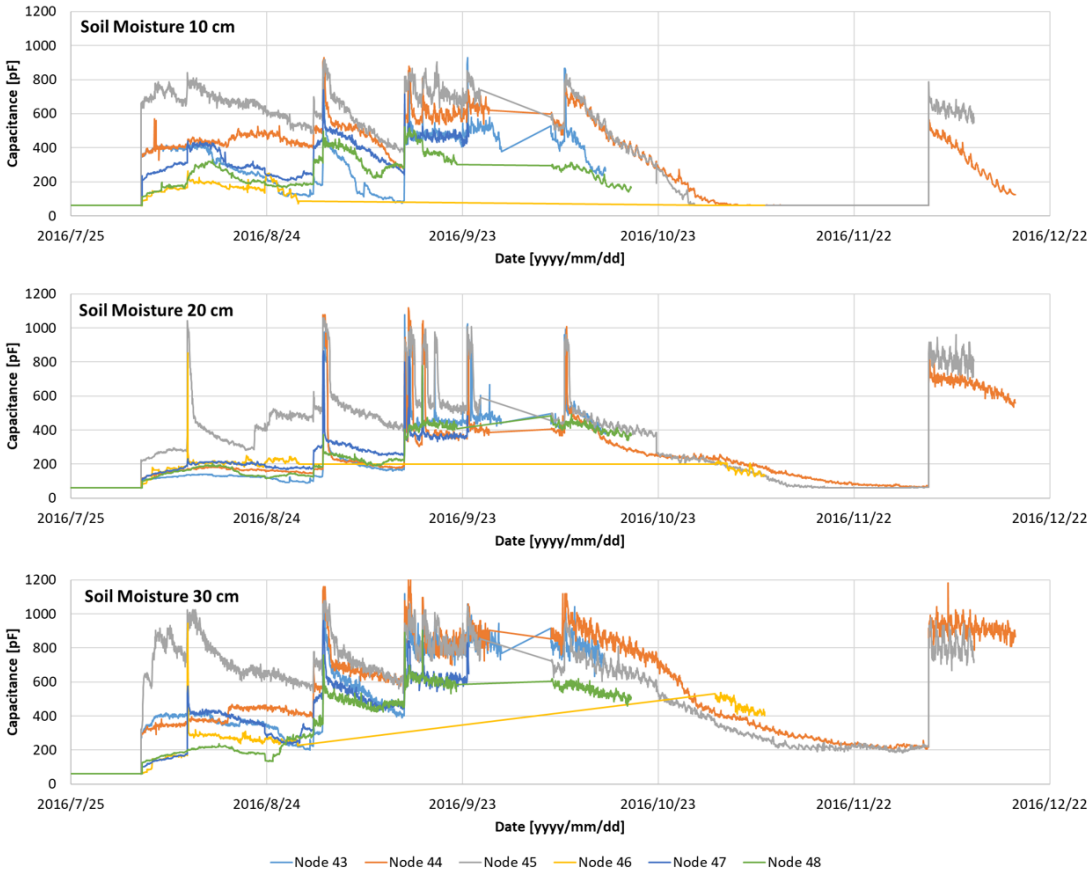

Figure 5.35: Soil moisture data captured by M2 sensors in orange field in Benoda

moisture in 10 cm was dried up by the end of October. However, some water was remained in soil deeper than 20 cm until the end of November. Sudden increase of soil moisture in 12/3 was caused by irrigation. In addition to drip irrigation, ridge irrigation was used in parallel as it can supply bunch of water quickly. The irrigation happened in 12/3 would be ridge irrigation.

5.36 presents temperature data. In kharif season, temperature differences between daytime and night was around 10 to 15 °C; however, in rabi season, it was expanded to 25 to 30 °C. Although temperature differences were not large, it was quite humid in kharif season. Soil temperature in 10 cm was varied in rabi season. That is because soil was dried up and cooling by vaporization heat cannot be expected. Compared to 10 cm depth, soil temperature in 20 and 30 cm depth were stable. Soil temperature sensor (20 cm)of node 48 may be broken around 10/11 as it output strange values. The large temperature differences and quite high humidity significantly shorten the life of alkaline batteries as shown in Figure 5.37. The batteries were gone only in a half and a month while it was designed to be operable for a year without changing batteries. The batteries are exchanged in 10/6 and node 44, 45 worked for 2 months after the replacement; however, 43, 48 immediately lose the power just in two weeks. That would be caused by failing to be in sleep mode and missed to reduce energy consumption while waiting. Also smartphone included in GW2 also had problem on Li-ion battery because Li-ion battery damaged by too high temperature. Also it was found that some smartphones stop working and shutdown when it detect the too high temperature. Thus there is a risk to have accidental shutdown which cannot be resolved remotely.

As far as we using alkaline batteries and smartphone, sufficient lifetime will not be available in tropical climate and alternative power source need to be considered.

5.4.2 Frozen Soil (Sinhidaka, Hokkaido, Japan)

In contrast, subarctic area imposes challenges to soil moisture sensor as well. As introduced in section 5.2.1, soil freezing happened in a place where it will be rarely snow but extremely cold. Shinhidaka town previously Shizunai town is one of the location having such characteristics and actually it is where deep soil freezing is observed. As shown on Figure 5.38, there is almost no snow in early December but the surface of the soil had been frozen already. It was an experimental pasture land managed by Hokkaido University. Soil physicists are working for research about methods of soil conditioning and evaluation of greenhouse gas emission from the soil. Our 5 M2 sensors (node 81, 88, 89, 90, and 92) and 2 GW2 gateways (X and Y) were tested in the extremely cold environment from October 7, 2016 to July 5, 2017. They were tested in 2 different fields. Node 81 and gateway X were deployed in a field of Niikappu and the other sensors and gateway Y were deployed in a field of Shizunai. Note that alkaline batteries were exchanged by Li batteries and antenna poles were added before the midwinter. Node 89 was broken around 10/20 by water exposure on the circuit board. That is probably caused by animal attack. Gateway Y was fallen into bad state from December 15, 2016 to January 5, 2017. These troubles were not very related with the cold climate

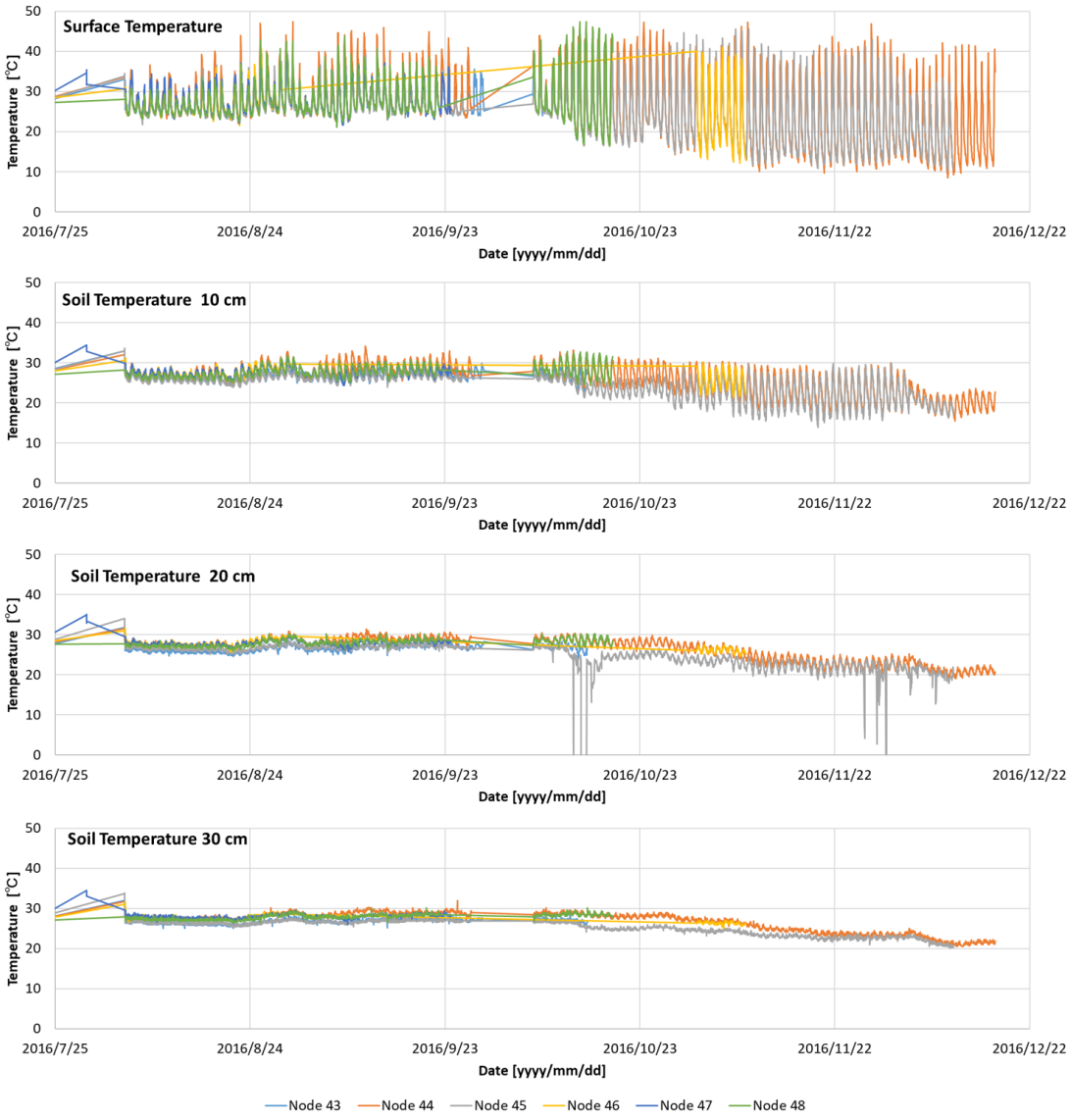

Figure 5.36: Temperature data captured by M2 sensors in orange field in Benoda

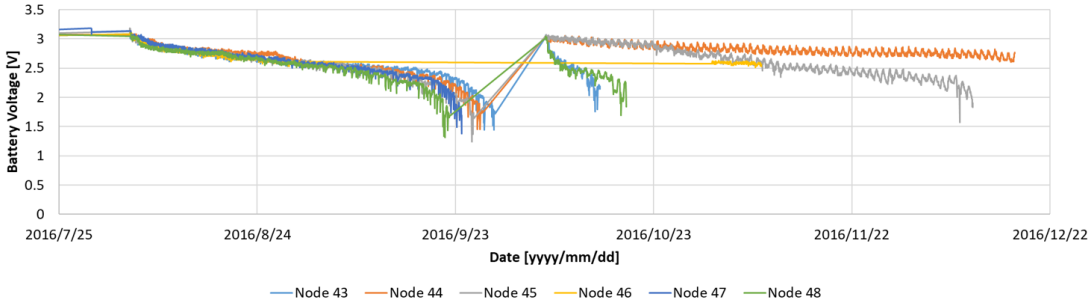

Figure 5.37: Battery voltage of M2 sensors deployed in orange field in Benoda

Figure 5.38: Experimental pasture field in Shinhidaka and deployed M2 sensor with antenna pole

and data was locally stored other than node 89 so data presented in following figures were retrieved data from micro-SD cards.

Figure 5.39 shows soil moisture data collected by M2 sensors as node 81 is placed in another field, it should be different to the other sensors. As soil type would not be very different from soil sample used for M2 calibration, approximated equation was reused for the analysis while it was not very accurate. From October to December, there are a lot of quick soil moisture increasing and decreasing triggered by precipitations. In early December, the soil started to be frozen and soil moisture seemed be lower because our soil moisture sensor cannot detect water content inside ice. Relative permittivity of ice is much smaller than permittivity of liquid water so frozen soil would be considered as dried soil for this sensor. The melting of frozen soil begun in middle March and totally melted at the beginning of April.

Figure 5.40 shows temperature data collected by M2 sensors. Surface temperatures are reached to near -20 °C in January. However, it is interesting that surface temperature reached to 20 to 25 °C in maximum in the same period. Thus, temperature differences are reached around 30 °C which was as large as in dry season in India.

Soil in 10 cm was totally frozen from the beginning of January to beginning of March. Probably soil in 20 cm would start freezing at that time. Until April 5 2017, some frozen soil or ice was included in the soil because the soil temperatures were stuck in a few °C

There was no concern of batteries as it was preliminary replaced by lithium batteries. A challenge caused by soil freezing is that the installed probe slipped out of soil and measurement depths were changed during the measurement. The maximum moving length was around 5 cm. This is caused by pressure by frozen soil. When the soil is frozen, its volume would be a bit inflated. So the occurred pressure push the probe to slip.

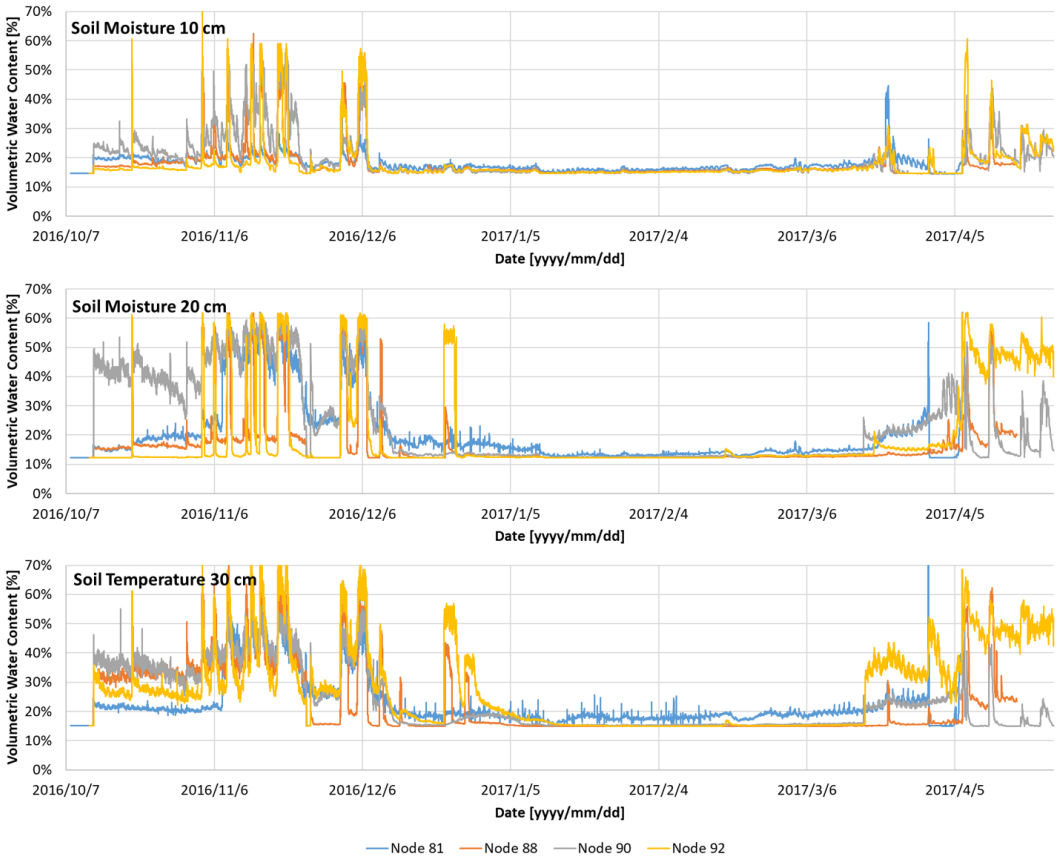

Figure 5.39: Soil moisture data captured by M2 sensor node in Shinhidaka, Hokkaido, Japan

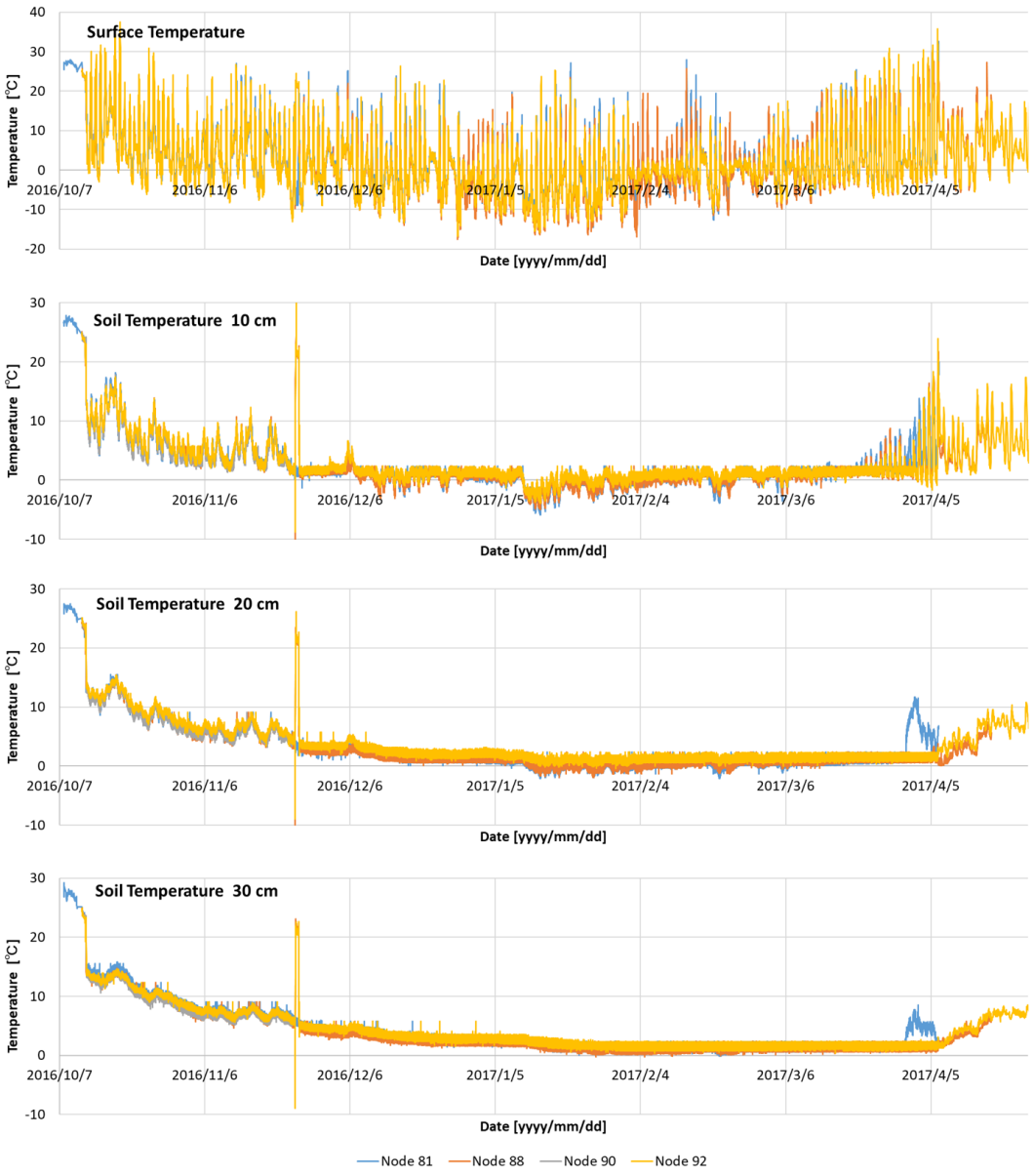

Figure 5.40: Temperature data captured by M2 sensor node in Shinhidaka, Hokkaido, Japan

5.5 Summary

In this chapter, various deployments of developed soil monitoring networks was presented. Through the experimental deployments, potential of the developed sensor was proven. Controlling soil moisture considering the soil moisture data will be a key to improve farming productivity. Japan and India have different motivation and requirements but it can be satisfied the current system design. The remaining issue is too quick power down in extreme conditions. By using lithium battery, it would be avoided but lithium batteries are much costly than alkaline batteries. Introducing energy harvesting or microwave wireless power transfer should be leveraged to battery-less operation which will be more robust in extreme conditions. Another issue is success rate for installing sensor probe was still low. Around half of the cases, the contact between soil and sensor electrodes is not appropriate. Also the installation quality is significantly varied by the who works on it. Preparing jig and making detailed soil moisture sensor installation should be discussed.

Chapter 6

Conclusion

6.1 Summary of Thesis

A design of cost effective soil moisture monitoring network for agriculture was introduced in this thesis. The appealing feature of the monitoring network is sufficient accuracy with affordable price. We initially targeted to holding down the price of sensor network around 10 % of currently commercialized soil moisture sensors. Fabricating probe with printed electronics technologies and leveraging capacitive sensing module for touch sensors, low-cost sensor node was developed. The sensor node can capture soil moisture and temperature data in multiple depth and collect data through wireless sensor network. The expected sales price of the sensor node is around $300 US dollars which is much lower than currently available capacitive base soil moisture sensors. If we would like to do similar measurement with wireless connectivity using commercialized sensors, over $ 3000 dollars will be required so it has been in the target price we set for its development.

However, the earlier version of our sensor system, which is called M1 and GW1 in the Chapter 4, were not very matured. Its measurement accuracy, packaging, energy consumption, and reliability were not sufficient to meet demands of farmers so we had received a lot of feedback through experimental deployments. Prioritizing the issues listed up and various improvements were introduced through iterative updates. 3 major updates were introduced in 2 years and the sensor system was significantly improved through the quick feedback from the actual fields. The first updates included mainly hardware update on sensing unit for miniaturization and reduction of energy consumption. The second updates included drastic design change on probe shape and packages of the sensor node in which the sensor probe is easily detachable. The third updates focuses on accuracy improvement and almost desired characteristics were acquired. Through these updates, the latest sensor system have been reached a bar to be practically used for precision agriculture. The soil moisture monitoring network have been released as a product from SenSprout inc by leveraging the technologies developed in the research. As sensor quality reached sufficient level, the next stage of development have been kicked off for smart irrigation where soil moisture sensors capture soil condition and irrigation system automatically makes decision based on the data. Internet connectable irrigation valve controller is developed and we have started some initial validations as shown in Figure 6.1.

Field deployments introduced in Chapter 5 have already implied the potential for introducing soil monitoring system in terms of quality control on crops. Regardless of labor efficiency and quality control, irrigation optimization simply gives reduction of water consumption which is urgent matter for countries having dry climate such as India. Therefore, several deployments of the soil monitoring system have been running in India. Soil monitoring system is necessary to maximizing production amount per water consumption as well as evapotranspiration estimation using whether stations.

In addition to the practical developments on soil monitoring network, energy harvesting and wireless power transfer are attractive technologies to reduce operational cost. Reducing initial cost is definitely important and achieved by printed electronics as men-

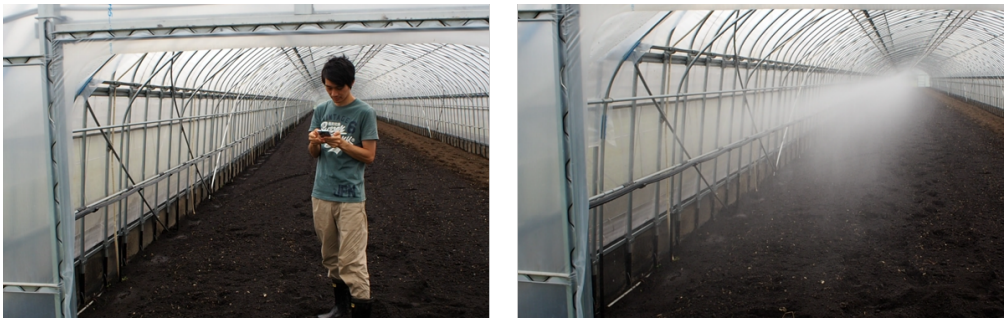

Figure 6.1: (Left) Remotely controlling irrigation valve from a smartphone (Right) then irrigation will be started.

tioned before but the operational cost especially labor cost for battery replacement need to be considered. One of the most serious barrier to spreading wireless sensor networks in large scale is energy supply. The most of the sensors are driven batteries but it requires battery replacements while battery life is kept expanding by reducing the energy consumption of components and introducing suitable algorithm for energy management. Nevertheless, as far as they rely on batteries, it eventually requires battery replacements. It may not be serious matter if the number of deployed sensors are limited to a few dozen and yearly battery replacement is enough for continue operations. Actually, the developed soil moisture sensors mentioned Chapter 4 are designed to have 1 year battery life because almost all growing season is less than a half year except fruit farming and sensors will be uninstalled from field. Before the next deployment, batteries should be exchanged and this operation is accepted as the number of deployed sensors are very limited, which is usually less than 10 as demonstrated in Chapter 5. However, it is not scalable operation when the number of sensors are increased to a few hundreds or more so battery-less operation is preferred. Using energy harvesting is the first alternative for battery-less operation and solar panels are often exploited for agricultural sensing indeed (e.g. our gateways deployed in India). Even if solar power is suitable for gateway or wether station, it would be difficult to fit it on the sensor node because the size of sensor node is limited, the sensor node could be covered by canopy which block sunshine, and the panel may have splash by soil and dust which harm performance of solar panel. Moreover, if we consider fully buried soil sensor, solar power cannot be expected.

RF energy is perpetual in urban area since bunch of wireless signals are emitted for broadcasting, communicating, and sensing. Such ambient RF signal can be converted to energy for sensor nodes as demonstrated by a prototype of RF energy harvesting sensor device using TV radio wave in Chapter 2. Farming production in suburban area is fundamental for fresh food supply to mega-city like Tokyo and ambient RF energy may be expected as power source in suburban area. Of course, balcony of high-rise building is the most preferred location for capturing ambient RF signals so it is possible to develop ambient RF powered soil moisture sensor for balcony and roof gardening.

Also temperature differences between surface temperature and soil temperature in

deep area will be possible energy source. As shown on temperature measurements results in Chapter 5, temperature differences were observed in any farm fields so it would be universal power source for soil moisture sensors. Thus, possibility of thermos energy harvesting for soil moisture was explored. Thermos energy harvesting leveraging Seebeck effect on semiconductors to convert temperature differences to electrical energy. It is inverse of Peltier effect so common Peltier modules can be used for harvester. Even if harvested energy is in μW order, it would be sufficient to enabling hourly measurements and data transmission with modern ultra-low power MCUs and communication modules. As temperature difference between surface temperature and soil temperature is not constant and vibrating in daily and yearly basis. Therefore, appropriate energy management method like proposed adaptive duty cycle controls introduced in Chapter 2 should be considered.

On the other hand, there are cases that energy harvesting from ambient RF energy and soil temperature differences is not applicable. For example, in greenhouse, no strong RF signals will be observed and temperature differences are not very large since temperature in greenhouse is controlled to be as stable as possible. If that is the case, intentional RF source for RF energy harvesting should be prepared then it works as a microwave wireless power transfer (WPT). The first prototype of low-cost soil moisture sensor in Chapter 2 considered the scenario.

The temperature differences between surface and underground is perpetual for outdoor culture but if the budget for initial investment is highly limited as intending quite large scale deployment, it may be difficult to rely on thermos energy harvesting. Heat conductors used for pulling soil temperature to surface are usually made by copper or aluminum which is relatively costly compared to the other components. As components for RF energy harvesting and microwave power transfer could be quite cheap, using RF energy will be suitable for large scale deployments. If bunch of sensor nodes are deployed in the large field, movable RF energy source is desired to cover the area since distance from power source is fundamental for transmission efficiency of microwave WPT. In rapid growth on unmanned aerial vehicles (UAVs), UAVs have started to be used in agricultural area for remote sensing and pesticide. Thus, there is an idea that adding RF source for WPT on UAVs and exploit them to delivering energy and collecting sensor data simultaneously. In order to efficiently deliver energy to sensor node through WPT, appropriate navigation strategy including sensor node position estimation introduced in Chapter 3 is required.

Combining these energy harvesting and microwave WPT, the most of scenarios of soil monitoring could be covered with a suitable battery-less solution. While these battery-less solutions have not been matured for field deployments yet, it should be the next item of development to improve cost-efficiency not only on initial cost but also operational cost.

In conclusion, the all works presented in the thesis intended to reduce the cost of soil monitoring network while keeping sufficient accuracy. Fabrication cost and energy supply are the most focused matters for these works and printed electronics, energy harvesting techniques, and microwave WPT are proposed as solutions. Even if the currently

Figure 6.2: (Left) Alert on too high temperature, (Right) Damaged battery exposed to too high temperature

Figure 6.3: Antenna poles for expanding communication range. Left: for gateway Omitama, Ibaraki, Japan. Middle: for sensor node (Obihiro, Hokkaido, Japan), Right: for both (Hyderabad, Telangana, India)

Figure 6.4: Damaged M2 sensor node. Left: the cracked sensing unit (Obihiro, Hokkaido, Japan) Right: The probe is no longer waterproof (Hyderabad, Telangana, India)

deployed sensor monitoring networks do not have energy harvesting and wireless power transfer, that will be integrated and be in the field in the near future.

6.2 Future Works

The remaining works are mainly improving repeatability and robustness of the monitoring system then introducing battery-less solutions in the field. While we have driven a lot of experimental deployments as show in 5 and brushing up the design of the sensor system; however, we have faced various failure cases in deployments.

First, we had reliability problem on gateways. As smartphone owns main part of the gateways, we need to rely on Android phone which is not very designed for leaving outside for quite long time and keeping a app running . It seems working in the most of the time but sometimes stop working by some rare incidents. More dedicated investigation and vilification are required. The phone are not durable for extremely high temperature 6.2. Not only reliability improvement, we need to prepare some ways to remotely fix the issue as a remote assistance service for unexpected errors and investigations.

Second, the communication range of IEEE 802.15.4/IEEE 802.15.4 g would not be sufficient. In spec, the communication module has around 1 km range in line-of-sight but it would be difficult to get line-of-sight in practical deployments then the communication range is around 100 m. It can be mitigated by installing antenna with some poles like Figure 6.3 but it requires additional cost and labor so it would not be reasonable solution considering scalability. 100 m is enough for cover a greenhouse but usually farmers want to deploy sensors in multiple houses and want to cover them by a single gateway. It is obvious that 100 m is too short for large scale farming. Emerging low power wide area (LPWA) is alternative on the communication module. For example, LoRA usually have several km communication range while its throughput is extremely low. As long as sensing interval of soil moisture sensing is normally set as every 1 hour and the data size is small enough, the low throughput is not a matter. Thus, it would be a desired communication module for this purpose.

Third, durability of sensor probe is not enough for repeating deployments. As shown in Figure 6.4, sensor probes sometimes mechanically damaged. On the left photo (Obihiro, Hokkaido, Japan), the rope supporting the crops cut the head of the sensor node when strong wind vibrate the pole the rope connected. In the right photo (Hyderabad, Telangana, India), heat shrink film was damaged and the probe was no longer water proof. Probably water would infiltrate into the damaged part as the copper patterns are a little rusted. We need to suppose such unexpected damage on probes will happen rather than make highly durable sensor but expensive. Currently commercialized sensors tend to take the later option but it is a reason why price of these sensors are remain to be high as there is a trade-off between cost and durability. Even if the sensor probe might be broken by relatively rare incidents, it would be still practical if it is easy enough to fix it. Introducing detachable sensor probes is the first improvement for enabling easy repair but also knowledge transfer for fixing issues is also important.

Currently, we mostly owning installation and maintenance by visiting the fields but it should be owned by users to make deployments scalable. Thus, simplifying installation and maintenance processes is mandatory. Also easily usable instructions should be prepared and users need to be educated to use the sensors. On the other hand, introducing crowed sourcing for maintenance would be interesting because using low-cost labor for fixing issues would be more cost-effective than prevent the issue by design changes which may make sensor design complicated.

Fourth, the repeatability of the soil moisture sensor still need to be improved. Currently the accuracy highly depends on who install the sensor because standard processes of installing sensor have not been defined. As our sensor probe is sensitive to contact between soil and sensor probe, it is quite important to get an appropriate contact; however, the reasonable way to have not been figured out yet. To standardize the installation process, some specified tools or jigs will be required to support installing sensors. Once effective standard is defined on installation, repeatability will be much improved.

These are considered as a future work for sensor developments. On the other hand, actual issues on energy harvesting and WPT have not been clarified yet since they have not been tested in the fields. While some candidates of improvements have been listed up based on assumptions, it is not able to determine what is the most important issue for the system without real deployments. Once a deployable prototype is ready, it should be tested at first and collect feedback to prioritize the issues we should tackle.

Acknowledgements

I would like to thank Prof. Yoshihiro Kawahara for invaluable mentoring from my master's course to ph D course. I am grateful to Dr. Tohru Asami for giving advices and supports on the research. Through the defense of my doctor's thesis, Prof. Kaoru Sezaki, Prof. Jun Adachi, and Prof. Hideya Ochiai gave valuable comments and feedback so I would like to appreciate. I would like to thank Meiko Fujita, Hideyuki Kanai and Noriko Mizuno for their administrative affairs in Kawahara Lab and Kenji Tsushio for supports and advices on the projects.

I would appreciate to Lab members of Asami and Kawahara lab as they mutually supported research activities. Especially, Tatsuya Sasaki, Dr. Yoshiaki Narusue, Duoung Minh Quan, Yuta Morisawa, Yu Suzuki, Yasutomo Shirahama, Ryosuke Kobayashi, Naoto Hayashi, Kouta Suzuki, Natsuki Ikeda, and Takumi Nishiyasu owned a part of the developments and operations related with the thesis. Prof. Manos M. Tentzeris and Dr. Rushi Vyas supported my research related with RF energy harvesting during my internship in Georgia Institute of Technology so I would appreciate it and following supports.

Prof. Masaru Mizoguchi, The University of Tokyo, and Prof. Yuki Kojima, Gifu University, gave knowledge about soil physics which I was not familiar at the start of the research project so my understanding on soil physics is rely on them. Kazuhiro Nishioka and Tai-Shen Chen supported experiments in the field. This work for soil moisture probe developments was supported by grants from a project of the NARO Bio-oriented Technology Research Advancement Institution (Integration Research for Agriculture and Interdisciplinary Fields).

The production and development work for soil moisture sensors are delivered by Sen-Sprout Inc. I would like to appreciate Naoya Miyamoto, Yasuhito Sakuraba, Lisa Kikuchi, Kazuhito Mine, Ritmo Sato, Tohru Shirakawa, Yukiya Sasa, Masahide Chiba, Kazme Egawa and the other members.

Prof. Junichiro Shiomi and his lab member kindly supported thermoelectric energy harvesting project in term of heat transfer circuit design and heat transfer simulation. Without their support, reasonable analysis and design were not achievable.

For experimental deployments, a lot of supporters gave opportunities and helped me to deploying sensors in various fields in Japan so I would like to thanks Yosuke Tamatsukuri, Dr. Du Jianming (Union-farm), Akihiro Ikemori (Ikemori farm), Arata Nagatake, Prof. Ryusuke Hatano (Hokkaido University), Tomoki Yoneda, Takafumi Takase (Kajistudo Co., Ltd.), Yoshinori Komatsu, Nobutaka Fukagawa (Kashima Antlers FC), Masanori Tanaka (IGM), Seiji Yonezawa, and all the other supporters.

It is not possible to expand the experimental fields in global without kind supports by

Prof. George Vellidis and his lab members (University of Georgia), Prof. J. Adinarayana, Prof. Surya Durbha, Dr. Suryakant Sawant, Saurabh Suradhaniwar (Indian Institute of Technology, Bombay), Naho Shigeta (INFOBRIDGE Marketing & Promotion Co., Ltd.), Dr. S. Wani, Dr. K. Srinivas (ICRISAT India) As experiments in Hyderabad, India are part of SICORP Collaborative Hub for International Research Program between Japan and India. Thus, I would like to thanks the project leaders Prof. Seishi Ninomiya (The University of Tokyo) and Prof. U. B. Desai (Indian Institute of Technology, Hyderabad). Also thanks to Prof. P. Rajalakshmi and her lab members for kind supports on fields.

This research is granted by the graduate program for social ICT Global Creative Leaders (GCL) supported by the ministry of education, culture, sports, science and technology, Japan as a part of the Program for Leading Graduate School. The GCL program gave financial support and provided great opportunities to expand the research in global scale. The GCL members gave informative feedback on my research and projects. Especially, Tastuya Iizuka, Mathew Ishige, Hirotoshi Ogawa, Yuki Sano, Fumika Taguma were involved to my GCL student project “Akiyagri” and worked hard for it so I would appreciate them. For Global Design Workshop (GDWS), I would like to thank all GDWS committees for giving feedback on my workshop design and also thank to Sony Creative Lounge and DMM.make AKIBA for providing the space for the workshop. As outcomes through the workshop are included in the thesis, I appreciated contributions by participants of the workshops.

At last, I would like to thank to my family as they always supported me from all the aspects to pursue phD course.

Reference

[1] A. Fares and A.K. Alva, "Evaluation of capacitance probes for optimal irrigation of citrus through soil moisture monitoring in an entisol profile," Irrigation Science, vol.19, no.2, pp.57–64, Jan. 2000. https://doi.org/10.1007/s002710050001

[2] G. Vellidis, M. Tucker, C. Perry, C. Kvien, and C. Bednarz, "A real-time wireless smart sensor array for scheduling irrigation," Computers and Electronics in Agriculture, vol.61, no.1, pp.44–50, 2008. Emerging Technologies For Real-time and Integrated Agriculture Decisions. http://www.sciencedirect.com/science/article/pii/S0168169907001706

[3] Y. Kim, R.G. Evans, and W.M. Iversen, "Remote sensing and control of an irrigation system using a distributed wireless sensor network," IEEE Transactions on Instrumentation and Measurement, vol.57, no.7, pp.1379–1387, July 2008.

[4] G. Bouyoucos and A. Mick, "Improvements in the plaster of paris absorption block electrical resistance method for measuring soil moisture under field conditions.," Soil Science, vol.63, no.6, pp.455–466, 1947.

[5] E.J. Spaans and J.M. Baker, "Calibration of watermark soil moisture sensors for soil matric potential and temperature," Plant and Soil, vol.143, no.2, pp.213–217, 1992.

[6] K. Noborio, R. Horton, and C. Tan, "Time domain reflectometry probe for simultaneous measurement of soil matric potential and water content," Soil Science Society of America Journal, vol.63, no.6, pp.1500–1505, 1999.

[7] G.J. Bouyoucou and A.H. Mick, "A fabric absorption unit for continuous measurement of soil moisture in the field," Soil Science, vol.66, no.3, pp.217–232, 1948.

[8] W. Gardner and D. Kirkham, "Determination of soil moisture by neutron scattering.," Soil Science, vol.73, no.5, pp.391–402, 1952.

[9] I. Long and B. French, "Measurement of soil moisture in the field by neutron moderation," European Journal of Soil Science, vol.18, no.1, pp.149–166, 1967.

[10] G.C. Topp, J.L. Davis, and A.P. Annan, "Electromagnetic determination of soil water content: Measurements in coaxial transmission lines," Water Resources Research, vol.16, no.3, pp.574–582, 1980. http://dx.doi.org/10.1029/WR016i003p00574

[11] K. Noborio, "Measurement of soil water content and electrical conductivity by time domain reflectometry: a review," Computers and Electronics in Agriculture, vol.31, no.3, pp.213–237, 2001. http://www.sciencedirect.com/science/article/pii/S0168169900001848

[12] F. Dalton, W. Herkelrath, D. Rawlins, and J. Rhoades, "Time-domain reflectometry: simultaneous measurement of soil water content and electrical conductivity," Science, vol.224, pp.989–991, 1984.

[13] G. Topp, J. Davis, and A. Annan, "Electromagnetic determination of soil water content using tdr: Ii. evaluation of installation and configuration of parallel transmission lines," Soil Science Society of America Journal, vol.46, no.4, pp.678–684, 1982.

[14] H.H. Nissen, P. Moldrup, and K. Henriksen, "High-resolution time domain reflectometry coil probe for measuring soil water content," Soil Science Society of America Journal, vol.62, no.5, pp.1203–1211, 1998.

[15] W. Skierucha and A. Wilczek, "A fdr sensor for measuring complex soil dielectric permittivity in the 10–500 mhz frequency range," Sensors, vol.10, no.4, pp.3314–3329, 2010.

[16] M. Nakashima, M. Inoue, K. Sawada, and C. Nicholl, "Measurement of soil water content by amplitude domain reflectometry method and its calibration," Journal of Groundwater Hydrology, vol.40, no.4, pp.509–519, 1998.

[17] T. Dean, J. Bell, and A. Baty, "Soil moisture measurement by an improved capacitance technique, part i. sensor design and performance," Journal of Hydrology, vol.93, no.1-2, pp.67–78, 1987.

[18] J. Bell, T. Dean, and M. Hodnett, "Soil moisture measurement by an improved capacitance technique, part ii. field techniques, evaluation and calibration," Journal of Hydrology, vol.93, no.1-2, pp.79–90, 1987.

[19] M. Tomer and J. Anderson, "Field evaluation of a soil water-capacitance probe in a fine sand.," Soil Science, vol.159, no.2, pp.90–98, 1995.

[20] A. Nadler and Y. Lapid, "An improved capacitance sensor for in situ monitoring of soil moisture," Soil Research, vol.34, no.3, pp.361–368, 1996.

[21] H. Bogena, J. Huisman, C. Oberdörster, and H. Vereecken, "Evaluation of a low-cost soil water content sensor for wireless network applications," Journal of Hydrology, vol.344, no.1, pp.32–42, 2007.

[22] M.S. Seyfried and L.E. Grant, "Temperature effects on soil dielectric properties measured at 50 mhz," Vadose Zone Journal, vol.6, no.4, pp.759–765, 2007.

[23] S.R. Evett, J.A. Tolk, and T.A. Howell, "Soil profile water content determination: Sensor accuracy, axial response, calibration, temperature dependence, and precision," Vadose Zone Journal, vol.5, no.3, pp.894–907, 2006.

[24] S.R. Evett, R.C. Schwartz, J.A. Tolk, and T.A. Howell, "Soil profile water content determination: Spatiotemporal variability of electromagnetic and neutron probe sensors in access tubes," Vadose Zone Journal, vol.8, no.4, pp.926–941, 2009.

[25] T. Kelleners, D. Robinson, P. Shouse, J. Ayars, and T. Skaggs, "Frequency dependence of the complex permittivity and its impact on dielectric sensor calibration in soils," Soil Science Society of America Journal, vol.69, no.1, pp.67–76, 2005.

[26] F. Kizito, C. Campbell, G. Campbell, D. Cobos, B. Teare, B. Carter, and J. Hopmans, "Frequency, electrical conductivity and temperature analysis of a low-cost capacitance soil moisture sensor," Journal of Hydrology, vol.352, no.3, pp.367–378, 2008.

[27] F. Padilla and F. Pugnaire, "Rooting depth and soil moisture control mediterranean woody seedling survival during drought," Functional Ecology, vol.21, no.3, pp.489–495, 2007.

[28] R.C. Bales, J.W. Hopmans, A.T. O'Geen, M. Meadows, P.C. Hartsough, P. Kirchner, C.T. Hunsaker, and D. Beaudette, "Soil moisture response to snowmelt and rainfall in a sierra nevada mixed-conifer forest," Vadose Zone Journal, vol.10, no.3, pp.786–799, 2011.

[29] S. Sudevalayam and P. Kulkarni, "Energy harvesting sensor nodes: Survey and implications," IEEE Communications Surveys Tutorials, vol.13, no.3, pp.443–461, July 2011.

[30] C. Moser, L. Thiele, D. Brunelli, and L. Benini, "Adaptive power management in energy harvesting systems," the conference on Design, automation and test in Europe, pp.773–778, DATE '07, Nice, France, May 2007.

[31] G.K. Ottman, H.F. Hofmann, A.C. Bhatt, and G.A. Lesieutre, "Adaptive piezoelectric energy harvesting circuit for wireless remote power supply," Power Electronics, IEEE Transactions on, vol.17, no.5, pp.669–676, sep 2002.

[32] A. Kansal, J. Hsu, S. Zahedi, and M.B. Srivastava, "Power management in energy harvesting sensor networks," ACM Trans. Embed. Comput. Syst., vol.6, no.4, pp.1–38, Sept. 2007.

[33] C.M. Vigorito, D. Ganesan, and A.G. Barto, "Adaptive control of duty cycling in energy-harvesting wireless sensor networks," 4th Annual IEEE Communications Society Conference on Sensor, Mesh and Ad Hoc Communications and Networks (SECON) 2007, pp.21–30, June 2007.

[34] R. Vyas, Y. Kawahara, B. Cook, T. Asami, and M. Tentzeris, "E-wehp: An embedded wireless energy harvesting platform for powering on embedded sensors using existing, ambient digital tv signals present in the air," IEEE Transactions on Microwave Theory and Techniques, pp.1–8, Aug. 2012.

[35] A. Parks, A. Sample, Y. Zhao, and J.R. Smith, "A wireless sensing platform utilizing ambient rf energy," IEEE Topical Meeting on Wireless Sensors and Sensor Networks (WiSNET), pp.1–3, Austin, TX, Jan. 2013.

[36] Y. Kawahara, H. Lee, and M.M. Tentzeris, "Sensprout: Inkjet-printed soil moisture and leaf wetness sensor," Proceedings of the 2012 ACM Conference on Ubiquitous Computing, pp.545–545, UbiComp '12, ACM, New York, NY, USA, 2012. http://doi.acm.org/10.1145/2370216.2370302

[37] T. Suzuki, Y. Narusue, K. Nishioka, Y. Kawahara, and Tohru Asami., "Design of a microwave power transmission system for farm field sensing by an unmanned aerial vehicle," IEICE General Conference, pp.B–18–46, Shiga, March 2015.

[38] D.L. Mascarenas, E.B. Flynn, M.D. Todd, T.G. Overly, K.M. Farinholt, G. Park, and C.R. Farrar, "Experimental studies of using wireless energy transmission for powering embedded sensor nodes," Journal of Sound and Vibration, vol.329, no.12, pp.2421–2433, 2010. Structural Health Monitoring Theory Meets Practice. http://www.sciencedirect.com/science/article/pii/S0022460X09008384

[39] B. Griffin and C. Detweiler, "Resonant wireless power transfer to ground sensors from a uav," 2012 IEEE International Conference on Robotics and Automation, pp.2660–2665, May 2012.

[40] J. Shi, J. Wang, A.Y. Hsu, P.E. O'Neill, and E.T. Engman, "Estimation of bare surface soil moisture and surface roughness parameter using l-band sar image data," IEEE Transactions on Geoscience and Remote Sensing, vol.35, no.5, pp.1254–1266, Sept. 1997.

[41] J. Taneja, J. Jeong, and D. Culler, "Design, modeling, and capacity planning for micro-solar power sensor networks," the 7th international conference on Information processing in sensor networks, pp.407–418, IPSN '08, St Louis, MI, April 2008.

[42] A. Dolgov, R. Zane, and Z. Popovic, "Power management system for online low power rf energy harvesting optimization," IEEE Transactions on Circuits and Systems I: Regular Papers, vol.57, no.7, pp.1802–1811, July 2010.

[43] T. Le, K. Mayaram, and T. Fiez, "Efficient far-field radio frequency energy harvesting for passively powered sensor networks," Solid-State Circuits, IEEE Journal of, vol.43, no.5, pp.1287–1302, May 2008.

[44] K. Gudan, S. Chemishkian, J. Hull, M. Reynolds, and S. Thomas, "Feasibility of wireless sensors using ambient 2.4ghz rf energy," 11th IEEE International Conference on Sensors (SENSORS) 2012, pp.1–4, Taipei, Taiwan, Oct. 2012.

[45] U. Olgun, C.-C. Chen, and J.L. Volakis, "Design of an efficient ambient wifi energy harvesting system," IET Microwaves, Antennas Propagation, vol.6, no.11, pp.1200–1206, Aug. 2012.

[46] G. Andia Vera, A. Georgiadis, A. Collado, and S. Via, "Design of a 2.45 ghz rectenna for electromagnetic (em) energy scavenging," Radio and Wireless Symposium (RWS), 2010 IEEE, pp.61–64, New Orleans, LA, Jan. 2010.

[47] M. Roberg, E. Falkenstein, and Z. Popovic, "High-efficiency harmonically-terminated rectifier for wireless powering applications," Microwave Symposium Digest (MTT), 2012 IEEE MTT-S International, pp.1–3, Montreal, Canada, June 2012.

[48] D. Costinett, E. Falkenstein, R. Zane, and Z. Popovic, "Rf-powered variable duty cycle wireless sensor," 40th European Microwave Conference, p.41, Paris, France, Sept. 2010.

[49] H. Nishimoto, Y. Kawahara, and T. Asami, "Prototype implementation of wireless sensor network using tv broadcast rf energy harvesting," 12th ACM international conference adjunct papers on Ubiquitous computing - Adjunct, pp.373–374, Ubicomp '10 Adjunct, Copenhagen, Denmark, Sept. 2010.

[50] R. Vyas, H. Nishimoto, M. Tentzeris, Y. Kawahara, and T. Asami, "A battery-less, energy harvesting device for long range scavenging of wireless power from terrestrial tv broadcasts," IEEE MTT-S International Microwave Symposium Digest (MTT) 2012, pp.1–3, Montreal, Canada, June 2012.

[51] Yagi Antenna.Inc, "UwPA: UHF antenna," `http://www.yagi-antenna.co.jp/`, 2005.

[52] D. Willkomm, S. Machiraju, J. Bolot, and A. Wolisz, "Primary users in cellular networks: A large-scale measurement study," 3rd IEEE Symposium on New Frontiers in Dynamic Spectrum Access Networks (DySPAN) 2008, pp.1–11, Chicago, IL, Oct. 2008.

[53] Texas Instruments, "eZ430-RF2500," `http://www.ti.com/tool/EZ430-RF2500T`, 2017.

[54] T. Yoshiaki, S. Shino, and K. Kobasyashi, "Process for preparing conductive material," Sep. 2011.

[55] Brother Industries, Ltd., "DCP-J525N inkjet printer," `http://www.brother.co.jp/product/printer/inkjet/dcpj525n/index.htm`, 2017.

[56] Fujifilm Corporation, "Photo paper for inkjet printer WPA460PRO," `http://fujifilm.jp/personal/supply/kassai/luster_photo/pro/index.html`, 2012.

[57] F. Yuan and N. Soltani, "Design techniques for power harvesting of passive wireless microsensors," 51st Midwest Symposium on Circuits and Systems (MWSCAS) 2008, pp.289–293, Aug. 2008.

[58] Seiko Instruments Inc., "Ultra-low voltage operation charge pump IC for step-up DC-DC converter startup S-882Z series," `http://datasheet.sii-ic.com/pub/ic/old_dtst/old_dt_e/charge_p/S882Z_E.pdf`, 2017.

[59] Skyworks Solutions, Inc., "Surface mount mixer and detector Schottky diodes," http://www.skyworksinc.com/uploads/documents/Surface_Mount_Schottky_Diodes_200041AC.pdf, 2017.

[60] K.W. Lui, A. Vilches, and C. Toumazou, "Ultra-efficient microwave harvesting system for battery-less micropower microcontroller platform," IET Microwaves, Antennas Propagation, vol.5, no.7, pp.811–817, May 2011.

[61] Avago Technologies, "HSMS-286x surface mount RF Schottky barrier diodes," http://www.avagotech.com/docs/AV02-1388EN, 2017.

[62] A. Collado and A. Georgiadis, "Improving wireless power transmission efficiency using chaotic waveforms," IEEE MTT-S International Microwave Symposium Digest (MTT) 2012, pp.1–3, Montreal, Canada, June 2012.

[63] G.W. Collins, Fundamentals of digital television transmission, Wiley, 2001.

[64] P.R. Kumar and P. Varaiya, Stochastic systems: estimation, identification and adaptive control, Prentice-Hall, Inc., Upper Saddle River, NJ, 1986.

[65] S.S. Gevorgian, T. Martinsson, P.L.J. Linner, and E.L. Kollberg, "Cad models for multilayered substrate interdigital capacitors," IEEE Transactions on Microwave Theory and Techniques, vol.44, no.6, pp.896–904, June 1996.

[66] Elephantech Inc., "AgIC Circuit Marker," https://www.elephantech.co.jp/en/#historical-products, 2017.

[67] C.-S. Yoo and I.-K. Ahn, "Low cost gps/ins sensor fusion system for uav navigation," Digital Avionics Systems Conference, 2003. DASC '03. The 22nd, vol.2, pp.8.A.1–8.1–9vol.2, Oct. 2003.

[68] V. Honkavirta, T. Perala, S. Ali-Loytty, and R. Piche, "A comparative survey of wlan location fingerprinting methods," 2009 6th Workshop on Positioning, Navigation and Communication, pp.243–251, March 2009.

[69] A. Arya, P. Godlewski, and P. Melle, "Performance analysis of outdoor localization systems based on rss fingerprinting," 2009 6th International Symposium on Wireless Communication Systems, pp.378–382, Sept. 2009.

[70] S.C. Ergen, H.S. Tetikol, M. Kontik, R. Sevlian, R. Rajagopal, and P. Varaiya, "Rssi-fingerprinting-based mobile phone localization with route constraints," IEEE Transactions on Vehicular Technology, vol.63, no.1, pp.423–428, Jan. 2014.

[71] F.K.W. Chan, H.C. So, J. Zheng, and K.W.K. Lui, "Best linear unbiased estimator approach for time-of-arrival based localisation," IET Signal Processing, vol.2, no.2, pp.156–162, June 2008.

[72] G.J. Toussaint, P.D. Lima, and D.J. Pack, "Localizing rf targets with cooperative unmanned aerial vehicles," 2007 American Control Conference, pp.5928–5933, July 2007.

[73] S.A.A. Shahidian and H. Soltanizadeh, "Optimal trajectories for two uavs in localization of multiple rf sources," Transactions of the Institute of Measurement and Control, vol.38, no.8, pp.908–916, 2016.

[74] J.F. Dickson, "On-chip high-voltage generation in mnos integrated circuits using an improved voltage multiplier technique," IEEE Journal of Solid-State Circuits, vol.11, no.3, pp.374–378, June 1976.

[75] S. Li and H. Gao, "Propagation characteristics of 2.4ghz wireless channel in cornfields," Communication Technology (ICCT), 2011 IEEE 13th International Conference on, pp.136–140, Sept. 2011.

[76] Decagon Device Inc., "Soil Moisture Sensors (Volumetric Water Content)," `http://www.decagon.com/en/soils/volumetric-water-content-sensors/`, 2015.

[77] G. Blewitt, "Basics of the gps technique: observation equations," Geodetic applications of GPS, pp.10–54, 1997.

Publication

Journal

[P1] R. Shigeta, T. Sasaki, D.M. Quan, Y. Kawahara, R. Vyas, M. Tentzeris, and T. Asami, "Ambient-rf-energy-harvesting sensor node with capacitor-leakage-aware duty cycle control," Selected papers from the IEEE SENSORS 2012 Conference: Special Issue for IEEE Sensors Journal, pp.1–8, July 2013.

[P2] Y. Kojima, R. Shigeta, N. Miyamoto, Y. Shirahama, K. Nishioka, M. Mizoguchi, and Y. Kawahara, "Low-cost soil moisture profile probe using thin-film capacitors and a capacitive touch sensor," Sensors, pp.1–14, 2016.

[P3] R. Shigeta, K. Suzuki, F. Okuya, and Y. Kawahara, "Trilateration-inspired sensor node position estimation for uav-assisted microwave wireless power transfer," SICE Journal of Control, Measurement, and System Integration, vol.10, no.5, pp.350–359, 2017.

International conference

[P4] R. Shigeta, Y. Kawahara, and T. Asami, "Demo: Capacitor leakage aware duty cycle control for energy harvesting wireless sensor networks," 9th ACM Conference on Embedded Networked Sensor Systems, pp.387–388, SenSys '11, Seattle, WA, Nov. 2011.

[P5] R. Shigeta, T. Sasaki, D.M. Quan, Y. Kawahara, R. Vyas, M. Tentzeris, and T. Asami, "Ambient-rf-energy-harvesting sensor node with capacitor-leakage-aware duty cycle control," 11th IEEE International Conference on Sensors (SENSORS) 2012, pp.1–4, Taipei, Taiwan, Oct. 2012.

[P6] Y. Kawahara, W. Wei, Y. Narusue, R. Shigeta, T. Asami, and M. Tentzeris, "Virtualizing power cords by wireless power transmission and energy harvesting," IEEE Radio Wireless Week (RWW), pp.37–39, Austin, TX, Jan. 2013.

[P7] Y. Kawahara, X. Bian, R. Shigeta, R. Vyas, M.M. Tentzeris, and T. Asami, "Power harvesting from microwave oven electromagnetic leakage," Proceedings of the 2013 ACM International Joint Conference on Pervasive and Ubiquitous Computing, pp.373–382, UbiComp '13, ACM, New York, NY, USA, 2013. http://doi.acm.org/10.1145/2493432.2493500

[P8] Y. Shirahama, R. Shigeta, Y. Kawahara, and T. Asami, "Implementation of wide range soil moisture profile probe by coplanar plate capacitor on film substrate," 14th IEEE International Conference on Sensors (SENSORS) 2015, pp.1758–1761, Busan, Korea, Nov. 2015.

[P9] Y. Kawahara, N. Miyamoto, Y. Kojima, R. Shigeta, K. Nishioka, N. Kabaya, S. Miyamoto, and M. Mizoguchi., "Low-cost sensing system design for agriculture.," WCCA-AFITA 2016, pp.SS–1613–16, Korea, June 2016.

[P10] R. Shigeta, N. Miyamoto, Y. Kojima, Y. Kawahara, and T. Asami., "Low-cost soil matric potential sensor by thin-film electrodes with gypsum plate," IEEE SENSORS 2016, pp.A–20–407(Poster), Orland, FL, Nov. 2016.

[P11] K. Suzuki, R. Shigeta, Y. Kawahara, and T. Asami, "Bilateration-based position estimation of sensor nodes for uav-assisted wireless power transfer systems," Adjunct Proceedings of the 13th International Conference on Mobile and Ubiquitous Systems: Computing Networking and Services, pp.66–71, MOBIQUITOUS 2016, ACM, New York, NY, USA, 2016. http://doi.acm.org/10.1145/3004010.3004015

Patent

[P12] 川原圭博, 繁田　亮, 宮元直也, 西岡一洋, 小島悠揮, 白浜妥知, 森澤雄太., 「水分量検出装置」(特願 2016-036026) Feb. 26th, 2016.

Domestic workshop

[P13] 繁田　亮，川原圭博，浅見徹.，"漏れ電力を考慮した rf エネルギーハーベスティングセンサネットのための最適駆動点決定手法,"マルチメディア，分散，協調とモバイル DICOMO 2012 シンポジウム，4E–2，石川，July 2012.

[P14] 繁田　亮，小林亮介，川原圭博，浅見徹.，"Uav からの無線給電によるバッテリーレス農業用センサシステムにおける最適給電点追跡手法,"電子情報通信学会 技術報告，vol.115, ASN2015-73，no.290，pp.127–132，Nov. 2015.

[P15] 林　直人，繁田　亮，高木　雅，川原圭博，浅見徹.，"インドの農村部での土壌センシングシステムの実証:期待と現実,"マルチメディア，分散，協調とモバイル DICOMO 2016 シンポジウム，pp.565–571，三重，July 2016.

[P16] 繁田　亮，鈴木康大，川原圭博，浅見徹.，"[奨励講演]uav からの無線給電による農業用センサシステムのためのセンサ位置推定手法,"電子情報通信学会 技術報告，vol.116，no.308, ASN2016-54，pp.73–78，Nov. 2016.

[P17] 鈴木康大，繁田　亮，川原圭博，浅見徹.，"汎用マイコンで可能な反射時間計測による簡易 tdr を利用した低価格水位計の開発,"電子情報通信学会 技術報告，vol.116，no.308, ASN2016-54，pp.97–102，Nov. 2016.

[P18] 角谷和宣, 繁田 亮, 川原圭博, 浅見 徹, 蒲谷直樹., “低価格移動式農業用ロボットのためのウェブカメラを用いた自己位置推定手法,” 電子情報通信学会 技術報告, vol.116, no.308, ASN2016-54, pp.79–84, Nov. 2016.

[P19] 繁田 亮, 宮元直也, 川原圭博., “測定深度選択可能なセンサ電極交換式土壌水分プロファイルプローブ,” 電子情報通信学会 技術報告, vol.117, no.310, ASN2017-72, pp.59–64, Nov. 2017.

[P20] 鈴木康大, 繁田 亮, 宮元直也, 佐々木和浩, 川原圭博., “測定深度選択可能なセンサ電極交換式土壌水分プロファイルプローブ,” 電子情報通信学会 技術報告, vol.117, no.310, ASN2017-77, pp.121–126, Nov. 2017.

[P21] 飯塚達哉, 繁田 亮, 川原圭博., “測定深度選択可能なセンサ電極交換式土壌水分プロファイルプローブ,” 電子情報通信学会 技術報告, vol.117, no.310, ASN2017-69, pp.41–46, Nov. 2017.

[P22] 池田夏輝, 繁田 亮, 塩見淳一郎, 川原圭博., “土中温度差発電駆動型土壌センサの熱・電気回路モデルと地温データを用いた発電量評価,” 電子情報通信学会 技術報告, vol.117, no.310, ASN2017-68, pp.35–40, Nov. 2017.

[P23] 西保 匠, 繁田 亮, 川原圭博., “芝管理用埋没設置型センサにおける 920mhz 帯 ieee802.15.4g の通信安定性評価,” 電子情報通信学会 技術報告, vol.117, no.310, ASN2017-67, pp.29–33, Nov. 2017.

Domestic conference

[P24] 繁田 亮, 新熊亮一, 笠井裕之, 山口和泰, 高橋達郎., “ソーシャルな関係性を有するネットワークデータ表現とその抽出法,” 電子情報通信学会総合大会, B–7–59, 東京, Sept. 2011.

[P25] 繁田 亮, 川原圭博, 浅見徹., “キャパシタの漏れ電力を考慮した energy harvesting センサネットのためのデューティサイクル制御手法,” 電子情報通信学会ソサイエティ大会, B–19–29, 北海道, Sept. 2011.

[P26] 繁田 亮, 川原圭博, 浅見徹., “キャパシタの漏れ電力を考慮した energy harvesting センサネットのための通信制御手法,” 電子情報通信学会総合大会, B–19–35, 岡山, March 2012.

[P27] 繁田 亮, 卞 暁瑩, 川原圭博, 浅見徹., “電子レンジ漏れ電波を用いた rf エネルギーハーベスティングセンサノードの一検討,” 電子情報通信学会総合大会, 岐阜, March 2013.

[P28] 鈴木 有, 繁田 亮, 川原圭博, 浅見徹., “エナジーハーベスティングを用いた静電容量センサにおける供給電圧と精度のトレードオフ分析,” 電子情報通信学会ソサイエティ大会, B–19–45, 富山, Sept. 2012.

[P29] 林直人，繁田　亮，川原圭博，浅見徹.，“SenSprout: 環境電波からの無線給電を利用した低コスト土壌モニタリングセンサの設計,” 電子情報通信学会ソサイエティ大会，B–18–11，福岡，Sept. 2013.

[P30] 繁田　亮，川原圭博，M. Tentzeris，浅見徹.，“Ambient rf energy harvesting の研究動向とアプリケーション,” 電子情報通信学会総合大会，岐阜，March 2013.

[P31] 興梠智紀，繁田　亮，白浜妥知，小島悠揮，川原圭博，浅見徹.，“薄膜土壌水分プロファイルプローブの逐次的校正手法,” 電子情報通信学会ソサイエティ大会，B–18–26，仙台，Sep. 2015.

[P32] 繁田　亮，興梠智紀，川原圭博，浅見徹.，“薄膜土壌水分プロファイルプローブにおける線間容量除去手法,” 電子情報通信学会総合大会，B–18–14，福岡，Mar. 2016.

[P33] 興梠智紀，繁田　亮，小島悠揮，川原圭博，浅見徹.，“低コストマイコンを使った薄膜土壌水分センサ測定値の周波数依存性の評価,” 電子情報通信学会総合大会，B–18–15，福岡，Mar. 2016.

[P34] 鈴木康大，繁田　亮，川原圭博，浅見徹.，“Uav を用いた給電システムにおける給電効率情報のフィードバックに基づいたセンサ位置推定による最適給電点探索手法,” 電子情報通信学会総合大会，B–18–33，福岡，Mar. 2016.

[P35] 小林亮介，成末義哲，繁田　亮，川原圭博，浅見徹.，“無線給電型土壌水分センサ実現のためのフェージング対策手法,” 電子情報通信学会総合大会，B–18–13，福岡，Mar. 2016.

[P36] T.T. Duc，R. Shigeta，Y. Kawahara, and T. Asami.，“Error reduction in capacitive based water level sensor for paddy field,” 電子情報通信学会総合大会, B–18–16, 福岡, Mar. 2016.

[P37] 宮元直也，繁田　亮，西岡一洋, 川原圭博.，“低コスト樹液流センサおよび土壌水分センサを用いたアスパラガスの栽培環境モニタリング,” 電子情報通信学会総合大会，B–18–13，名古屋，Mar. 2017.

[P38] 林　直人，繁田　亮，川原圭博，浅見徹.，“分散的に設置された無線センサシステムのメンテナンスに向けた知識集約型クラウドソーシングの検討,” 電子情報通信学会総合大会，B–18–14，名古屋，Mar. 2017.

[P39] 角谷和宣，繁田　亮，川原圭博，浅見徹.，“カメラ映像による自己位置推定を用いた精密農業のための低価格自律移動ロボットの試作と評価,” 情報処理学会全国大会，5T–02，名古屋，Mar. 2017.

Award

[A1] 最優秀賞，GCL 2017 年 夏のプレゼンコンペ, 8th Oct. 2017.

[A2] 若手研究奨励賞，電子情報通信学会 ASN 研究会, 15th May. 2016.

[A3] 最優秀賞，GCL 2015 年 夏のプレゼンコンペ, 6th Oct. 2015.

[A4] One of the 25 most downloaded Sensors Journal papers in the month of September, IEEE SENSORS Journal 2013, 31th Oct. 2013.

[A5] The 2012 Student Paper Competition Award - Second Place, IEEE SENSORS 2012, 30th Oct. 2012.

[A6] ヤングリサーチャー賞，DICOMO2012, July 2012.